UNIVERSITY OF LIVERPOOL

Characterisation of Nascent Mesoderm Derived from Mouse Embryonic Stem Cells Grown in 3-D and 2-D Culture Systems

Thesis submitted in accordance with the requirements of the University of Liverpool for the degree of Doctor in Philosophy

by

Jing Zhou

November 2016

Acknowledgements

I would like to thank my supervisors, Professor Patricia Murray and Professor Alan Morgan, for their continuous input and guidance throughout the Ph.D. progress.

I would also like to acknowledge the China Scholarship Council for funding this study.

I am grateful to many members from the Stem Cell Group and the Technology Directorate of the University of Liverpool, for their genuine help and professional support on completing this research project. In particular, Dr. Antonius Plagge, for his assistance over the entire process of generating the reporter cell line; Dr. Jack Sharkey, for his assistance in the animal experiments during the process of the mESC *in vivo* administration and imaging data acquisition; Miss Lauren Scarfe, for her help with the preparation of the paraffin slides; Dr. Sandra Pereira Cachinho, for her help with the FACS; Ms. Carolyn Rainer, for her help with the flow cytometry analysis; and Dr. Marco Marcello and Dr. Joanna Wnetrzak, for their help on the confocal laser scanning microscopy, respectively.

Thanks also to Mrs. Angela Platt-Higgins (Institute of Integrative Biology, University of Liverpool) for her assistance with H&E staining, and to pathologist Dr. Rajeev Shukla (Alder Hey Children's NHS Foundation Trust) for his support on histopathological analysis.

My deepest gratitude is to my family, without whom this work could never have been achieved. I owe it all to them!

Abstract

Mouse embryonic stem cells (mESCs) are derived from the inner cell mass of the blastocyst. When cultured in 3-D suspension in the absence of feeder cells, they form aggregates called embryoid bodies (EBs) that spontaneously differentiate to generate an outer layer of extra-embryonic endoderm with underlying basement membrane, an inner layer of primitive ectoderm, as well as a central proamniotic-like cavity. Furthermore, EBs can undergo a process that resembles gastrulation and can generate derivatives of the three embryonic germ layers. EBs are therefore very useful as model systems for investigating the early stages of mammalian development, and also for generating specific lineages such as ectoderm, mesoderm and endoderm, which can be used to investigate the mechanisms regulating the differentiation of specific lineages, as well as for regenerative medicine research. However, when used as a source for generating specific cell types of interest, EBs can be problematic, because only a proportion of cells within each EB will differentiate to become the required cell type. For this reason, there has been much interest in developing more efficient 2-D culture systems for directing the differentiation of mESCs to specific cell types. However, it is not clear whether cell types differentiating in EBs are equivalent to the corresponding cell types generated in 2-D differentiation cultures and have the same differentiation potential. To address this question, this study has compared the properties of nascent mesoderm arising in EBs with nascent mesoderm arising in 2-D differentiation culture.

In order to do this, a mESC reporter line was created where a gene encoding the far-red fluorescent protein E2-Crimson (E2C) was knocked into the *Rosa26* locus of an *E14-Bra-GFP* mESC line. This line enabled GFP^+ nascent mesoderm cells to be isolated using fluorescence activated cell sorting so that the expression of key genes could be analysed, and then the fate of the cells could be tracked in

living mice *in vivo* or following incorporation into developing organs *ex vivo* due to the fact that they constitutively express E2C.

After confirming that the novel reporter *E14-Bra-GFP/Rosa26-E2C* mESC line displayed typical mESC properties and behaved similarly to unmodified mESC lines, the effectiveness of the E2C reporter for tracking cells *in vivo* and *in vitro* was assessed. Although E2C expression was stable, the fluorescence signal was quite weak, which meant that while it was possible to detect E2C in cells *in vitro* and on histological sections, tracking them in living mice was not feasible. For this reason, the study focused on comparing the gene expression profile of mesoderm isolated from EBs and 2-D cultures using quantitative reverse transcription PCR (RT-qPCR), and then their differentiation potential was assessed by incorporating the mesodermal cells into mouse kidney rudiments *ex vivo*. The most striking result from the RT-PCR analysis was that the mesodermal cells isolated from the EBs expressed >20-fold higher levels of the lateral plate mesoderm gene, *Foxf1*, compared to the mesoderm cells derived from the 2-D culture system. Surprisingly, neither the mesodermal cells isolated from the EBs, nor those isolated from the 2-D system integrated into developing nephrons within kidney rudiments cultured *ex vivo*. This result was unexpected because the kidney is derived from the mesodermal lineage, specifically the intermediate mesoderm, and so it was anticipated that nascent mesoderm cells would be able to contribute to the developing kidneys. However, further analysis showed that the EB-derived mesoderm cells differentiated into $PECAM^{+}$ endothelial-like cells within the rudiments. It is known that the lateral plate mesoderm gives rise to the vasculature in the developing embryo, so the fate of the EB-derived nascent mesodermal cells accompanied with their high levels of *Foxf1* suggested that they were likely to have been already specified as lateral plate mesoderm. In contrast, the mesodermal cells derived from the 2-D culture system showed a limited capacity to generate PECAM-1^{+} cells, and instead, appeared to integrate into the renal stroma. It can therefore be concluded that Bra^{+} mesodermal cells generated using

different *in vitro* culture systems have different properties, and might already be specified to more differentiated mesodermal lineages, such as paraxial, intermediate or lateral plate mesoderm. To facilitate future progress, it would be useful to generate dual reporter mESC lines that enabled the expression of *Bra* and a marker of either paraxial, intermediate or lateral plate mesoderm to be monitored simultaneously in real-time during *in vitro* differentiation culture.

Abbreviations

2-/3-D	Two-/three-dimensional
AV	Adenoviral vector
AAV	Adeno-associated viral vector
BM	Basement membrane
BMP	Bone morphogenetic protein
Bra	Brachyury
CapM	Cap mesenchyme
Cdx2	Caudal type homeobox 2
CMV	Cytomegalovirus
DAPI	4',6-diamidino-2-phenylindole
DEME	Dulbecco's Modified Eagle's Medium
DT	Distal tubule
DTA	Diphtheria toxin A
E2C	E2-Crimson
EB	Embryoid body
ECM	Extra-cellular matrix
EDTA	Ethylenediaminetetraacetic acid
ExEc	Extraembryonic ectoderm
FACS	Fluorescence-activated cell sorting
FBS	Foetal bovine serum
Fgf(r)	Fibroblast growth factor(receptor)
Fox	Forkhead box
FP	Fluorescent protein
FR	Far-red
GAPDH	Glyceraldehyde 3-phosphate dehydrogenase
gDNA	Genomic DNA
Gdnf	Glial cell-derived neurotrophic factor
GFP	Green fluorescent protein
H&E	Haematoxylin and eosin
HA	Homologous arm
HL	Henle's loop
Hox	Homeobox
HR	Homologous recombination
IM	Intermediate mesoderm
ICM	Inner cell mass
Klf4/5	Kruppel-like factor 4/5
KSC	Kidney stem cell
Lhx1	LIM-domain homeobox 1
LIF	Leukaemia inhibitory factor
LPM	Lateral plate mesoderm
LV	Lentiviral vector
mESC	Mouse embryonic stem cell
MM	Metanephric mesenchyme
NIR	Near-infrared
NRT	Non-reverse transcriptase
NTC	Non-template control
Oct4	Octamer-binding transcription factor 4
Osr1	Odd-skipped-related 1
pA	Poly-A
PBS	Phosphate-buffered saline
PECAM-1	Platelet endothelial cell adhesion molecule-1
PEn	Parietal endoderm
PFA	Paraformaldehyde
PGK	Phosphoglycerate kinase
PM	Paraxial mesoderm
PNA	Rhodamine-labelled peanut agglutinin
PrEc	Primitive ectoderm
PrEn	Primitive endoderm
PS	Primitive streak
PT	Proximal tubule
RA	Retinoic acid
RFP	Red fluorescent protein
ROCK	Rho-associated, coiled-coil containing protein kinase
ROSA	Reverse orientation splice acceptor
RT-qPCR	Quantitative real-time polymerase chain reaction
RV	Renal vesicle / retroviral vector
SA	Splice accepter
SB	S-shaped body
SC	Subcutaneous
SD	Splice donor / Standard deviation
SDS	Sodium dodecyl sulphate
SEM	Standard error of mean
Sox2	Sry-like high-mobility group box 2
TB	Tail bud
Tbx6	T-box protein 6
TE	Trophectoderm
UB	Ureteric bud
VEn	Visceral endoderm
Wt1	Wilm’s tumour 1

Table of Contents

List of Tables and Figures

List of Tables

List of Figures

Chapter 1

Introduction

Overview

Since their derivation in the 1980s, mouse embryonic stem cells (mESCs) have served as invaluable tools for understanding the cellular and molecular mechanisms that regulate mammalian development, and for determining the signaling pathways required for the differentiation of specific cell lineages. For instance, by culturing mESCs in suspension, three-dimensional aggregates called embryoid bodies (EBs) are formed, which are excellent model systems that mimic the early stages of mouse development. As such, they have given us important insights into the underlying mechanisms that drive morphogenesis and embryo patterning (Robertson, 1987; Murray and Edgar, 2004). In addition, by culturing mESCs under 2-D adherent culture conditions in defined media, it has been possible to determine the role of specific growth factors and signaling pathways responsible for regulating self-renewal (Nichols and Smith, 2012), and directing mESC differentiation to the three embryonic germ layers (i.e., ectoderm, mesoderm and endoderm (Turner *et al.*, 2014). However, what remains unclear at present is whether the ectodermal, mesodermal and endodermal cells that are formed in EBs are equivalent to those that form under 2-D culture conditions.

Making use of an mESC line where green fluorescent protein (GFP) is knocked into the *brachyury* locus (a gene that is expressed in nascent mesoderm), this thesis addresses this important question by comparing the properties of mesodermal cells derived from mESCs cultured as EBs with those derived under 2-D conditions. Specifically, the expression levels of key genes were investigated, and the differentiation potential of the mesodermal cells were compared by investigating their ability to generate renal cell types in developing mouse kidney rudiments. To facilitate this, the gene encoding the far-red fluorescent protein, E2-Crimson, was knocked into the *Rosa26* locus of the aforementioned Bra-GFP reporter mESC line to enable the fate of the cells to be monitored *in vivo* and *in vitro*.

1.1 Development of the mouse embryo

The mouse (*Mus musculus*) is a classic model organism that is commonly used in mammalian developmental biology. It takes 9 weeks for the mouse to develop from a fertilized egg into a mature adult, with the first 3 weeks being *in utero*, and the remaining 6 weeks, post-natal (Wolpert *et al*., 2015). According to the Theiler stages of mouse development, the *in utero* stages of development are as follows, where 'E' refers to 'embryonic day': fertilisation (E0-0.9), cleavage (E1.0), morula formation (E2.0), blastocyst formation (E3.0-E4.5), implantation (E5.0-E6.0), gastrulation (E6.5-E8.0), turning (E8.5), organogenesis (E10.0-E14.0), fetal growth and development (E14.0-E19.0/E22.0) (Theiler,

1989).

1.1.1 Peri-implantation development of the mouse embryo

The peri-implantation stage of mouse embryo development includes the events that occur between E3.0 and E6.0. After fertilisation, the embryo undergoes a series of cleavage divisions, forming the morula at around E2.0. At E3.0, the morula undergoes compaction, which involves the cells up-regulating the cell adhesion molecule, E-cadherin, and becoming tightly associated with each other. The cells that are positioned on the periphery of the embryo following compaction give rise to the first epithelium of the embryo, which is called the trophectoderm (TE), while those positioned inside the embryo contribute to the inner cell mass (ICM) (Fleming, 1987; Andrzej *et al*., 1967; Plachta *et al*., 2011). The TE drives fluid transport inside the embryo to form a fluid-filled cavity known as the blastocoel. At this stage the embryo is called a blastocyst. The TE cells of the blastocyst deposit a basement membrane (BM) at their basal surface. Following blastocyst formation, the cells on the surface of the ICM differentiate to form the primitive endoderm (PrEn), depositing a basement membrane in-between themselves and the remaining ICM (Nadijcka and Hillman, 1974). Following implantation, PrEn cells differentiate into the visceral endoderm (VEn) and parietal endoderm (PEn) – both giving rise to extraembryonic tissues (Gardner, 1982). The PrEn cells in direct contact with the TE BM differentiate into the PEn, which migrate laterally along the TE BM to form the parietal yolk sac. The main

function of the PEn is to deposit a thick BM called Reichert's membrane that is thought to protect the embryo from maternal immune cells (Salamat *et al*., 1995). The PrEn cells that directly overlie the ICM differentiate to VEn, which provides nutrients that support the growth of the early embryo and also plays an important role in patterning the embryo (Gardner, 1982). Shortly after implantation, the cells of the ICM differentiate to become the epiblast (or primitive ectoderm, PrEc) (Artus and Chazaud, 2014). These PrEc cells become polarized to form tall columnar ectodermal cells that form a pseudostratified epithelium. Shortly afterwards, the cells at the centre of the ICM undergo programmed cell death to form the proamniotic cavity (Murray and Edgar, 2000) (Figure 1.1). PrEc cells positioned at the future posterior part of the embryo then undergo gastrulation, giving rise to the three embryonic germ layers, i.e. ectoderm, mesoderm and endoderm.

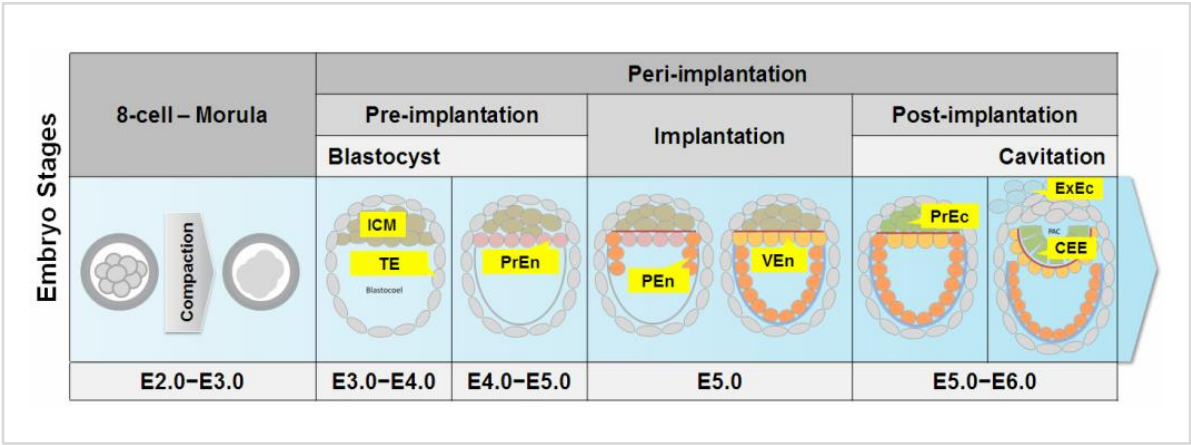

Figure 1.1 Schematic diagram of mouse embryo development from the blastocyst to gastrulation stages. ICM, inner cell mass; TE, trophectoderm; PrEn, primitive endoderm; PEn, parietal endoderm; VEn, visceral endoderm; PrEc, primitive ectoderm; ExEc, extraembryonic ectoderm; CEE, columnar ectodermal epithelium.

1.1.2 Gastrulation and germ layer differentiation

The formation of the primitive streak (PS) marks the onset of antero-posterior axis determination in the developing mouse embryo (Rodriguez *et al*., 2005; Stern, 2004). The epiblast cells egress through the PS to generate the nascent mesoderm in-between the epiblast and the overlying VEn. Within the following 12 h, the PS elongates anteriorly to the distal region of the egg cylinder, where the node forms (Arnold and Robertson, 2009). This process establishes a dorso-ventral axis orthogonal to the antero-posterior axis of the embryo. As the PS expands, the posterior PS contributes mainly to the extraembryonic mesoderm. The anterior PS gives rise to the axial mesoderm, paraxial mesoderm, and the outer layer of definitive endoderm that displaces the remaining VEn. This is followed by generation of the intermediate and lateral plate mesoderm from the middle PS (Nagy *et al*., 2003; Tam *et al*., 1987) (Figure 1.2). Detail of the germ layer contribution is shown in Figure 1.3 and Table 1.1.

The PS comprises an early PS stage at around E6.5 and a late PS stage at E7.5 (Tam and Behringer, 1997). It has been shown that b*rachyury* (*Bra*, also known as *T*) is the key marker of the entire PS and is a pan mesodermal marker that is expressed until the stage of tail bud formation. *Bra* is one of the crucial members of the T-box transcription factor family (Bollag *et al*., 1994; Herrmann *et al*., 1990) initially identified due it its role in the mouse short-tail mutation (Herrmann and Kispert, 1994).

Table 1.1 Germ layer and lineage formation during gastrulation of the mouse embryo*

Regions	Germ Layers	Dominant Lineage Constitution
Anterior Primitive Streak	Axial Mesoderm	Notochord
	Paraxial Mesoderm	Head tissues, vertebral column, bone, cartilage, tendon and ligament, skeletal muscle, dermis of dorsal skin
	Definitive Endoderm	Digestive tract, respiratory tract (lung), liver, pancreas, prostate, thymus, thyroid
Middle Primitive Streak	Intermediate mesoderm	Kidney, lower urinary tract, reproductive system
	Lateral Plate Mesoderm	Limb, heart, spleen, adipose, endothelium, smooth muscle, circulatory system
Posterior Primitive Streak	Extraembryonic Mesoderm	Yolk sac, amnion, allantois
Ectoderm	Definitive Ectoderm	Outer layer of hair, skin, lining of nose and mouth, brain and nervous system

*Gilbert, 2013 & Wolpert *et al*., 2015.

In the mouse embryo, the onset of *Bra* expression is observed at E5.5 in a ring of distal extraembryonic ectoderm. At approximately E6.5, the expression was restricted to the posterior PrEc domain where PS initiates (Rivera-Pérez and Magnuson, 2005). *Bra* was subsequently found to play an important role in mesoderm development (Herrmann and Kispert, 1994; Takada *et al*., 1994). During mesoderm formation, *Bra* expression is found in the posterior epiblast/PS, node/notochord, allantois and tail bud (Kispert and Herrmann, 1994; Kispert *et al*., 1995; Papaioannou, 2014; Concepcion and Papaioannou, 2014; Wilkinson *et al*., 1990; Showell *et al*., 2004; King *et al*., 1998; Conlon *et al*., 1995). *Bra* deficiency

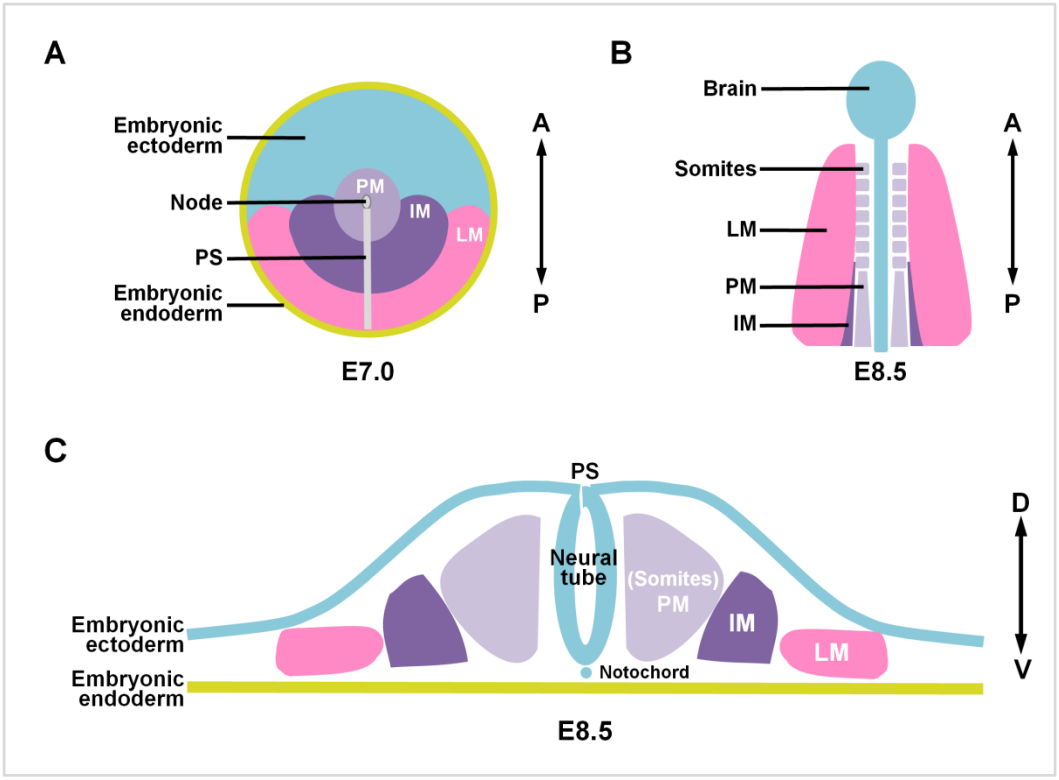

Figure 1.2 Schematic demonstration of mesoderm patterning during the mouse embryo development. A, dorsal view of the gastrulated embryo at E7.0, showing specification of ectoderm and endoderm and formation of the primitive streak (PS) and the derived paraxial, lateral plate and intermediate mesoderm (PM, LPM, IM) along the anterior-posterior axis (A-P); B, dorsal view of the E8.5 embryo, showing patterning of PM, LPM, IM along the anterior-posterior axis; C, cross section of E8.5 embryo at the posterior region, showing the specification of PM, LPM, IM along the dorsal-ventral (D-V) axis.

results in a lack of migrating mesodermal cells and a failure of PS, notochord and tail bud formation (Herrmann and Kispert, 1994). Moreover, notochord elongation and tail bud differentiation is dependent upon sufficient levels of *Bra* along the rostro-caudal axis (Kispert and Herrmann, 1994). Genetic and functional studies have revealed that Bra functions endogenously as a transcription activator for specific mesoderm genes by binding to a palindromic target sequence through a conserved region of T-domain. Bra downstream targets such as *eFGF* (embryonic fibroblast growth factor), *Bix1/4* and *XWnt1* have been isolated in *Xenopus*

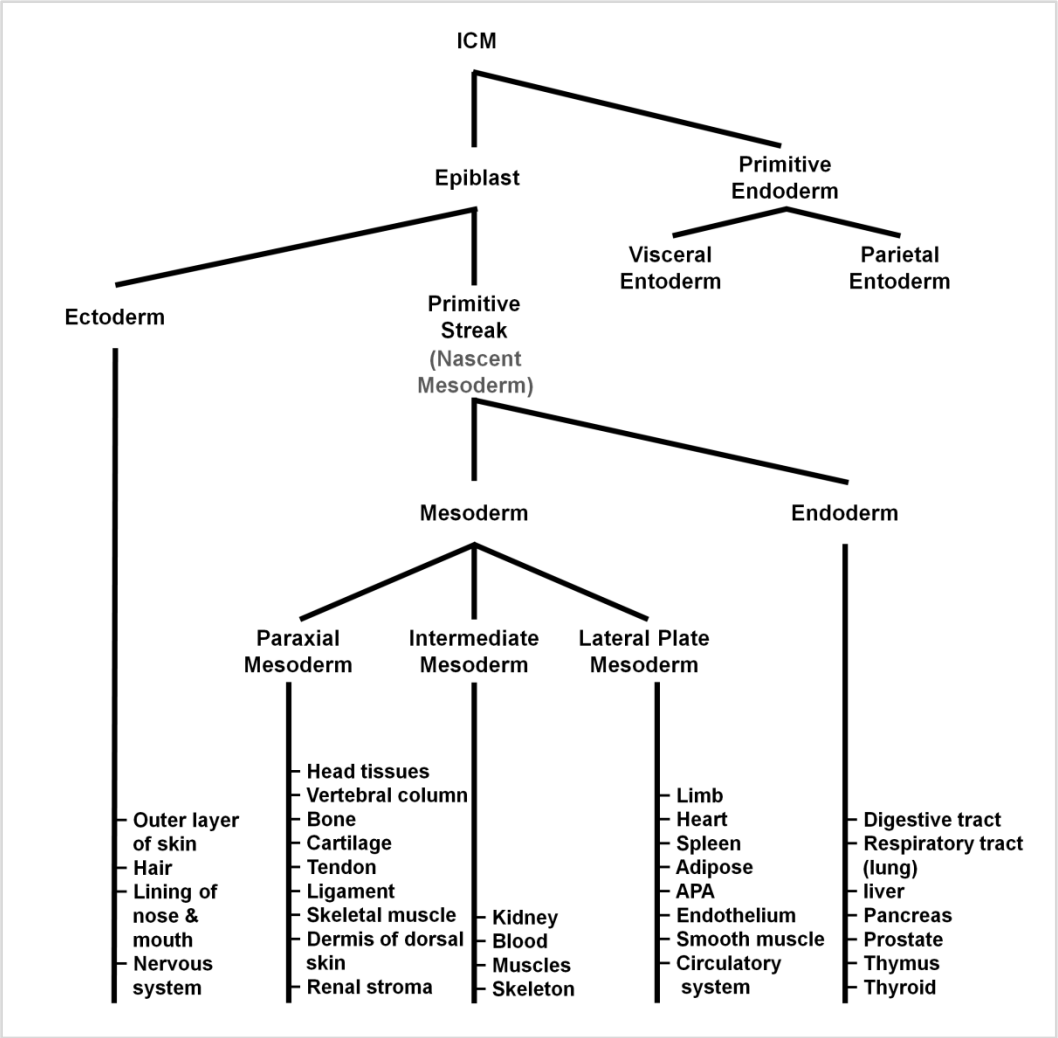

Figure 1.3 Schematic fate map of germ layer and lineage relationship of mouse embryo development. ICM, inner cell mass.

experiments (Kispert and Herrmann, 1993; Kispert *et al*., 1995; Casey *et al*., 1998; Kusch, 2002; Showell *et al*., 2004).

Promoter analysis has shown that *Bra* is a target of the Wnt/β-catenin signalling pathway that requires Wnt3 and Wnt3a (Arnold *et al*., 2000; Liu *et al*., 1999; Yamaguchi *et al*., 1999). At the egg cylinder stage, *Wnt3* expression is detected at E5.5 in a small region of posterior VEn overlying the epiblast at the

epiblast/extraembryonic ectoderm boundary and is evident in both VEn and posterior epiblast by E6.0, preceding the onset of *Bra* expression (Rivera-Pérez and Magnuson, 2005). It has been suggested that Wnt3 promotes localised generation of activated β-catenin in the cells fated to give rise to mesoderm (Takada *et al*., 1994; Rivera-Pérez and Magnuson, 2005; Liu *et al*., 1999). Wnt3a also plays an essential role in PS mesoderm formation and movement. Loss of Wnt3a activity results in abnormal PS and a deficiency of trunk paraxial mesoderm (Takada *et al*., 1994; Yoshikawa *et al*., 1997).

The bone morphogenetic protein (BMP) and FGF signalling pathways carry additional functions during PS mesoderm formation and migration. Mutation of *Bmp4* leads to a deficiency in ventral mesoderm differentiation (Winnier *et al*., 1995). It is proposed that BMP signalling induces the mesoderm to pattern along the dorsal-ventral axis in a dose-dependent manner, in which high levels stimulate lateral plate mesoderm fate while low levels promote intermediate mesoderm fate. Paraxial mesoderm fate is, however, repressed in the presence of BMP signals (James and Schultheiss, 2005). Moreover, the BMP signalling is regulated by its antagonists such as Chordin and Noggin (Canalis *et al*., 2003). Inhibition of BMP4 promotes neural differentiation in mESC cultures (Gratsch and O'Shea, 2002). In mouse fibroblast growth factor receptor 1(FGFR1) mutants, abnormal accumulation of ingressed mesodermal cells has been observed in the PS where *Bra* expression is attenuated but E-cadherin expression is up-regulated. It is

evident that perturbing E-cadherin expression de-represses *Wnt3a* expression and rescues *Bra* expression, indicating a molecular link between FGF and Wnt signalling (Yamaguchi *et al*., 1994; Ciruna and Rossant, 2001).

Apart from their functions in the PS development, Bra and Wnt proteins orchestrate as an autologous regulatory loop to create and maintain a posterior mesoderm progenitor niche during somitogenesis (Martin and Kimelman, 2010). Retinoic acid (RA) signalling has been shown to repress the expression of Zebrafish *Bra* ortholog *ntl* via the RA receptor (RAR) in the somite progenitors, leading to a disruption of posterior mesoderm specification. Conversely, Ntl prevents the effects of RA by directly activating expression of the RA-degrading enzyme gene, *cyp26a1* (Martin and Kimelman, 2010).

1.2 *In vitro* models of mouse development

The small size and inaccessibility of the peri-implantation mouse embryo makes it difficult to study. However, shortly following the isolation of embryonic stem cells (ESCs) from mouse blastocysts in the 1980s (Evans & Kaufman, 1981; Martin, 1981) it was found that by culturing ESCs in suspension, aggregates are formed that could recapitulate some of the key events of peri-implantation mouse development. For this reason, these aggregates were termed ‘embryoid bodies’ and provide an excellent model system for studying the early events of mouse development (Robertson, 1987).

1.2.1 Mouse embryonic stem cells (mESCs)

mESCs were first successfully derived from the ICM of either diapause blastocysts of mouse strain 129/SvE (Evans and Kaufman, 1981) or early blastocysts of mouse (ICR×SWR/J) embryos (Martin, 1981; Martin and Evans, 1981; Nichols and Smith, 2012; Hogan *et al*., 1994; Kawase *et al*., 1994; Suzuki *et al*., 1999). When maintained *in vitro* on a layer of fibroblast feeder cells in the presence of foetal bovine serum, mESCs can be maintained in a self-renewing and pluripotent state, thus resembling the cells within the ICM of the mouse blastocyst (Evans and Kaufman, 1981; Martin, 1981). More recently, more defined conditions for propagating mESCs have been developed that typically comprise feeder-free and serum-free culture in the presence of leukaemia inhibitory factor (LIF) and inhibitors of specific signalling pathways (e.g., the mitogen-activated protein kinase (MEK) inhibitor, PD032590, and the glycogen synthase kinase 3 (GSK-3) inhibitor, CH99021 (Wray *et al*., 2010; Dunn *et al*., 2014). It is known that LIF activates the signal transducer and activator of transcription 3 (Stat3), which promotes self-renewal by inducing expression of Klf4 (Nichols and Smith, 2012). However, LIF can also activate MAPK/Erk (mitogen-activated protein kinase/extracellular signal-regulated kinase) pathways that can drive mESC differentiation. This is the reason why the inclusion of a MEK inhibitor can promote mESC self-renewal (Niwa *et al*., 1998; Matsuda *et al*., 1999; Guo *et al*., 2009; Burdon *et al*., Batlle-Morera *et al*., 2008).

Several master regulatory transcription factors expressed in the ICM of the blastocyst are essential for maintaining mESC self-renewal and pluripotency, of which octamer-binding transcription factor 4 (Oct4, also known as POU5F1) and homeoprotein Nanog are essential for maintaining stemness. A key role of Oct4 in the ICM is to supresses caudal type homeobox 2 (Cdx2), thus ensuring that the expression of this transcription factors is restricted to the TE (Arnold and Robertson, 2009). *Nanog* is initially expressed at a low level in some of the morula cells but reaches a higher expression level in the blastocyst and is essential for maintaining the cells in an undifferentiated state. Together with another epiblast transcriptional factor Sry-like high-mobility group box 2 (Sox2), Oct4 induces the expression of Nanog to regulate mESC pluripotency (Basilico *et al*., 1997; Mitsui *et al*., 2003). Other transcription factors, including Kruppel-like factor (Klf) 4 (Li *et al*., 2005; Hall *et al*., 2009) and Klf5 (Ema *et al*., 2008) interact with the core regulatory network, and their role in maintaining stemness is indispensable (Luo *et al*., 1997; Davenport *et al*., 2003; Narducci *et al*., 2002; Jiang *et al*., 2008).

Under proper culture conditions and without stemness promoting factors, the mESCs undergo spontaneous differentiation and give rise to the derivatives of all three germ layers, i.e. ectoderm, mesoderm and endoderm (Keller, 2005; Smith, 2001). The *in vitro* differentiation of mESCs offers approaches to understand cell fate decision and could also have uses in regenerative medicine by generating

important cell types that could be used to treat degenerative diseases. General protocols to promote *in vitro* mESC differentiation include: i) suspension culture to promote embryoid body (EB) formation, ii) use of defined supplements such as extra-cellular matrix (ECM), growth factors and signalling molecules within two-dimensional (2-D) or three-dimensional (3-D) culture, iii) enhancement of specific gene expression by genetic manipulation of mESCs and iv) use of supportive stromal cells in co-culture conditions (Kurosawa, 2007). Among such, the use of the EB system is particularly advantageous because of the similarities between the development of EBs and the peri-implantation mouse embryo (Robertson, 1987).

1.2.2 EB model system

When cultured in suspension *in vitro* in the absence of feeder cells and LIF, mESCs spontaneously form spheroid multicellular aggregates called embryoid bodies (EBs) (Wobus *et al*., 1984; Doetschman *et al*., 1985). According to their development stages, EBs are categorised as simple (2–4 days post plating), cavitating (4–5 days post plating), and larger cavitated (over 8 days post plating) EBs (Kurosawa, 2007; Abe *et al*., 1996). The development of EBs mimics peri-implantation mouse embryo development (Wobus *et al*., 1984; Doetschman *et al*., 1985). A typical EB has an outer layer of PrE, an inner layer of PrEc, a basement membrane separating them, as well as a central cavity that resembles the proamniotic cavity (Figure 1.4) (Shen and Leder, 1992). The PrEc

differentiates to generate derivatives of definitive ectoderm, endoderm and mesoderm (Wobus *et al*., 1984; Doetschman *et al*., 1985; Keller *et al*., 1993). Specification of mesoderm was observed in EBs generated from R1 mESCs, and also identified by the expression of *Bra* in EBs formed by D3 and E14 mESC lines (Park *et al*., 2004; Doetschman *et al*., 1985; Fehling *et al*., 2003). Similar to the effect *in vivo*, BMP4 was found to promote mesodermal formation in the EBs (Park *et al*., 2004). However, once the EBs have differentiated towards mesoderm, the presence of high concentrations of BMPs could suppress the nascent mesoderm from giving rise to renal lineages in EBs (Bruce *et al*., 2007).

Several approaches have been developed to generate EBs within the laboratory (Figure 1.5). Mouse EBs cultivated in suspension using bacterial-grade petri dishes have been successfully induced towards neurogenesis (Plachta *et al*., 2004), cardiogenesis (Klug *et al*., 1996), vasculogenesis (Risau *et al*., 1988; Feraudet *et al*., 2001) and chondrogenesis (Hwang *et al*., 2006). Because individually distributed mESCs encounter each other in a spontaneous and random manner, the resulting EBs are heterogeneous in morphology, hence forming an irreproducible mixture of derivative populations (Wartenberg *et al*., 1998). As a modification, methylcellulose culture introduces semi-solid methylcellulose media into the bacterial-grade petri dish culture and thus provides good reproducibility, resulting in a population of EBs that is more homogeneous. Hanging drop culture is another frequently-used method to produce EBs. By plating a small volume of cell

suspension onto the lid of petri dishes, it is possible to achieve good control of EB size and number so that they are homogeneous and reproducible. The drawbacks

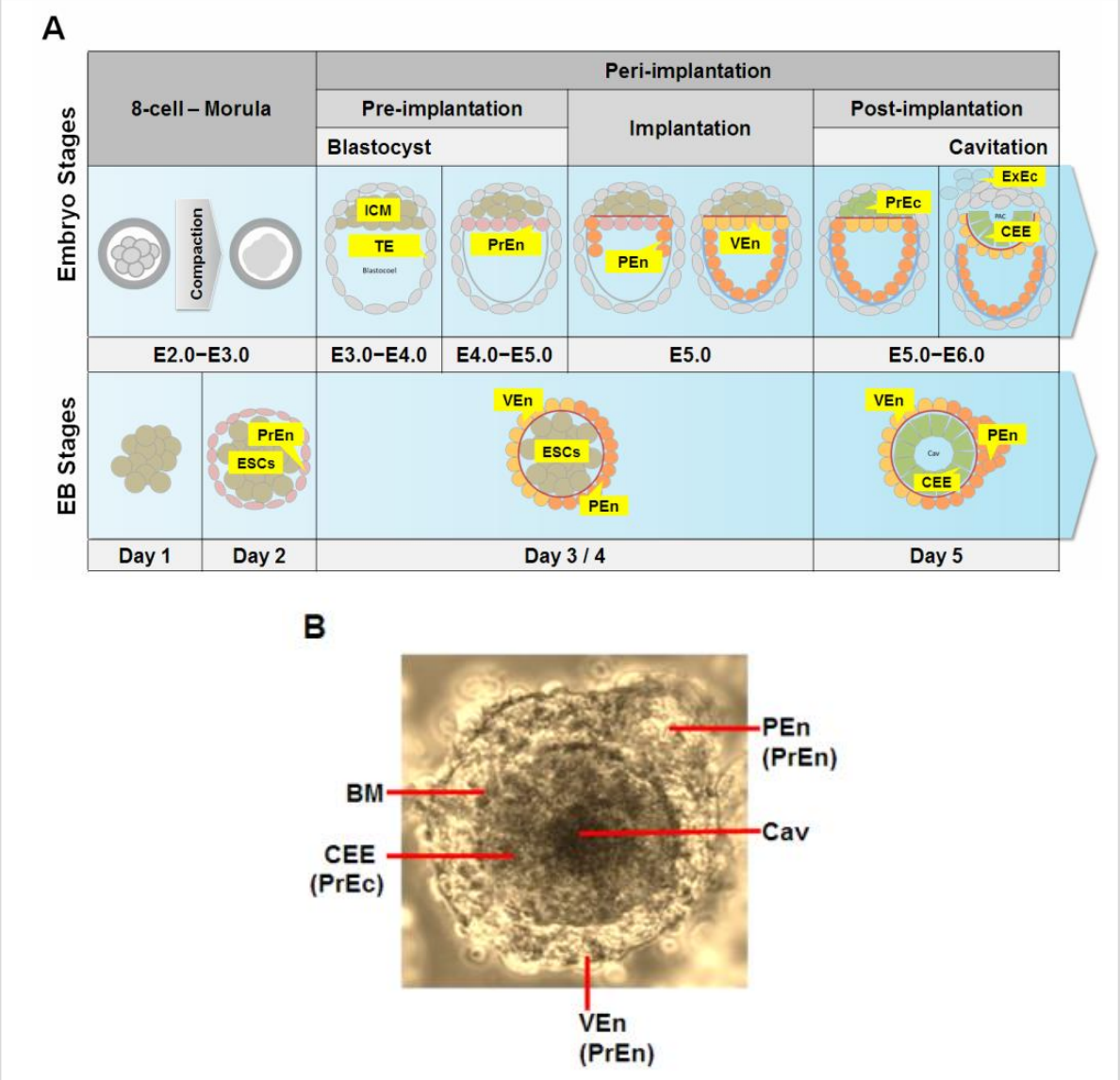

Figure 1.4 Schematic Illustration comparing the development between the early mouse embryo (A, top panel) and EBs (A, bottom panel, and B). Day 5 mESC-derived EBs comprise of an outer layer of primitive endoderm (PrEn) and an inner layer of columnar primitive ectoderm (PrEc) surrounding a proamniotic-like cavity, Cav) separated from each other by a basement membrane (BM). The PrEc can give rise to the definitive ectoderm, endoderm and mesoderm, mimicking early mouse embryo development. ICM, inner cell mass; TE, trophectoderm; PEn, parietal endoderm; VEn, visceral endoderm; ExEc, extraembryonic ectoderm; CEE, columnar ectodermal epithelium.

of the hanging drop method are the limited number of EBs that can be generated, as well as the time-consuming preparation process, which increases the possibility of introducing microbial contamination (Höpfl *et al*., 2004). To address this, low-adherence culture dishes have been designed. Suspension culture using round-bottom 96-well plates that are treated with specific cell adhesion repellents show efficient formation of uniform EBs with homogeneous size and shape (Konno *et al*., 2005; Shinji *et al*., 1988; Suslov *et al*., 2002; Koike *et al*., 2005). This method facilitates monitoring of the differentiation of EBs with defined seeding densities (Kurosawa, 2007).

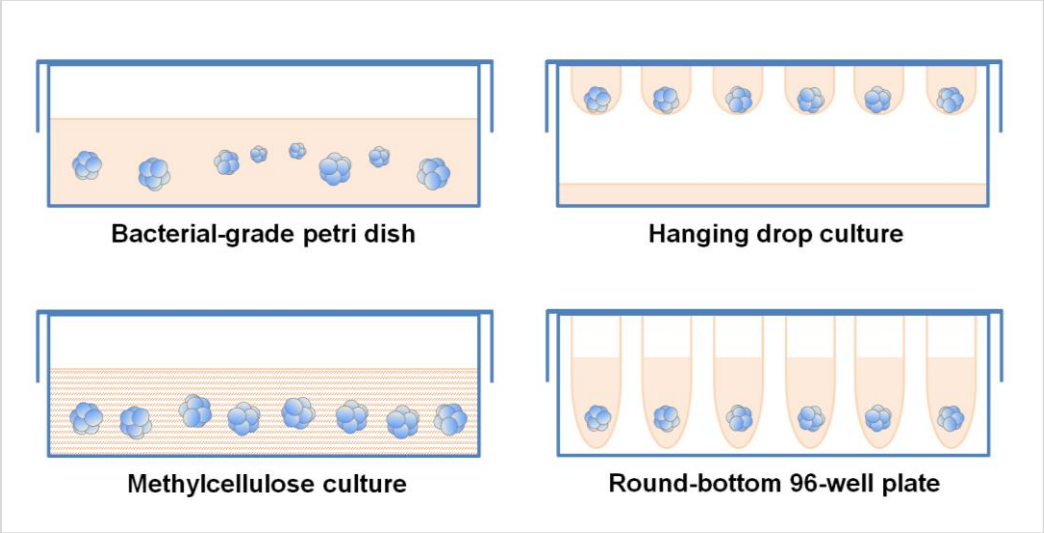

Figure 1.5 Schematics of four types of laboratory approaches to produce EBs from mESCs. Under standard culture conditions and without stemness promoting factors, the mESCs spontaneously differentiate into the germ layer derivatives of ectoderm, mesoderm and endoderm.

1.2.3 2-D induction system

EBs are a very good *in vitro* differentiation model of early embryo development.

However, as a source of specific types of differentiated cells, such as mesoderm, EBs can be problematic. This is because the heterogeneous nature of the EBs means that the extent of differentiation towards any specific cell type can vary considerably between EBs. The complex 3-D structure also hinders the visualisation of the differentiation process at an individual cell level. For this reason, various 2D differentiation protocols have been developed to direct differentiation to specific cell-types more efficiently. Typically, 2D culture systems include defined, serum-free growth media. This is because serum contains unknown factors that may cause variations in cell differentiation, and also makes it difficult to investigate the role of specific growth factors in driving differentiation (Turksen, 2002). In addition, feeder cells are usually eliminated as they may influence the outcome of differentiation (Pollard and Walker, 1997). In addition to culture media, extra cellular matrix (ECM) molecules that comprise the ESC culture substrate also regulate self-renewal and differentiation. Coating tissue culture plates with substrates including gelatin, laminin, fibronectin, or collagen type-IV may improve mESC adherence and survival, and in such ways, several studies have demonstrated *in vitro* derivation of mono-layer mESCs into lineages of neural progenitors, endothelial cells, paraxial mesoderm, intermediate mesoderm and renal precursors using chemically defined media (Ying and Smith, 2003; Blancas *et al*., 2013; Blancas *et al*., 2011; Sakurai *et al*., 2009; Oeda *et al*., 2013; Furue *et al*., 2005; Bruce *et al*., 2007).

Recently, Tuner *et al* showed that *Activin/Nodal* and *Wnt* signalling pathways promote mesoderm formation in monolayer mESC culture, and the mesodermal cells differentiated from mESCs displayed *Bra* expression, similarly to the nascent mesoderm that develops in the primitive streak of developing mouse embryos and of 'gastrulating' EBs. By using a combination of Activin A (activates the *Activin/Nodal* pathway) and Chiron (activates the *Wnt3a* pathway), this group developed a highly efficient strategy for inducing E14 mESCs to differentiate into nascent mesoderm. After 2-day culture in neural differentiation medium and a further 2-day culture in medium supplemented with Activin A and Chiron, robust *Bra* expression was observed in over 90% in the population (personal communication) (Turner *et al*., 2014a and 2014b).

However, although mesoderm differentiation occurred within both the 3-D and 2-D mESC culture systems, it is not clear whether the differentiated cells (e.g. mesodermal cells) that are generated by the 2-D protocols are equivalent to those that form in the EBs and this still needs to be elucidated.

1.3 *In vitro* and *in vivo* fluorescence-based cell tracking technology

During the past two decades, considerable advances have been made in the field of fluorescent probe-based imaging technology, especially in terms of the range of specific fluorescent probes and commercial instrumentation.

1.3.1 Non-genetic cell labelling

A variety of different non-endogenously-expressed fluorescent probes have been produced for cell labelling. According to the cell compartment that is labelled, they are classified as membrane, cytoplasmic, endocytic or nuclear labels. The membrane labels include a range of lipophilic, carbocyanine fluorescent chemicals, which bind to the lipid bilayer of cell membranes with their aliphatic fraction. Commonly used examples of lipophilic membrane labels include PKH and DiI (Lo Celso *et al*., 2008; Horan and Slezak, 1989; Parish, 1999; Hendrikx *et al*., 1996; Ashley *et al*., 1993; Haldi *et al*., 2006; Yusuf *et al*., 2009; Sipkins *et al*., 2005; Lane *et al*., 2011; Sanchez-Aguilera *et al*., 2011; Wagner *et al*., 2010; He *et al*., 2012). The cytoplasmic, endocytic and nuclear labelling probes include amine-reactive probes (e.g. Carboxyfluorescein succinimidyl ester, CFSE, and carboxyfluorescein diacetate succinimidyl ester, CFDA-SE) (Lyons and Parish, 1994), nanocrystals (e.g. quantum dots, QDs), and bisbenzimides (e.g. Hoechst 33342), respectively. Because of the ability to bind to cytosolic components or DNA and thus to provide uniform staining, they have been applied to study mammalian cells (Parish, 1999; Lyons and Parish, 1994; Kohler *et al*., 2009; Lewandowski *et al*., 2010; Lin *et al*., 2007; Muller-Borer *et al*., 2007; Rosen *et al*., 2007; Link and El-Sayed, 2000; Mohamed *et al*., 2000; Mempel *et al*., 2006). These non-genetic probes are available in multiple colours and have the advantage of being able to label cells rapidly and efficiently. However, membrane binding dyes were found to readily transfer to host cells, thus giving false-positive staining

(Li *et al*., 2013; Serbedzija *et al*., 1989). Moreover, the rapid dilution of the fluorescent signal upon cell division has limited their application, particularly in longer-term cell tracking (Lyons and Parish, 1994; Parish, 1999; Muller-Borer *et al*., 2007; Zhu *et al*., 2014).

1.3.2 Genetic cell labelling

Fluorescent reporter genes provide stable expression of the fluorescent signal in the cells in which they are expressed, hence being ideal for long-term cell tracking. This can be obtained through genomic manipulation by using viral transduction or plasmid transfection to establish labelled transgenic cell lines.

1.3.2.1 Virus-mediated transgenesis

Viral transduction has been created as a molecular protocol by which cloned genetic materials can be transferred and inserted into cells of interest by using viruses or viral vectors as tools (Hamer and Leder, 1979). Three main types of viral vector have been designed: adenoviral or adeno-associated viral vectors (AVs or AAVs), retroviral vectors (RVs), and lentiviral vectors (LVs) (Kay *et al*., 2001). AVs or AAVs are episomal DNA-based vectors that can infect both dividing and non-dividing cells; however, they do not replicate nor integrate into the recipient genome (Trono, 2000; Adamson *et al*., 2011; Hansen1 *et al*., 2000; Wickham *et al*., 1993). RVs are RNA-based vectors which replicate by reverse transcriptase. They are the first type of viral vector used to establish transgenic

mESC lines (Robertson *et al*., 1986). A disadvantage, however, is that they can only be used to transduce proliferating cells (Yamagata *et al*., 2012). LVs are a sub-class of RVs that are able to infect both dividing and non-dividing cells (Naldini *et al*., 1996; Roe *et al*., 1993). The transduction efficiency of these vectors is dependent on the species and cell-type (Smith-Arica *et al*., 2003; Asano *et al*., 2002; Lois *et al*., 2002; Pfeifer *et al*., 2002; Cheery *et al*., 2000). The site and copy number of the viral-based integration is unpredictable. Of note, there is a high prevalence of transcriptional silencing of the transgene *in vitro* and *in vivo* which may be due to DNA methylation (Jaenisch *et al*., 1985; Laker *et al*., 1998; Yoder *et al*., 1997; Jähner and Jaenisch, 1985).

1.3.2.2 Gene targeting and knock-in of fluorescent reporters

Gene targeting is achieved by homologous recombination (HR), which occurs between two co-introduced DNA molecules upon the exchange of their genetic sequences (Folger *et al*., 1982). Gene targeting refers to the homologous recombination between the endogenous chromosome and exogenous DNA sequences (Capecchi, 1989a). Following on from the discovery that mESCs could be introduced into blastocysts to generate chimeras, and the development of transgenic mESC lines, the first genetically manipulated mouse was soon generated (Bradley *et al*., 1984; Thomas and Capecchi, 1987, 1990; McMahon and Bradley, 1990). This breakthrough paved the way for the widespread generation of genetically modified mouse strains using mESCs. To achieve this,

targeting vectors are constructed. Four main types of vectors, replacement, knock-in, conditional and insertion, are designed to suit specific approaches. Amongst them, the knock-in vectors serve as exogenous gene carriers to incorporate the reporter genes into the chromosomal locus of interest, subsequently leading to the disruption of the targeted locus with expression of the transgene (Adams and van der Weyden, 2008).

For transgenic cell lineages and mouse lines, fluorescent reporter genes are commonly used. The wild-type GFP is a protein of 238 amino acids derived from the jellyfish *Aequorea victoria* that has limited toxicity when expressed in cells (Johnson *et al*., 1962; Shimomura *et al*., 1962). However, native GFP has some drawbacks, including a tendency of the protein to undergo dimerisation, dual excitation maxima (i.e., excited by both blue and ultraviolet light), poor photostability and poor folding at 37 ℃. To overcome these, a wide variety of GFP variants with enhanced properties have been designed for use. Engineered GFP mutants, such as enhanced GFP (eGFP) (Yang *et al*., 1996; Cormack *et al*., 1996), AcGFP1 (Chen *et al*., 2002; Gurskaya *et al*., 2003), and ZsGreen1 (Matz *et al*., 1999; Haas *et al*., 1996), provide brighter emission of green fluorescence that is detectable by common filters with single excitation maxima and a reduced frequency of oligomerisation. Other novel GFP derivatives, for instance, blue, cyan, yellow and orange fluorescent proteins have now been developed, covering the entire visible spectrum (Alford *et al*., 2013).

Red fluorescent proteins (RFPs) have emission maxima that span from the yellow-orange (575 nm–610 nm wavelength) to far-red (710 nm–850 nm wavelength) regions of the spectrum, thereby advancing the fluorescence protein spectral range to include longer wavelengths (Alford *et al*., 2013). Lukyanov and colleagues identified naturally-occurring reef coral RFPs, including amFP486 (Matz *et al*., 1999), eqFP578 (Merzlyak *et al*., 2007), and DsRed (or drFP583) (Matz *et al*., 1999).

In order to deliver the transgenes, vectors are usually linearised and electroporated into the recipient cells, which involves physical transfer in an electric field that may cause cell damage (Neumann *et al*., 1982). This accounts for the relatively low efficiency of homologous recombination gene targeting. Another reason is the limited capacity of the cell enzymatic machinery that leads to low frequency of homologous recombination but high frequency of random recombination (Mansour *et al*., 1988; Capecchi, 1989b; Vasquez *et al*., 2001). Increasing the length of homologous arms enhances the frequency of homologous recombination (Thomas and Capecchi, 1987; Deng and Capecchi, 1992). To efficiently select the correctly integrated recombinants, the selection markers are crucial. A neomycin (*neo*) cassette is the most commonly used. An additional negative selection gene, such as the diphtheria toxin A-fragment (DT-A) gene, can significantly increase the yield of correct targets (Yagi *et al*., 1993; Yagi *et al*., 1990). The resultant recombinants bare genetically-expressed fluorescent proteins that produce

constant fluorescent signals and they are thus suitable for long-term cell tracking studies.

Recently, Fehling *et al* generated an *E14-Bra-GFP* mESC line to investigate mesodermal differentiation *in vitro*. In this line, an eGFP mini gene cassette was targeted into the *Bra* locus, replacing approximately two-thirds of exon 1 of *Bra*. GFP expression was under the control of the *Bra* promoter, which means that cells that undergo mesoderm differentiation are marked by GFP fluorescence (Fehling *et al*., 2003). Using this cell line, Fehling *et al* developed an EB culture protocol that yielded a high proportion of GFP^+ cells. The GFP^+ cells isolated *in vitro* have shown the ability to generate mesodermal derivatives including the haematopoietic and cardiac lineages, as well as neuromesodermal progenitors (Fehling *et al*., 2003; Zhang *et al*., 2014; Org *et al*., 2015; Tsakiridis and Wilson, 2015), although there is a lack of evidence that the expression pattern of GFP can accurately recapitulate that of endogenous *Bra* expression in the mouse embryo.

The latest breakthrough of generating transgenic lines is achieved by the clustered regularly interspaced short palindromic repeats (CRISPR)-based technologies. CRISPRs were first identified in *Escherichia coli* (Ishino *et al*., 1987). CRISPR loci and the co-localised endonuclease CRISPR-associated proteins (Cas) have been widely described as essential components of the adaptive immune system in bacteria and archaea (Doudna and Charpentier, 2014). In this system, CRISPR

RNAs (crRNAs) direct Cas to bind the target sequence (called spacer) of the invading DNA via complementary base pairing and cleave the DNA, generating double strand breaks (Wiedenheft *et al*., 2009). The most common approach uses CRISPR-Cas9 protein and single guide RNA (sgRNA) or duplex of crRNA:trans-activating crRNA (tracrRNA) to direct DNA cleavage. A protospacer adjacent motif (PAM) at the 3' end of the spacer is also required to ensure the cleavage specificity (Doudna and Charpentier, 2014). DNA breaks can be repaired by non-homologous end joining, which leads to stochastic insertions and/or deletions at the target site, or homology-directed recombination, which results in introduction of desired sequence in the presence of donor DNA templates (Komor *et al*., 2017). This has made it possible to apply CRISPR-Cas9 technology to target genome modification in human and mouse cells (Cong *et al*., 2013; Jinek *et al*., 2013; Mali *et al*., 2013). Moreover, recent studies have reported the generation of gene-targeted mouse models via CRISPR-Cas9 injection into the zygote, indicating a convenient and time-saving approach without the need for genetically modifying mESCs (Yang *et al*., 2014; Wang *et al*., 2013). Of note, in this way, the efficiencies distinctly varied, with only 10–20% efficiency regarding the large fragment insertion (e.g. gene reporter). This, together with other limitations including high off-target mutation rate in human cells, suggests future efforts should focus on enhancing the outcomes of homology-directed repair (Ran *et al*., 2015; Kuscu *et al*., 2014; Fu *et al*., 2013; Hsu *et al*, 2013).

1.3.3 *In vitro* and *in vivo* optical imaging technology

1.3.3.1 *In vitro* optical imaging

Since the invention of the first fluorescence microscope, there has been continuous development in the field of optical imaging (Rusk, 2009). With advances in a broad spectrum of fluorescent probes and computer technology, highly specialised microscopes have made *in vitro* imaging an invaluable experimental methodology. For instance, the Cell-IQ® system (Chip-Man Technologies, Finland) provides an integrated instrument combining an inverted phase-contrast/fluorescent microscope and a simplified tissue culture incubator, thus enabling automated real-time monitoring of proliferation, migration, morphology and fluorescence in living cells. Studies have been performed to monitor the behaviour of human mesenchymal stems and human embryonic stem cell differentiation under adapted *in vitro* conditions (Walter *et al*., 2010; Hicks *et al*., 2009; Nat *et al*., 2007; Narkilahti *et al*., 2007).

1.3.3.2 *In vivo* optical imaging

In vivo optical imaging enables the study of living organisms by monitoring and characterising physical and biological processes within specific cells or tissues of interest. Fluorescence-based labelling serves as an ideal tool for *in vivo* imaging in animals. However, due to the photon absorption by tissue haemoglobin (<650 nm wavelength region) and water (>900 nm wavelength region), the majority of the visible fluorescence (e.g. GFP green emitted light) is absorbed within 500 μm of

the surface tissue of the recipient animal. To circumvent this, an optical window of approximately 650 nm–900 nm of the near infra-red wavelength region of the spectrum is favourable, which allows maximum depth of fluorescence penetration (Weissleder, 2001). In addition, cell nuclei and mitochondria cause light scattering within the optical window (Wang and Wu, 2007), whereas the intensity can be reduced by using longer wavelengths (Shcherbo *et al*., 2007). This requires fluorescent probes which have the emission spectra within the far-red (FR) region (710 nm–850 nm wavelength, which is part of the near-infrared spectrum). From this perspective, a series of DsRed- or eqFP578-derived FR fluorescent proteins (FPs) have been developed, comprising i) monomers mPlum (Wang *et al*., 2004), mRasperry (Wang *et al*., 2004), mKate (Shcherbo *et al*., 2007), mKate2 (Shcherbo *et al*., 2009), mRFP (Campell *et al*., 2002), and pseudomonomer tdKatushka (Shcherbo *et al*., 2009), and ii) oligomers DsRed (Matz *et al*., 1999), Katushka (Shcherbo *et al*., 2007), RFP637 (Kredel *et al*., 2008), RFP639 (Kredel *et al*., 2008), and E2-Crimson (Strack *et al*., 2009).

Wild-type DsRed is a 28-kDa natural fluorescent tetramer isolated from *Discosoma sp.* (Campell *et al*., 2002). It has excitation and emission peaks at approximately 560 nm and 585 nm, respectively (Strack *et al*., 2009). In comparison to most GFP derivatives, it is insensitive to pH and resistant to photobleaching but is prone to form precipitated aggregates that are cytotoxic (Baird *et al*., 2000). A series of modified DsRed variants are commercially

available with higher solubility, including monomeric mutants such as DsRed-monomer (Campell *et al*., 2002), mCherry, mStrawberry (Campell *et al*., 2002; Shaner *et al*., 2004; Wang *et al*., 2004), mPlum and mRaspberry (Shaner *et al*., 2004; Wang *et al*., 2004), dimeric mutants such as tdTomato (Campell *et al*., 2002; Shaner *et al*., 2004; Wang *et al*., 2004), as well as tetrameric mutants such as DsRed-Express (Bevis and Glick, 2002), DsRed-Express2 (Strack *et al*., 2008), DsRed2 (Bell *et al*., 2007; Yanushevich *et al*., 2002; Matz *et al*., 1999) and E2-Crimson (Strack *et al*., 2009) (Table 1.2).

E2-Crimson is a novel tetramer derived from DsRed-Express2 and retains DsRed-Express2's advantages including fast maturation, high solubility, high photostability and low cytotoxicity. Furthermore, it has the excitation and emission maxima of 611 nm and 646 nm, respectively. This means that it can be excited efficiently by standard far-red lasers of routinely-used optical instrumentation. Hence, it is suitable for multi-colour *in vivo* imaging for cell tracking (Strack *et al*., 2009)

To visualise the fluorescent signal, instruments such as the In Vivo Imaging System® (IVIS, PerkinElmer, UK) have been employed, which possess detectors for a wide optical spectrum between the blue and near infrared that facilitate intravital monitoring of cells expressing fluorescent reporters in small living animals (Chu *et al*., 2014).

Table 1.2 Properties of commercially available DsRed-derived red and far-red fluorescent proteins

Fluorescent Proteins	Quaternary Structure	Excitation/ Emission Maxima (nm)	Brightness Relative to eGFP (%)†	Maturation Half-time at 37°C (min)	References
DsRed-Express	Tetramer	554/586	92	36	a, b
DsRed-Express2	Tetramer	554/591	93	42	b
tdTomato	Dimer	554/581	591	60	c
DsRed-Monomer	Monomer	557/592	24	<60	d
DsRed2	Tetramer	563/582	150	390	a, e-g
mCherry	Monomer	587/610	98	15	c-d
mStrawberry	Monomer	574/596	162	55	c-d
mPlum	Monomer	590/649	25	100	c,h
mRaspberry	Monomer	598/625	80	55	c,h
E2-Crimson	Tetramer	611/646	180	26	i

† http://www.clontech.com
a Bevis and Glick, 2002
b Strack *et al*., 2008
c Shaner *et al*., 2004
d Campbell *et al*., 2002
e Bell *et al*., 2007
f Yanushevich *et al*., 2002
g Matz *et al*., 1999
h Wang, 2004
i Strack *et al*., 2009

1.4 Aims

The differentiation of *Bra*$^{+}$ mesoderm occurs spontaneously in developing EBs, and this process appears to mimic the differentiation of nascent mesoderm in the gastrulating mouse embryo. For instance, in both the embryo and in mESC-derived EBs, the nascent mesoderm appears to arise from a primitive ectodermal epithelium. In contrast, when mESCs are directed to differentiate to *Bra*$^{+}$ mesoderm under 2-D culture conditions, the mesodermal cells are not derived from primitive ectodermal epithelial cells, and instead, appear to

differentiate directly from undifferentiated mESCs. This raises the question of whether the mesoderm arising in the EBs is equivalent to the mesoderm that is generated in 2-D culture systems.

The main focus of this work was to compare the two mesoderm populations derived from the 3-D (i.e., EBs) and 2-D mESC culture systems and examine whether they are equivalent to each other. This was achieved by comparing their gene expression profile using quantitative RT-PCR and investigating their differentiation potential by incorporating the mesodermal cells into developing mouse kidney rudiments (the kidneys being derived from the mesodermal lineage). The specific objectives were as follows:

1. To generate a novel E2-Crimson (E2C)-expressing mESC reporter line by knocking the E2C gene into the *Rosa26* locus of the *E14-Bra-GFP* mESC line. This new line would allow the fate of the GFP^+ mesodermal cells to be followed in the developing kidneys due to the fact that they would constitutively express E2C;
2. To evaluate the effectiveness of the E2C fluorescence reporter for tracking the newly-generated *Bra-GFP/Rosa26-E2C* mESCs in living mice;
3. To characterise the mesoderm derived from the *Bra-GFP/Rosa26-E2C* reporter mESCs cultured under the 3-D and 2-D conditions by determining the expression levels of key genes using quantitative RT-PCR;
4. To evaluate the nephrogenic potential of the mesoderm derived from the

Bra-GFP/Rosa26-E2C reporter mESCs cultured under the 3-D and 2-D conditions. This was achieved by assessing the differentiation potential of the $E2C^{+}$ mesodermal cells following their incorporation into developing mouse kidney rudiments *ex vivo*.

Chapter 2

Materials and Methods

2.1 Cell lines and media

The cell lines used in this project are shown in Table 2.1. Details of media are listed in Table 2.6.

Table 2.1 List of cell lines

Cell Lines	Sources
SNL76/7 (STO)	ATCC, SCRC-1049
E14TG2a (mESC)	ATCC, CRL-1821
E14-Bra-GFP (mESC)	G. Lacaud, Manchester
GFP-KSCs (mouse neonatal kidney-derived stem cells)	In-house
tdTomato-transduced *E14-Bra-GFP* mESCs	

2.2 Thawing and freezing cells

For thawing cells, cryovials were removed from liquid nitrogen and placed in 37^{o}C water bath. Once defrosted, cell suspension was transferred to 15 mL conical tubes containing 10 mL medium and centrifuged at 200×g for 2 min. Supernatants were aspirated and cell pellets resuspended in fresh medium and transferred to tissue culture plates that had been pre-coated with gelatin (1g/L gelatin, Sigma,

G1890).

For freezing cells, medium was aspirated and cells were washed with 1× phosphate-buffered saline (PBS) (without Ca^{2+} and Mg^{2+}) (Sigma, D8537), trypsinised using 1×trypsin/EDTA (Sigma, T4174). The trypsin was neutralized using complete medium. Cell pellets were collected by centrifugation at 200×g for 2 min and resuspended in Recovery™ Cell Culture Freezing Medium (Thermo Fisher Scientific, 12648). Cells were counted and 1 mL of cell suspension containing approximately 10^6 cells was transferred into each cryovial. The cryovials were stored in freezing containers filled with 2-propanol at -80°C overnight, and then transferred to liquid nitrogen.

2.3 Preparation of mitomycin-C-inactivated STO feeder cells

24 h prior to the inactivation, the STO culture medium was replaced with 10 mL fresh medium. For the inactivation, half of the medium was removed and 5 mL medium was retained. Mitomycin-C (Sigma, M4287) was added to give a final concentration of 20 μg/mL. The dishes were incubated at 37°C in a humidified incubator with 5% CO_2 for 2 h. Cells were washed three times with 1×PBS (without Ca^{2+} and Mg^{2+}) and trypsinised with 1×trypsin/EDTA followed by neutralization with complete medium. Cell pellets were collected by centrifugation at 200×g for 2 min and resuspended in STO medium. Cells were counted and plated into gelatin-coated tissue culture dishes at a density of 5×10^4

cells/cm^2. Prior to plating the mESCs, feeder cells were washed once with 1×PBS (without Ca^{2+} and Mg^{2+}).

2.4 Sub-culture of STO and mESCs

STO cells were maintained in 10 cm tissue culture dishes at 37^{o}C in a humidified incubator with 5% CO_2. Cells were passaged twice per week at a split ratio of 1:4−1:6 until reaching passage 15.

mESCs were maintained in the 6-well feeder plates at 37^{o}C in a humidified incubator with 5% CO_2. Cells were passaged every other day at a split ratio of 1:6−1:10 until reaching passage 40.

For sub-culturing, cells were washed once with 1×PBS (without Ca^{2+} and Mg^{2+}) and trypsinised with 1×trypsin/EDTA followed by neutralization with complete medium. Following the centrifugation at 200×g for 2 min, supernatants were discarded and cell pellets were resuspended in specific culture medium. For STO cells, the cell suspension was transferred into 10 cm tissue culture dishes; for mESCs, cell suspension was transferred into the previously prepared STO feeder plates.

2.5 3-D EB system

To make EBs, early passages of mESCs maintained on STO feeder plates were

sub-cultured in feeder-free gelatinised 6-well tissue culture plates for 48 h. Cells were trypsinised, pelleted and resuspended in mouse EB medium. The cell suspension was then plated in 90 mm bacterial petri dishes (Sterilin, 101VR20) at a specific seeding density. The EBs were maintained for up to 9 days. Medium was changed every other day (5 mL/dish). Each EB dish was split 1:2 split on day 3 post plating. EB morphology and Bra-GFP expression was examined at specific time points (usually day 4 and 7). Experiments were performed in 3 independent biological replicates.

2.6 2-D system

Early passage *Bra-GFP/Rosa26-E2C* mESCs were harvested from feeder plates and sub-cultured in gelatinised 6-well tissue culture plates at a density of 5×10^4 cells/cm^2. Cells were incubated for 48 h followed by trypsinisation and re-plating into gelatinised 6-well plates at 1×10^5 cells/cm^2 for 24 h. Cells were then harvested and re-plated into 60 mm tissue culture dishes at a density of 4.7×10^3 cells/cm^2 with overnight incubation in mESC medium. The following morning, medium was changed to NDiff® 227 (Clontech, Y40002) for 48 h and then NDiff® 227 supplemented with Activin-A (R&d Systems, 338-AC) to a final concentration of 100 ng/L) and CHIR 99021 (Tocris, 4423) to a final concentration of 3 µM for a further 48 h incubation. Medium was changed on a daily basis.

2.7 Flow cytometry analysis

Single cell suspension in 1×PBS (1×10^6 cells/mL) was acquired by dissociating monolayer cell culture or aggregated EBs with 1×trypsin/EDTA similar to routine sub-culture protocols. Prior to the analysis, the suspension was filtered using a 40 µm strainer (BD Falcon, 352340)

To analyse the GFP^+ cells within the *Bra-GFP/Rosa26-E2C* mESCs -derived EBs or 2-D differentiated monolayer cultures, cells were examined using a BD FACScalibur (BD Biosciences) flow cytometer according to manufacturer's instructions, using a 488 nm laser to detect the GFP signal. For analysis of the GFP expression window in the EBs, wild-type E14TG2a-derived EBs were used as a negative control. For analysis of GFP expression in the 2-D system, undifferentiated *Bra-GFP/Rosa26-E2C* mESCs sub-cultured in gelatinised dishes in mESC medium for 24 h prior to induction were used as a negative control. Data were acquired by the BD CellQuest (BD Biosciences) software based on 10^4 events and analysed using the Cyflogic (CyFlo Ltd) software.

To determine the percentage of $E2C^+$ cells in the routinely-cultured *Bra-GFP/Rosa26-E2C* mESCs, cells were analysed using a BD FACSCanto (BD Biosciences) flow cytometer. Untransfected *E14-Bra-GFP* mESCs were used as a negative control. Data output was performed using BD FACSDiva (version 6.1.3) software.

2.8 Fluorescence-activated cell sorting (FACS)

FACS was used to isolate GFP^+ mesodermal cells derived from *Bra-GFP/Rosa26-E2C* mESCs cultured in 3-D and 2-D systems. Single cell suspensions in 1×PBS (containing 100 mL/L Sigma fetal bovine serum, FBS) at a density of 1×10^7 cells/mL were obtained by dissociation with 1× trypsin/EDTA of day-6 EBs or day-4 2-D monolayer cultures. Sorting was performed using the BD FACSAria (BD Biosciences) flow sorter. Day-6 EBs derived from wild-type E14TG2a mESCs and undifferentiated *Bra-GFP/Rosa26-E2C* mESCs sub-cultured in gelatinised dishes in mESC medium for 24 h prior to induction were used as negative controls for 3-D and 2-D systems, respectively. Data output was performed using BD FACSDiva (version 6.1.3) software.

2.9 Cell-IQ real-time imaging

EBs were formed from the *Bra-GFP/Rosa26-E2C* mESCs at a seeding density of 1.25×10^5 cells/mL and maintained in culture for up to day 9. On day 3 post plating, EBs were collected and plated onto solidified 2% agarose gel (20 g/L in 1×PBS) (Sigma, A9045) in glass bottom 6-well plates (MatTek, P06G-0-20-F). They were then embedded in a thin overlay of 1% agarose (10 g/L in EB medium). Each well was filled with 3 mL EB medium once the overlaid gels were set. Plates were sealed and maintained in Cell-IQ (Chip-Man Technologies Ltd) imaging facility. EBs were imaged by the Cell-IQ Imagen (Chip-Man Technologies Ltd) software on days 3 to 9 post plating on an hourly basis. Imaging data from both bright field

and 488 nm laser for the GFP fluorescence signal were documented. Raw data were analysed by the Cell-IQ Analyser (Chip-Man Technologies Ltd) and ImageJ (NIH) softwares.

2.10 Mouse embryonic kidney rudiment *ex vivo* culture

Kidneys were dissected from CD1 E13.5 mouse embryos and collected in a 1.5 mL microfuge tube in ice cold rudiment dissection medium. Following media aspiration, kidneys were washed once with and re-suspended in 1×PBS, and transferred to a 15 mL conical tube. Once settled (by gravity), they were trypsinised at 37^{o}C for a maximum of 15 min, with intermittent gentle tapping to disaggregate cells. Rudiment medium was added and the tube was incubated at 37^{o}C for 5 min to neutralise the trypsin. The tube was centrifuged at 1,800 ×g for 2 min. Cell pellets were re-suspended in 1 mL kidney rudiment medium for cell counting. In the meantime, FACS-sorted Bra-GFP^{+} cells derived from mESC 2-D or 3-D culture systems were centrifuged and resuspended in rudiment medium and counted.

A total of 2×10^{5} cells were used in each rudiment, wherein kidney rudiment cells and Bra-GFP^{+} cells were mixed at a ratio of 1:9 in 0.5 mL microfuge tubes followed by centrifugation at 1,800 ×g for 2 min. Cell pellets were gently removed from the tube wall and transferred onto the pre-cut Isopore Membrane Filter (Merck Millipore, RTTP02500) on metal grids in the 6-well plates.

Rudiments were cultured in rudiment culture medium with Rho-associated, coiled-coil containing protein kinase inhibitor (ROCKi, Y-27632, Merck Millipore, 688001) for 24 h followed by a further 4-day in the absence of ROCK inhibitor. Controls were also set up, including kidney rudiments comprising GFP^+ mouse neonatal kidney-derived stem cells (GFP-KSCs) (1:9 ratio of KSC: kidney rudiment cells), reaggregated kidney rudiments (formed by kidney rudiment cells only), and intact kidney rudiments. Experiments were performed in 3 independent biological replicates.

2.11 Administration and imaging of *Bra-GFP*/*Rosa26-E2C*

Bra-GFP/Rosa26-E2C and untransfected *E14-Bra-GFP* mESCs were harvested from the feeder plates and expanded in 10 cm gelatinised tissue culture dishes and cultured for 48 h to reach the required density. Cells were then trypsinised and pelleted following the routine tissue culture protocols.

Following a quick rinse with 1×PBS, cells were re-suspended in 1×PBS and counted. In a separate pilot experiment prior to the *in vivo* administration, E2C reporter pellets of 2 and 8×10^6 cells, respectively, were analysed using the IVIS® Spectrum Imaging System (PerkinElmer) to determine the level of E2C fluorescence. Cells were injected in 100 µL of PBS. The cell resuspensions were stored on ice immediately prior to *in vivo* administration.

Three female CB17 severe combined immunodeficient (SCID) mice (Charles River) were housed in accordance with the guidelines. Experiments were performed following the approved guidelines under a UK Home Office licence (Licence Number: 70/8741) under the Animals (Scientific Procedures) Act 1986 and approved by the University of Liverpool Animal Ethics Committee. At the age of 8−10 weeks old, mice were used for mESCs injection. Animals were anaesthetised with isoflurane and shaved to remove back fur. mESCs in 100 µL of 1×PBS were administered to the dorsal flank of individual mouse via subcutaneous injection at four different positions (top left, top right, bottom left and bottom right).

The following doses of 10, 7.5 and 5×10^6/100 µL *Bra-GFP/Rosa26-E2C* mESCs were injected in to three of the positions in a random manner. 10×10^6/100 µL untransfected *E14-Bra-GFP* mESCs were individually injected alongside the *Bra-GFP/Rosa26-E2C* engrafts in the same mouse as negative controls. Experiments were performed in three independent biological replicates. Data of the signal intensity in terms of the values measured at the regions of interest (ROI) were acquired on day 0, 1, 4, 7 and 9 post injection using the IVIS® Spectrum *In Vivo* Imaging System (PerkinElmer) and analysed with its Living Image® software.

2.12 Tumour volume measurement

Following the injection, the tumour size was measured using a digital caliper on day 4, 7 and 9 in terms of the length, width and height of the tumours. The length was measured in the direction of the dorsal longitude; the width was measured along the dorsal latitude; and the height was measured perpendicularly in-between the surface of the back and the upper surface of the tumours.

2.13 Fixation

For routinely-cultured cells

Medium was aspirated. Cells were washed once with 1×PBS followed by fixation with 4% paraformaldehyde (PFA) (Sigma-Aldrich, P6148) at room temperature for 5- min. Samples were washed three times with 1×PBS and stored for up to 1 week in 1×PBS at 4°C for immunofluorescence.

For EBs

EBs were collected into conical tubes and allowed to settle under gravity. Medium was discarded followed by fixation with 4% PFA at room temperature for 20 (day 4−7) or 30 (day 8−9) min. EBs were then washed three times with 1×PBS.

For mouse embryonic kidney rudiments

Day 0 and 5 rudiments together with the membrane were transferred to the 24-well plates and fixed with 4% PFA at room temperature for 15 min. Samples were gently washed once with 1×PBS and stored in 1×PBS at 4°C for

immunofluorescence.

For dissected tumours

Mice were sacrificed on day 9 when the tumours reached the size limit according to the Home Office guidelines. Tumours were harvested immediately afterwards and fixed with about 10-time volume of 4% PFA at 4°C overnight. If necessary, larger tumours were vertically cut into small pieces prior to fixation.

2.14 Sectioning

For EB frozen sections and tumours

Fixed EBs/tumours were soaked in 15% sucrose at 4°C overnight followed by embedding in the 7.5% molten gelatin. Samples were mounted onto cork disks with Shandon™ Cryomatrix™ embedding resin (Thermo Fisher Scientific, 6769006). They were then covered with embedding resin and cut with a cryostat at10–20 µm. Section and blocks were stored at at -80°C.

For tumour frozen sections

Fixed tumours were rinsed with 1×PBS followed by a concession immersing process of 15% and 30% sucrose at 4°C overnight, respectively. Tumours were then embedded with embedding resin and frozen in cryostat section machine. 10 µm sections were prepared onto the slides and stored at -80°C.

For tumour paraffin sections

Fixed tumours were rinsed with 1×PBS and transferred to 70% ethanol followed by a general paraffin embedding process (Hewitson and Darby, 2010). 5 µm sections slides were prepared.

2.15 Tumour histopathological analysis

Tumour paraffin sections were stained with haematoxylin and eosin (H&E) followed by histopathological examination.

2.16 Immunofluorescence staining

For routinely-cultured cells

Bra-GFP/Rosa26-E2C and untransfected *E14-Bra-GFP* mESC lines were sub-cultured from STO feeder layers to gelatinised dishes for 48 h. They were then plated into 8-chamber slides/35 mm gelatinised dishes. When reaching the required density, they were fixed and then immunostained for stemness markers such as Oct4 and Nanog. Samples were blocked in 10% serum solution containing 0.1% Triton-X 100 at room temperature for 1 h, and then incubated with the primary antibodies at specified concentrations at 4°C overnight. They were washed three times with PBS and incubated with secondary antibody solution in the dark at room temperature for 2 h. Detailed information of antibodies is listed in Table 2.2. All samples were then counter-stained with 4',6-diamidino-2-phenylindole (DAPI) (Thermo Fisher Scientific, D1306, 1:100,000) at room

temperature for 15 min. Slides were mounted with DAKO fluorescent mounting medium (Agilent Technologies, S3023) and sealed by nail polish. Controls were also included to check for non-specific binding of secondary antibodies, and these comprised samples where primary antibodies were omitted. Data were acquired using a Leica DM2500 (Leica) fluorescence microscope and the Leica Application Suite (LAS, Leica) integrated software.

For mouse embryonic kidney rudiments

Fixed rudiments on the membranes were blocked with 10% serum solution containing 0.1% Triton-X 100 at room temperature for 1 h, followed by incubation with primary antibodies for megalin, synaptopodin, Wt1, and E2-Crimson where necessary, at 4^{o}C overnight. They were then incubated with secondary antibodies at 4^{o}C overnight in the dark followed by counter-staining with 10 μg/μL rhodamine-labeled peanut agglutinin (PNA) (Vector, RL-1072) at room temperature for 1 h in the dark. Controls were also included as above to check for non-specific binding of secondary antibodies. Samples were mounted onto the slides using DAKO fluorescent mounting medium and sealed by nail polish. Data were documented by the Zeiss LSM 510 META (Zeiss) multiphoton confocal laser scanning microscope. Data analysis was performed by the ImageJ (NIH) software.

Table 2.2 List of antibodies used for immunofluorescence

Targets	Blocking Sera	Primary Abs (dilutions)	Catalogue No's (suppliers)	Secondary Abs (dilutions)	Catalogue No's (suppliers)
E2C	Chicken/ Goat	Rabbit IgG (1:1,000)	632496 (Clontech)	Chicken-anti-rabbit IgG 488 or Goat-anti-rabbit 594 (1:1,000)	AF A21441/ A11012 (TFS)‡
Oct4	Goat	Mouse IgG_{2b} (1:500)	sc-5279 (Santa Cruz)	Goat-anti-mouse IgG_{2b} 488 (1:1000)	AF A21141 (TFS)
Nanog	Chicken	Rabbit IgG (1:500)	ab80892 (Abcam)	Chicken-anti-rabbit IgG 488 (1:1000)	AF A21441 (TFS)
Megalin	Goat/ Donkey	Mouse IgG_1 (1:200)	DM3613P (Acris)	Goat-anti-mouse IgG_1 488 or Donkey-anti-mouse IgG (H+L) 647 (1:1,000)	AF A21121/ A31571 (TFS)
PECAM-1	Donkey	Rat IgG_{2a},κ (1:100)	550274 (BD)	Donkey-anti-rat IgG (H+L) 488 (1:1,000)	AF A21208 (TFS)
Synap-topodin	Goat/ Donkey	Mouse IgG_1 (1:2)	65194 (Progen)	Goat-anti-mouse IgG_1 488 or Donkey-anti-mouse IgG (H+L) 647 (1:1,000)	AF A21121/ A31571 (TFS)
Wt1	Goat/ Donkey	Mouse IgG_1 (1:100)	05-753 (Merck Millipore)	Goat-anti-mouse IgG_1 488 or Donkey-anti-mouse IgG (H+L) 647 (1:1,000)	AF A21121/ A31571 (TFS)

‡ AF, Alexa-Fluor; TFS, Thermo Fisher Scientific

For EB and tumour frozen sections

EB or tumour frozen section slides were blocked in 10% serum solution(s) and incubated with primary antibody solutions in a humidified chamber at room

temperature for 1 h, followed by incubation with E2-Crimson and/or PECAM-1 primary antibodies at 4°C overnight. The remaining steps followed the protocols for routinely-cultured cells.

2.17 Linearisation of the gene targeting construct

The targeting construct pDEST-ROSA26-E2C employed in this study was prepared by Dr. Antonius Plagge (University of Liverpool) and generated by using two vectors which were kindly given as gifts by Dr. Shinichi Aizawa's group (RIKEN, Japan) and Dr. Peter Hohenstein (University of Edinburgh), respectively. Based mainly on Hohenstein's vector, an 8.1 kb 5'-HA and a 3.5 kb 3'-HA was cloned from Aizawa's construct to replace the original 1 kb 5'-HA and 5 kb 3'-HA, respectively.

50 µg pDEST-ROSA26-E2C plasmid DNA was digested by *Pvu*I FastDigest® restriction enzyme (Thermo Fisher Scientific, FD0624) in 1×FastDigest® Green buffer (Thermo Fisher Scientific, B72). The reaction mixtures were incubated at 37°C for 2 h and further at -20°C overnight. The product was examined by 8 cm-length 0.8% agarose gel electrophoresis at 7 V/cm for 3 h in 1×TAE buffer, with the λ DNA/Hind III ladder (Thermo Fisher Scientific, 15612013) as a sizing marker to check the efficacy of the enzyme digest. Gel slices were collected and linearised DNA fragments were extracted and purified by Wizard® SV Gel and PCR Clean-Up System (Promega, A9282) according to the manufacturer's

protocols. DNA concentrations and purity were determined using a NanoDrop 2000 (Thermo Fisher Scientific, ND-2000). Where necessary, an ethanol precipitation was performed to further concentrate linearised DNA. Purified linearised DNA was dissolved in 1×TE buffer and stored at -20°C.

2.18 Generation of the knock-in mESC reporter line

E14-Bra-GFP mESCs at passage *7* were expanded in 10 cm feeder dishes. When reaching approximately 70% confluence, cells were trypsinised, pelleted and resuspended in 1×PBS (without Ca^{2+} and Mg^{2+}). The cell suspension was mixed with linearised targeting construct (DNA final concentration 1 µg/µL) and was transferred into cuvettes (800 µL each) for electroporation (240 V, 7.6 ms). Following the electroporation, cells were placed on ice and gently pipetted once by adding an extra 1 mL of mESC medium. Cell suspension was transferred to 10 cm feeder dishes and incubated at 37^{o}C in a humidified incubator with 5% CO_2. Two days post electroporation, G418 (Sigma, A1720) was added into the culture medium at a final concentration of 200 µg/mL, initiating the counter-selection process. Medium was changed daily and supplemented with G418 till day 9 of the selection. Viable colonies were picked and transferred to 96-well non-treated round-bottom plates containing 1×trypsin/EDTA (one colony per well). Colonies were dissociated and mESC medium was added to neutralise the trypsinisation. The solution was then transferred to 96-well tissue culture plates prepared with feeder cells and incubated at 37^{o}C in a humidified incubator with 5% CO_2. After

24 h expansion, cells in each well were trypsinised and neutralised with mESC medium to reach a total volume of 200 µL per well, 100 µL of which being transferred to gelatinised 24-well tissue culture plates for screening purpose whilst the remaining being sealed and frozen at -80^{o}C for subsequent expansion.

2.19 Genomic DNA extraction of mESCs

mESC pellets were collected in 1.5 mL microfuge tubes from dishes/plates following routine sub-culture protocols. They were resuspended in lysis buffer containing 100 µg/mL Proteinase K (Sigma, P6556) and incubated at 55^{o}C overnight. One volume of 2-propanol was added followed by centrifugation at 16,000 ×g for 1 min to obtain the genomic DNA (gDNA) as pellets. gDNA were washed twice with 70% ethanol and air dried. They were then re-dissolved in 1×TE buffer at 4^{o}C overnight followed by 65^{o}C for 15 min. DNA concentrations and purity was measured using NanoDrop 2000.

2.20 3'-homologous arm PCR analysis

3'- homologous arm (HA) PCR analyses were performed on the gDNAs of viable colonies expanded in 96-well feeder plates using a GoTaq® Long PCR reaction system (Promega, M4021) according to the manufacturer's manual. Detail of the composition of the PCR reaction system is listed in Table 2.3. gDNA template from untransfected *E14-Bra-GFP* mESCs served as the negative control. A non-template control was also included where template gDNA was substituted by

nuclease-free H_2O. PCP primer sequences were:

5'-GGCTTCTGAGGCGGAAAGA-3' (forward);

5'-CAACAATCAGCCTAAGGTAG-3' (reverse).

Table 2.3 Composition of the GoTaq® Long PCR reaction system

Components	Final Volume/Concentration
GoTaq® Long PCR Master Mix, 2×	1×
Forward/Reverse primers	50 µmol/L
gDNA template*	500 ng
Nuclease-free H_2O adjusted to a final volume of	25 µL

*For non-template control, the template gDNA was substituted by nuclease-free H_2O.

PCR amplification was performed by the G-STORM GS1 Thermal Cycler (G-Storm). The PCR programme was set up as follows:

Hot start at 95°C for 2 min, followed by PCR steps comprising denaturation at 94°C for 30 s, annealing at 65°C for 30 s, elongation at 65°C for 4 min, and final extension at 72°C for 10 min, for 30 cycles. Products were examined using 8 cm-length 0.8% agarose gel electrophoresis at 7 V/cm for 45 min in 1×TAE buffer, with 1 kb DNA ladder (Fisher Scientific, 15615-016) as a sizing marker to verify product molecular sizes.

2.21 Analysis of E2C expression in the PCR screened positive clones with fluorescence microscopy

Screened clones were plated on gelatin for 48 h and re-plated in gelatinised

8-chamber slides for culture. When reaching required colony size, they were fixed with 4% PFA followed by counter staining with DAPI as for immunofluorescence staining. After mounting, slides were examined by the Leica DM2500 (Leica) fluorescence microscope with the 561 nm laser and data were acquired by the Leica Application Suite (LAS, Leica) integrated software. STO feeder cells as well as untransfected and tdTomato-transduced *E14-Bra-GFP* mESCs were included as negative and positive controls, respectively.

2.22 Real-time reverse transcription-PCR of mRNA isolated from Bra-GFP$^+$ and Bra-GFP$^-$ cells derived from 3-D and 2-D culture systems

Quantitative real-time polymerase chain reaction (RT-qPCR) was performed using the Fast SYBR® Green Cells-to-CT™ Kit (Thermo Fisher Scientific, 4405659). Cell lysis, reverse transcription and qPCR amplification was performed according to the manufacturer's protocols. The reaction system was set up as described in Table 2.4.

Table 2.4 Composition of the Fast Real-time PCR reaction system

Components	Final Volume/Concentration
Fast SYBR® Green PCR Master Mix	10 µL
Forward/Reverse primers	312.5 nmol/L
RT Reaction template*	4 µL
Nuclease-free H_2O adjusted to a final volume of	20 µL

*For non-template control, the template cDNA was substituted by nuclease-free H_2O.

Three biological replicates for the Bra-GFP^{+} populations isolated from 3-D and 2-D systems, and two biological replicates for Bra-GFP^{-} populations derived from the 3-D and 2-D systems were assessed. For each RT reaction product analysed, two technical replicates were prepared. RT-qPCR reaction was performed using the BioRad CFX Connect Real-time PCR Detection instrument. The PCR programme was set up as follows:

The amplification steps were DNA polymerase activation at 95°C for 20 s, denaturation at 95°C for 3 s and annealing/extension at 60°C for 30 s. A melting curve was generated at the end of the 40th PCR cycle. The melting curve steps were 95°C denaturation for 10 s, 65°C annealing for cycles of 0.5°C increments every 5 s to detect the product melting temperature starting from 65°C to 95°C. Data were acquired using the incorporated Bio-Rad CFX Manager (version 3.1) software. Changes in the relative gene expression level and statistical analysis were also performed using the software, where $p<0.05$ was considered statistically significant. Primer information is shown in Table 2.5. Amplification annealing temperature (Ta) was 60°C for all primers. PCR reaction products were verified by 0.8% agarose gel electrophoresis at 7 V/cm with 100 bp HyperLadder™ IV (BIO-33029, Bioline) as sizing marker for amplicons molecular size (Appendix Figure 1). Non-template control (NTC) was performed for each analysed gene and the non-reverse transcriptase (NRT) control was also included to verify the elimination of gDNA.

Table 2.5 List of RT-qPCR primers*

Genes	Forward Sequences	Reverse Sequences	Amplicons Size (bp)	References
Bra	CATCGGAACAGC TCTCCAACCTAT	GTGGGCTGGCGT TATGACTCA	136	RTPrimerDB
β-actin	GTACCCAGGCAT TGCTGACA	CTGGAAGGTGGA CAGTGAGG	145	
Gapdh	CATCTTCCAGGA GCGAGACC	GAAGGGGCGGA GATGATGAC	150	
Fgf5	AAGTCAATGGCT CCCACGAA	TCCTCGTATTCCT ACAATCCCCT	88	
Foxd1	CAAGAATCCGCT GGTGAAGCC	ACAGGTTGTGAC GGATGCTG	88	
Foxf1	CCAAAACAGTCA CAACGGGC	TCACACACGGCT TGATGTCT	191	
Gdnf	CGCTGACCAGTG ACTCCAAT	AAACGCACCCCC GATTTTTG	222	In-house
Nanog	AAGCAGAAGATG CGGACTGT	GTGCTGAGCCCT TCTGAATC	232	
Oct4	TGGAGACTTTGC AGCCTGAG	CTTCAGCAGCTT GGCAAACTG	188	
Osr1	GCCCCCAAAAAG GAGAGAGT	AGCCACAGCTCA TCCTTTACC	161	
Pax2	TCCAGGCATCAG AGCACATC	GGCCGATGCAGA TAGACTGG	104	
Wt1	AATGCGCCCTAC CTGCCCA	CCGTCGAAAGTG ACCGTGCTGTAT	116	
Cdx2	QT00116739		114	
Tbx6	QT00098861		80,80,157	
Lhx1	QT01660792		87	
Foxa2	QT00242809		115	
Hoxa10	QT00240212		61	Qiagen
Hoxa11	QT00250404		97	
Hoxb1	QT00493906		128	
Hoxc9	QT00113218		138	
Hoxd11	QT00267337		97	

* Annealing temperature (Ta) was 60°C for all primers.

2.23 Statistical analysis

Data were analysed using Microsoft Excel or GraphPad Prism (version 5.01, GraphPad Software), except for the RT-qPCR data which were analysed by the Bio-Rad CFX Manager software. Processed data were plotted by GraphPad Prism. For the statistical analysis of all the data, the same number/replicates were analysed. Basic functions used were: mean, standard deviation (SD), standard error of the mean (SEM) and Student's *t*-test.

2.24 Composition of tissue culture media

Table 2.6 List of media and composition

Media	Composition
STO culture medium	Dulbecco's Modified Eagle's Medium (DMEM) (Sigma, D6546)
	100 mL/L FBS (Gibco, 10270)
	10 mL/L MEM non-essential amino acid (Sigma, M7145)
	10 mL/L L-glutamine (Sigma, G7513)
mESC culture medium	DMEM (Sigma, D6546)
	150 mL/L FBS, Sigma, F2442)
	10 mL/L MEM non-essential amino acid (Sigma, M7145)
	10 mL/L L-glutamine (Sigma, G7513)
	0.1 mmol/L β-mercaptoethanol (Gibco, 31350)
	1,000 U/mL Mouse LIF (Merck Millipore, ESG1107)
Mouse EB culture medium	DMEM (Sigma, D6546)
	100 mL/L FBS (Sigma, F2442)
	10 mL/L MEM non-essential amino acid (Sigma, M7145)
	10 mL/L L-glutamine (Sigma, G7513)
	0.1 mmol/L β-mercaptoethanol (Gibco, 31350)

(continued on next page)

(continued from previous page)

Table 2.6, continued.

Media	Composition	
mESC freezing medium (2×, for 96-well plates)	400 ml/L	mESC medium
	400 mL/L	FBS (Gibco, 10270)
	200 ml/L	DMSO (Sigma, D2650)
Mouse KSC Culture medium	DMEM (Sigma, D6546)	
	100 mL/L	FBS (Gibco, 10270)
	10 mL/L	MEM non-essential amino acid (Sigma, M7145)
	10 mL/L	L-glutamine (Sigma, G7513)
	0.1 mmol/L	β-mercaptoethanol (Gibco, 31350)
Rudiment dissection medium	MEME (Sigma, M5650)	
	10 mL/L	FBS (Gibco, 10270)
Rudiment culture medium	MEME (Sigma, M5650)	
	100 mL/L	FBS (Gibco, 10270)
	10 mL/L	L-glutamine (Sigma, G7513)
	10 mL/L	Penicillin/Streptomycin (Gibco, 15140122)

2.25 Composition of buffers

Table 2.7 List of buffers and composition

Solutions	Composition	
1× TAE buffer (pH 8.0)	40mmol/L	Tris base
	5mmol/L	Sodium acetate
	1mmol/L	Ethylenediaminetetraacetic acid (EDTA)
1× Cell lysis buffer (pH8.5)	100 mmol/L	Tris base
	5 mmol/L	EDTA
	200 mmol/L	NaCl
	2 g/L	Sodium dodecyl sulphate (SDS)

Chapter 3

Generation of the *Bra-GFP/Rosa26-E2C* mESC reporter line

3.1 Introduction

A key aim of this project was to characterize Bra^+ nascent mesoderm derived from mESCs cultured in 3-D as EBs or in 2-D differentiation culture conditions. An important part of the characterization was to investigate the differentiation potential of the mesodermal cells in (i) mouse kidneys *in vivo*, and (ii) mouse kidney rudiments *ex vivo*, as previously undertaken by our group (Rak-Raszewska *et al*., 2012a). To this end, it was important to be able to specifically select Bra^+ cells from the mESCs cultured under both the 3-D and 2-D conditions, and to track the mesodermal cells *in vivo* and *ex vivo*. In order to select Bra^+ cells, we made use of a Bra-GFP mESC line where GFP is expressed from within the *brachyury* locus, enabling mesodermal cells to be selected using fluorescence activated cell sorting (FACS) (Fehling *et al*., 2003). To enable the GFP^+ mesodermal cells to be tracked both in living mice and in kidney rudiments *ex vivo*, we introduced the far-red fluorescent protein, E2-Crimson (E2C) (Strack *et al*., 2009), into the constitutively active *Rosa26* locus of the Bra-GFP mESCs (Friedrich and Soriano, 1991). E2C has excitation and emission maxima of 611

nm and 646 nm, respectively, making it suitable for imaging in the near-infrared window (Strack *et al*., 2009). It has a number of advantages over other far-red fluorescent proteins, in that it is very bright (extinction coefficient of 126,000 M^{-1}/cm), has good photostability, and in various cell types, has shown limited phototoxicity (Strack *et al*., 2009; Christensen *et al*., 2015). Furthermore, it has been recently demonstrated that breast cancer cells expressing E2C could be imaged within rat lungs *in vivo*, suggesting that E2C is suitable for tracking cells *in vivo* in small rodents (Christensen *et al*., 2015). To introduce the E2C reporter into the *Rosa26* locus of the Bra-GFP mESC line, we used a homologous recombination approach outlined below. After the E2C reporter line had been generated, the mESCs were assessed to ensure that the expression of key mESC markers (i.e., Oct4 and Nanog) was not affected. Furthermore, the E2C reporter cells were checked to ensure they were still able to differentiate by ensuring they were able to form typical EBs.

Using homologous recombination to generate a transgenic mESC reporter line

Rosa26 is located on mouse chromosome 6 and spans approximately 9 kb (Monticelli, 2010). It comprises three exons and generates two non-coding and one highly-conserved anti-sense transcript encoding no protein product (Zambrowicz and Soriano, 1997). The *Rosa26* locus was originally identified by Soriano's group in the promoter-trap screening by integrating the *β-geo* (fused

β-gal and *neo*) cassette into mESCs derived from the 129Sv mouse strain via a retroviral targeting vector named ROSAβ-gal (reverse orientation splice acceptor β-gal). The resulting mutants showed constitutive and ubiquitous expression of a single copy of the transgene in all tissues at all pre- and post-natal developmental stages of the germ-line chimeric mice, albeit at different levels of expression. Moreover, none of the progeny exhibited any obvious phenotype (Friedrich and Soriano, 1991). Taken together, these reports highlight the usefulness of *Rosa26* to construct stable reporter mESC lines for tracking cells following transplantation (Soriano, 1999).

Soriano's strategy has provided a common approach for introducing transgenes into pluripotent mESCs. In brief, the strategy involves constructing a knock-in vector that contains the exogenous reporter gene cDNA sequence preceded by an adenoviral splice acceptor sequence, a positive selection marker (usually a neomycin resistance gene cassette), the *Rosa26* 5'- and 3'-homology arms (HAs) flanking the aforementioned elements, and a negative selection marker (commonly a diphtheria toxin A subunit, DTA). During the recombination between the *Rosa26* homology arms, the transgene integrates into the first intron of *Rosa26* at a unique *Xba*I site and is expressed constitutively under the control of the *Rosa26* promoter. The selection markers are expressed independently by assigned promoters, respectively. Incorrect recombinants have either the inactivation of neo expression or activation of DTA insertion which are lethal to

cells during counter selection. Viable clones that have correct integration of the targeting construct can be screened out following the selection. They can then be analysed by PCR amplification of cDNA sequences of the exogenous reporter gene as well as the genomic DNA sequences of the homologous arms (Abe *et al*., 2011; Hohenstein *et al*., 2008).

E14-Bra-GFP mESC line

The *E14-Bra-GFP* mESC line used in this study was a generous gift from Dr. Georges Lacaud at the Paterson Institute for Cancer Research, Manchester (Fehling *et al*., 2003). This mESC line was generated by knocking an eGFP mini gene into the locus of the pan-mesoderm marker *Bra* of the E14.1 cell line derived from blastocysts of the 129/Ola mouse strain (Hooper *et al*., 1987).

During the knock-in, the targeting vector was linearised and electroporated into the Bra-GFP mESCs followed by counter selection. Viable colonies were picked and expanded. Genomic DNA samples were collected for 3'-HA PCR analysis. Screened clones were thawed and expanded to examine expression of E2C.

The objectives of this chapter were to:

1. Linearise the targeting construct;
2. Undertake knock-in of the E2-Crimson transgene into the *Rosa26* locus;
3. Perform 3'-HA PCR screening for correctly targeted recombinants;

4. Analyse E2C expression in screened positive clones using fluorescence microscopy;
5. Analyse E2C expression using flow cytometry;
6. Assess the stemness and differentiation potential of the *Bra-GFP/Rosa26-E2C* mESC reporter line.

3.2 Results

3.2.1 Linearisation of targeting construct

To improve transfection efficiency, the first step was to linearise the targeting plasmid. *Pvu*I restriction enzyme digestion was therefore performed to linearise the vector and also release the targeting construct from the vector backbone. Following electrophoresis, a clear DNA band of approximately 19 kb showed successful *Pvu*I restriction enzyme digestion of the targeting vector DNA (Figure 3.1). The smaller fragment produced simultaneously by this digestion would not be observed on this fragment range of the gel electrophoresis image. The results demonstrated that the linearised pDEST-ROSA26-E2C plasmid DNA fragment was acquired for knock-in.

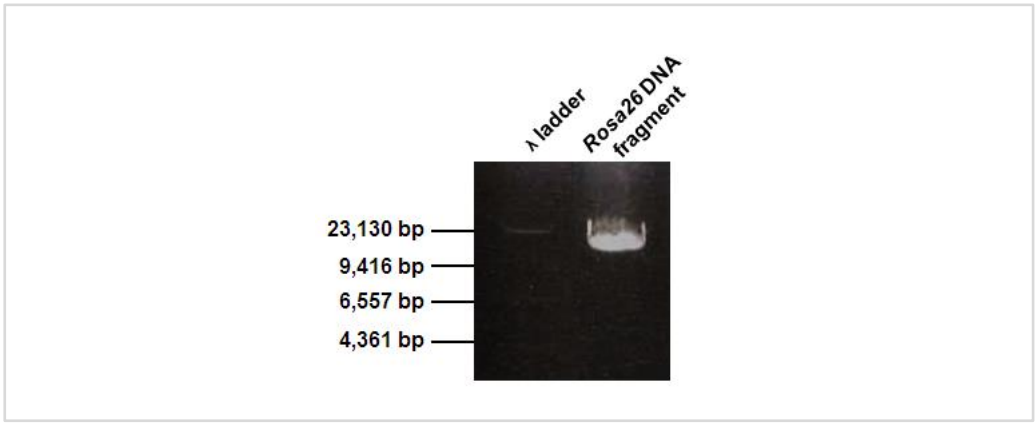

Figure 3.1 0.8% agarose gel electrophoresis of linearised pDEST-ROSA26-E2C plasmid DNA fragment confirmed purity following *Pvu*I restriction enzyme digestion and DNA extraction. Sample was loaded on an 8 cm-length 0.8% agarose gel run at 7 V/cm for 3 h in 1×TAE buffer.

3.2.2 *Rosa26* knock-in of E2-Crimson transgene

The linearised targeting construct was electroporated into *E14-Bra-GFP* mESCs

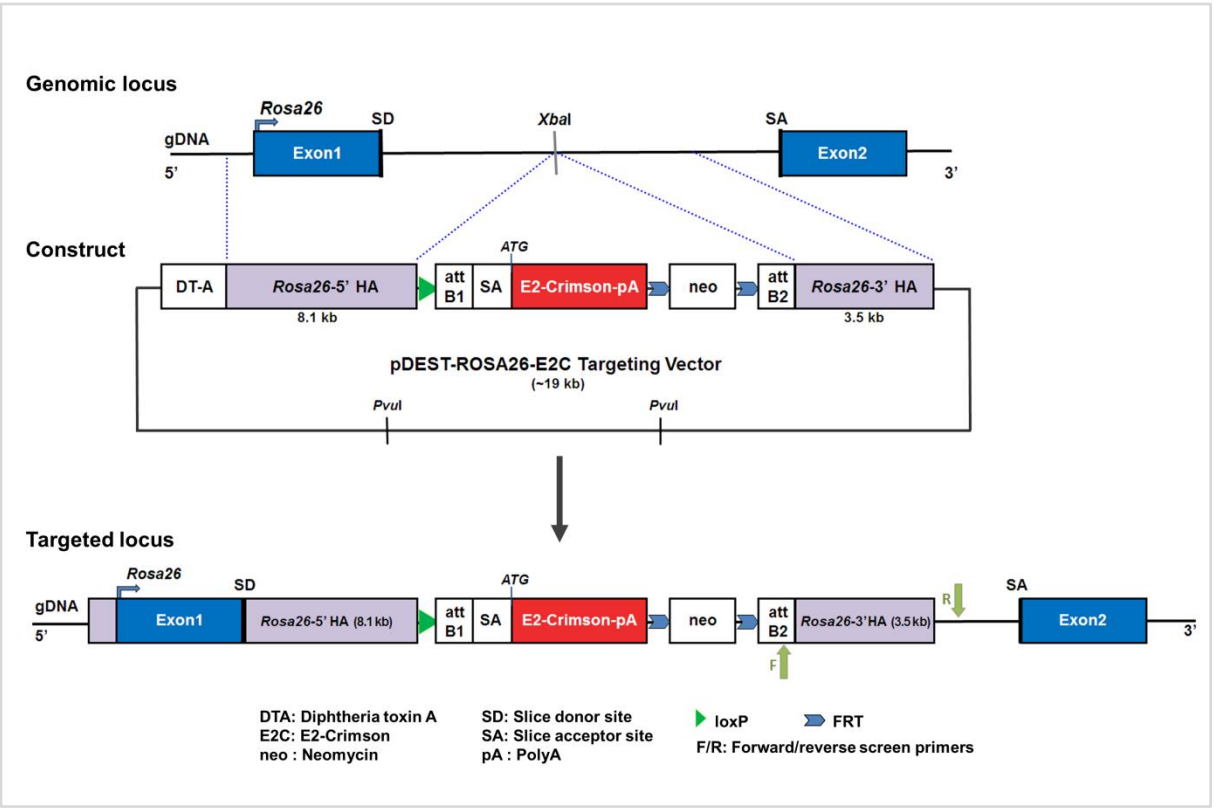

Figure 3.2 Schematic illustration of Schematic illustration of the *Rosa26* knock-in strategy and *E14-Bra-GFP* mESC chromosome with correct targeted insertion of pDest-ROSA26-E2C targeting vector. The vector contains two homology arms (HAs) that flank the E2-Crimson cassette that has a poly A (pA) additional signal, which will stop any further transcription downstream of the targeted insertion, and a downstream positive drug selection marker *neo* (Neomycin resistance). The insertion site in-between the HAs is identified by the *Xba*I restriction enzyme site. A lethal negative selection marker DTA is placed in the 5' upstream region adjacent to the targeting arm. The *Puv*I restriction enzyme sites are located in the vector backbone. When linearised for gene targeting, most of the vector backbone will be removed following *Puv*I restriction digestion. A *loxP* site (indicated with a green triangle) is located next to the 5' HA for future Cre-mediated recombination. FLP recombinase target (FRT) sites (indicated with blue arrow heads) flanking the *neo* cassette are designed for future manipulation with flippase (FLP) recombinase. In the correct recombinants, E2C cDNA is introduced into the *Rosa26* locus and is expressed under the control of the *Rosa26* promoter. The *neo* gene is also introduced into the *Rosa26* locus whereas the DTA cassette is lost. Clones that had an integrated DTA cassette would be killed by the toxin during the selection process. Neomycin expression is under the control of its own promoter within the cassette, which facilitates cell survival during G418 selection. Neo-deficient clones were depleted due to the loss of G418 resistance. Green arrows show the forward and reverse primer-binding sites for the designated 3'-HA screening.

and a 9-day counter selection was undertaken, following which, 244 viable clones were picked individually and were then expanded and cryopreserved in 96-well plates. It was assumed that the correct clones would only contain *E2C* and *neo* cassettes within intron 1 of the *Rosa26* locus (Figure 3.2).

3.2.3 3'-HA PCR screening for correctly targeted recombinants

In order to examine whether the viable clones were integrated correctly as a single copy cassette, we chose 35 expanded clones in a random manner for PCR analysis. 3'-HA PCR screening was applied to the gDNA templates from the 35 clones. Gel electrophoresis results showed significant bright bands in 18 of 35 clones, weaker DNA bands from 2 of 35, and no band with the remaining 15 clones as well as the control templates (Figure 3.3). The 18 clones with bright bands and the 2 with weaker bands showed the correct PCR product size of approximately 3.4 kb and thus were considered as positive recombinants. Positive recombinants comprised just over 50% of the resultant clones.

3.2.4 Analysis of E2C expression in screened positive clones using fluorescence microscopy

Following the 3'-HA PCR screening, the 18 positive and 3 randomly selected negative clones were individually expanded from the 96-well cryopreserved plates. Viable clones were sub-cultured in 8-chamber tissue culture slides and observed under a fluorescence microscope to investigate whether they expressed the *E2C*

transgene. The five positive clones were found to be fluorescent, and their intensity was comparable to that of tdTomato-transduced *E14-Bra-GFP* mESCs (produced in house). No fluorescence signal was detected within the negative clone wells (Figure 3.4).

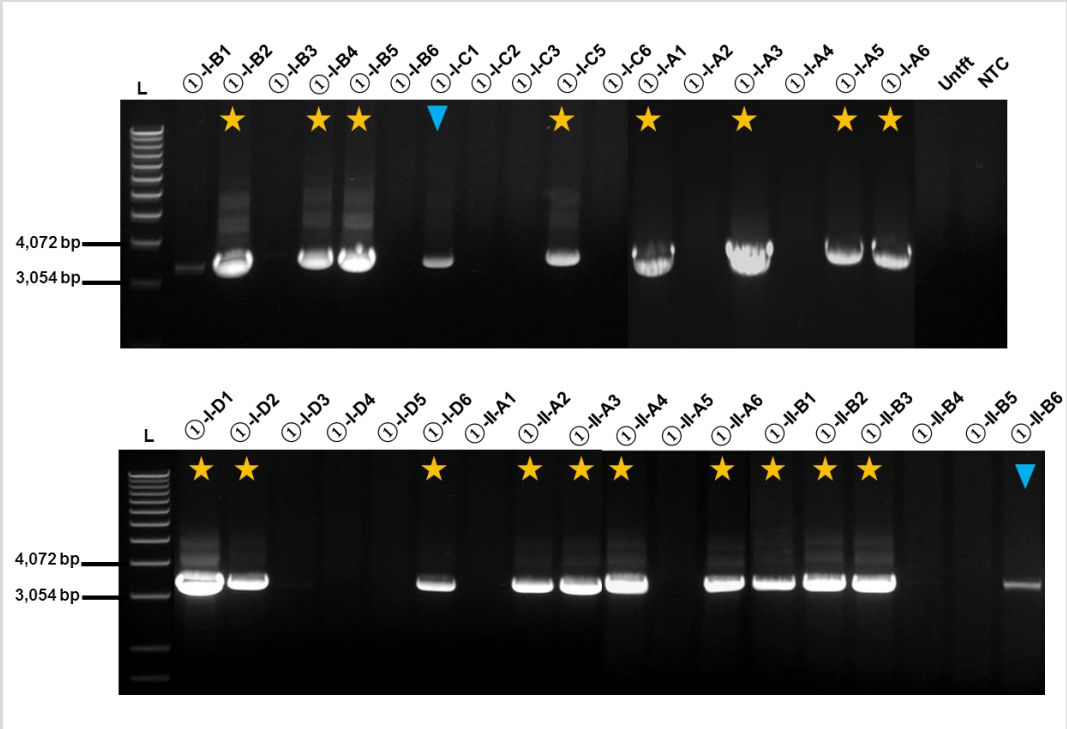

Figure 3.3 0.8% agarose gel electrophoresis of a total of 35 viable clones. PCR was performed with 25 µl GoTaq® Long PCR Master Mix system. 500 ng gDNA templates (numbered as ①-I-A to D and ①-II A to B) were amplified at the annealing temperature of 65°C for 30 cycles, with gDNA template from untransfected (Untft) *E14-Bra-GFP* mESCs cultured on gelatin as negative control. A non-template control (NTC) was also included where template gDNA was substituted by nuclease-free H_2O. Yellow stars show 3'-HA screened positive clones with bright bands (18 of 35) and blue arrow heads show positive clones with weaker bands of the correct size of 3,380 bp (2 of 35). Sample was loaded on an 8 cm-length 0.8% agarose gel run at 7 V/cm for 45 min in 1×TAE buffer. L,1 kb ladder.

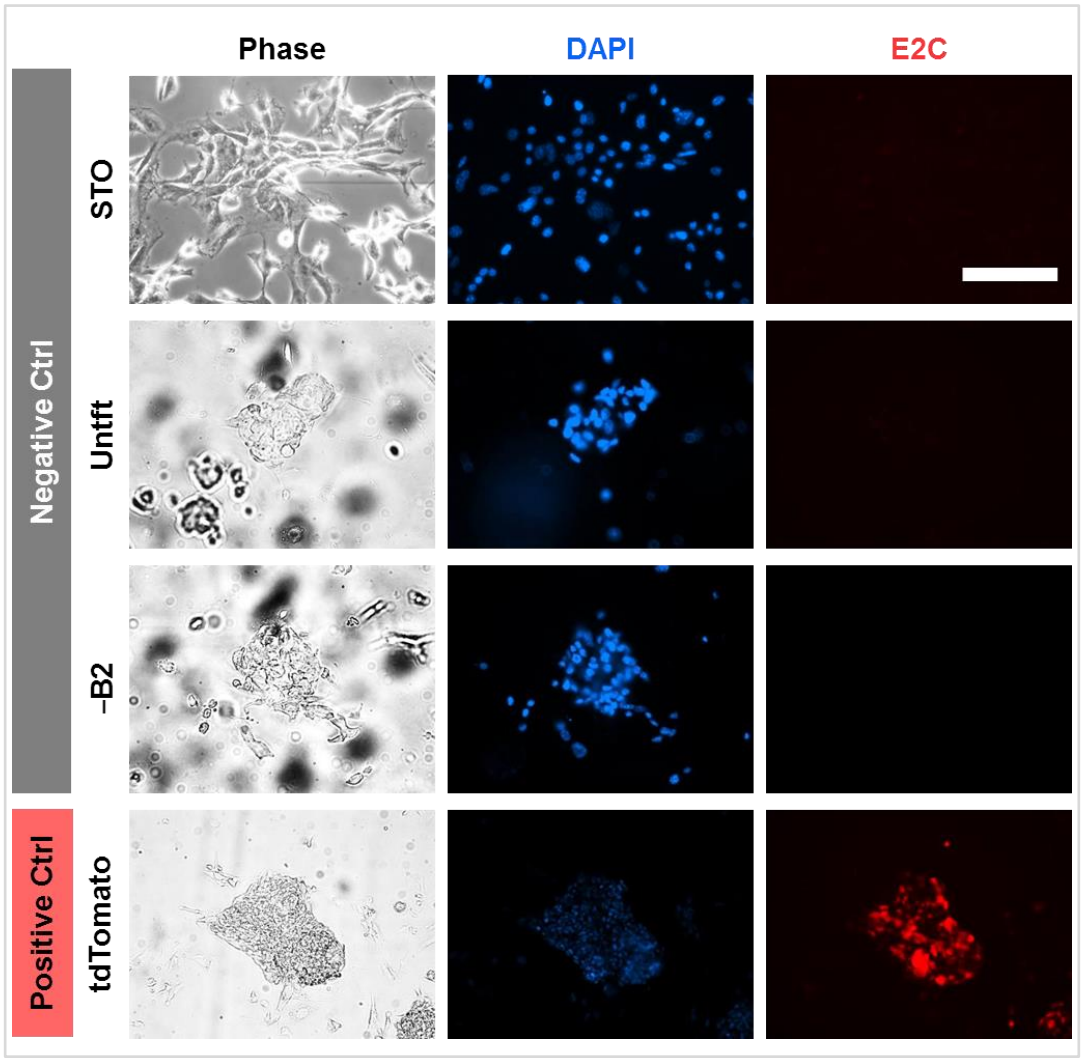

Figure 3.4 E2C expression was examined by fluorescence microscopy in 3'-HA PCR-screened positive and negative clones. Five positive clones were named according to their address in the 96-well plate (i.e., +B5, +C4, +D1, +E3, +G1). tdTomato-transduced *E14-Bra-GFP* mESCs were used as a positive control with STO feeder cells, untransfected (untft) *E14-Bra-/GFP* mESCs and a negative clone named –B2 comprised the negative controls. All samples were counter-stained with the nuclear stain DAPI. Scale bar, 100 µm (all graphs).

(continued on next page)

(continued from previous page)

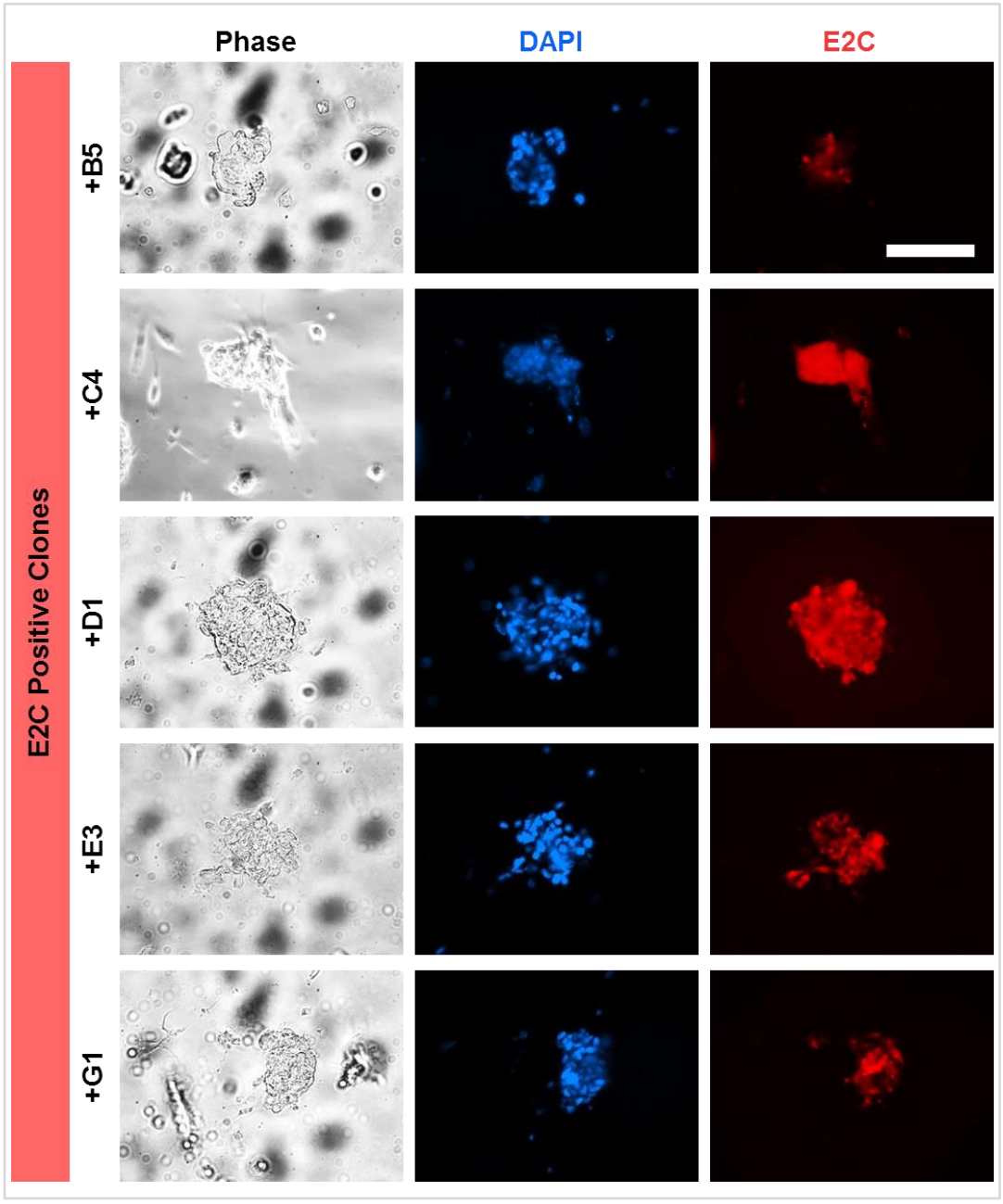

Figure 3.4, continued.

3.2.5 Flow cytometry analysis of E2C expression

In order to confirm that all cells within the positive clones expressed E2C, 4 of the E2C-expressing clones, namely +B5, +C4, +D1 and +E3, were selected for flow

cytometry analysis. The average E2C signal intensity of all the 4 clones was approximately 10^3. For Clones +B5, +C4 and +E3, over 93% of the population expressed E2C (data not shown), whereas 99% of clone +C4 expressed E2C, indicating a very high purity. +D1 comprised a smaller proportion (87%) of E2C-expressing cells (Figure 3.5). Apart from the fact that only 87% cells of the clone +D1were E2C positive, it also appeared that the mean fluorescence intensity was lower in this clone (375) than in the +C4 (729). +C4 was therefore selected for subsequent experiments.

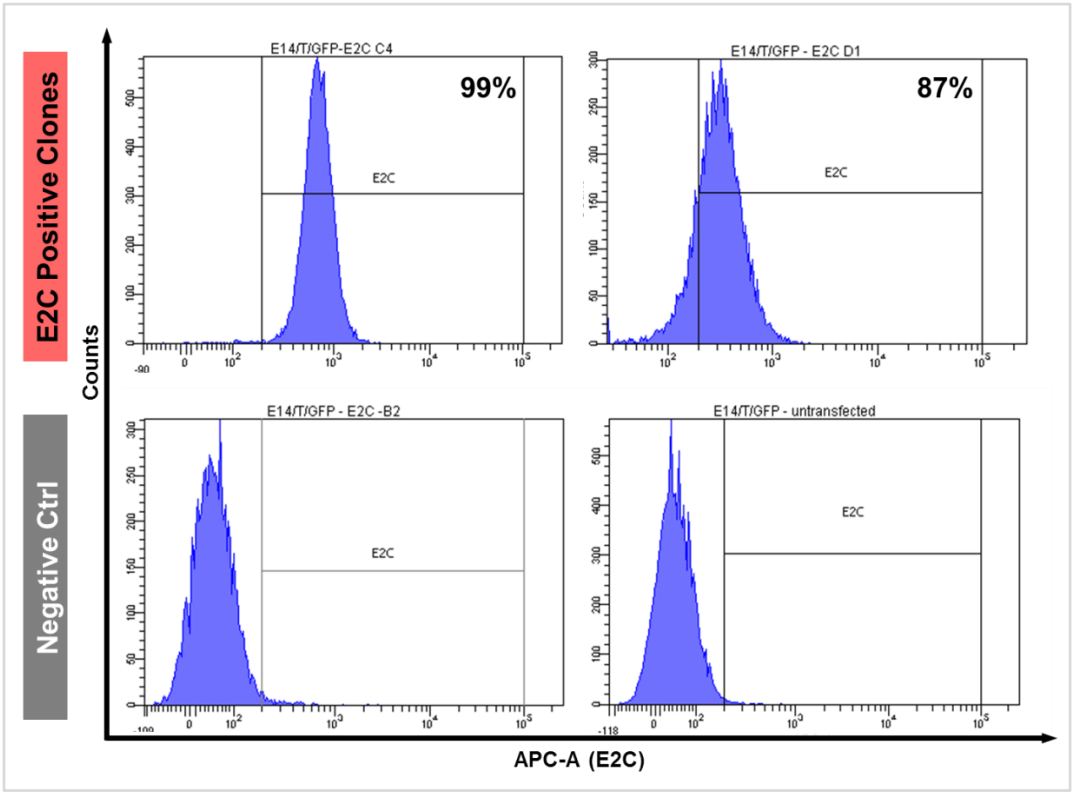

Figure 3.5 Flow cytometry analysis of E2C expression of the selected 3'-HA PCR-screened positive clones. Untransfected *E14-Bra-GFP* mESCs and a negative clone named –B2 was used as the negative control. 10,000 events were counted for each sample.

3.2.6 Stemness and differentiation potential of *Bra-GFP/Rosa26-E2C* mESC reporter line

To ensure the knock-in of E2C did not affect self-renewal or differentiation capacity, the cells were assessed for the expression of stemness markers and their ability to generate EBs. To examine the expression of stemness markers, the clone +C4 was plated into 8-chamber slides/35 mm dishes for immunofluorescent staining of Oct4 and Nanog. The results demonstrated specific nuclei located-staining of Oct4 and Nanog, respectively, of the +C4 colonies (Figure 3.6).

To evaluate whether typical EBs can be formed following the *E2C* knock-in manipulation, a specified density of cells from clone +C4 colonies were plated in bacterial petri dishes and cultivated for 7 days in EB medium. Aggregates were observed during the first 24 to 48 h followed by the formation of an outer PrEn layer. Cavitation was observed in the majority of EBs by day 7 (Figure 3.7). BM, PrEc, VEn and PEn were also identifiable by day 7 in the cavitated EBs, suggesting that the +C4 cells had retained their ability to differentiate to different lineages.

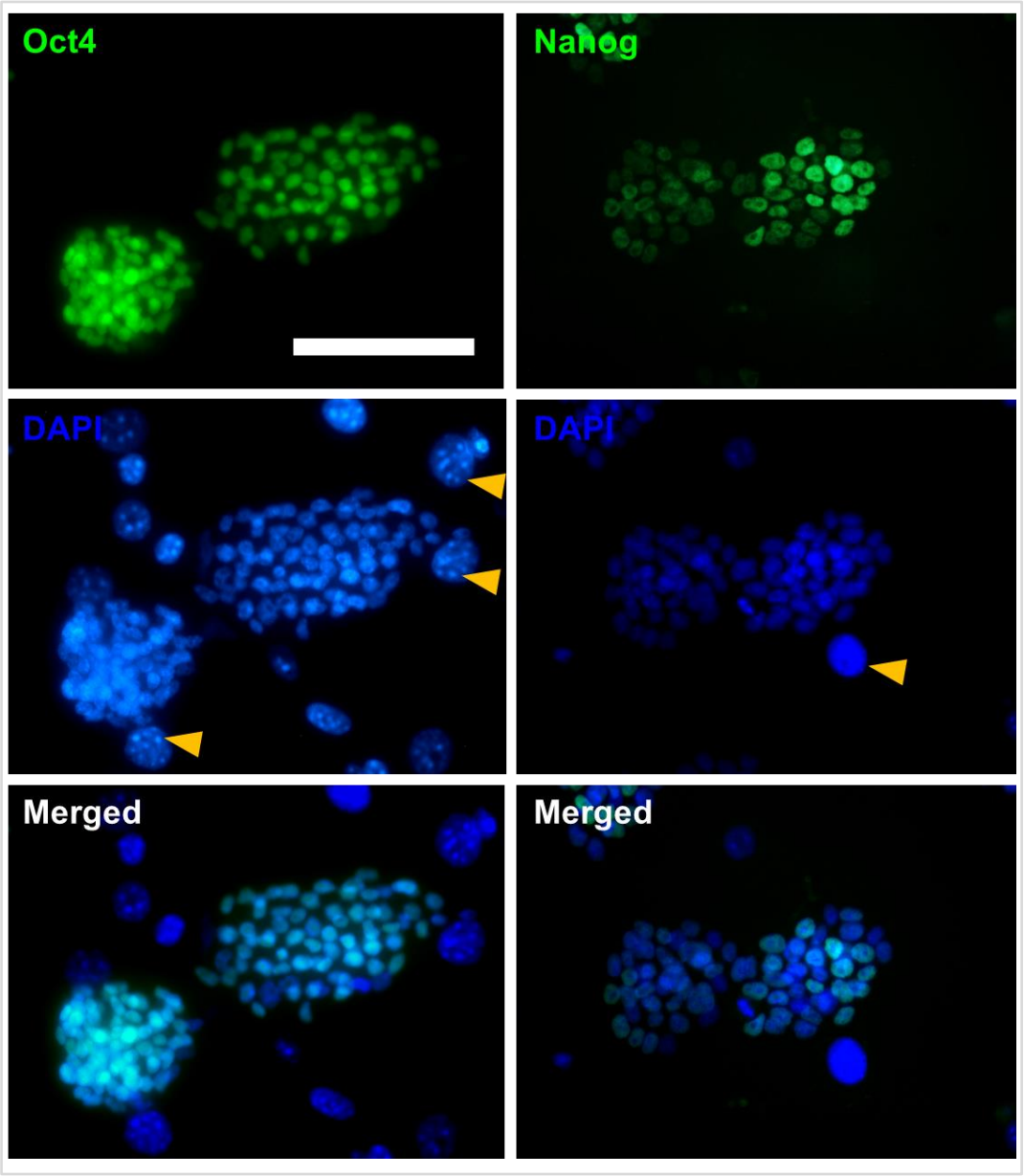

Figure 3.6 Expression of stemness markers Oct4 and Nanog was confirmed by immunofluorescent staining of clone +C4. All samples were counter-stained with DAPI. Yellow arrow heads show STO feeder cell nuclei. Scale bar, 100 µm (all graphs).

.

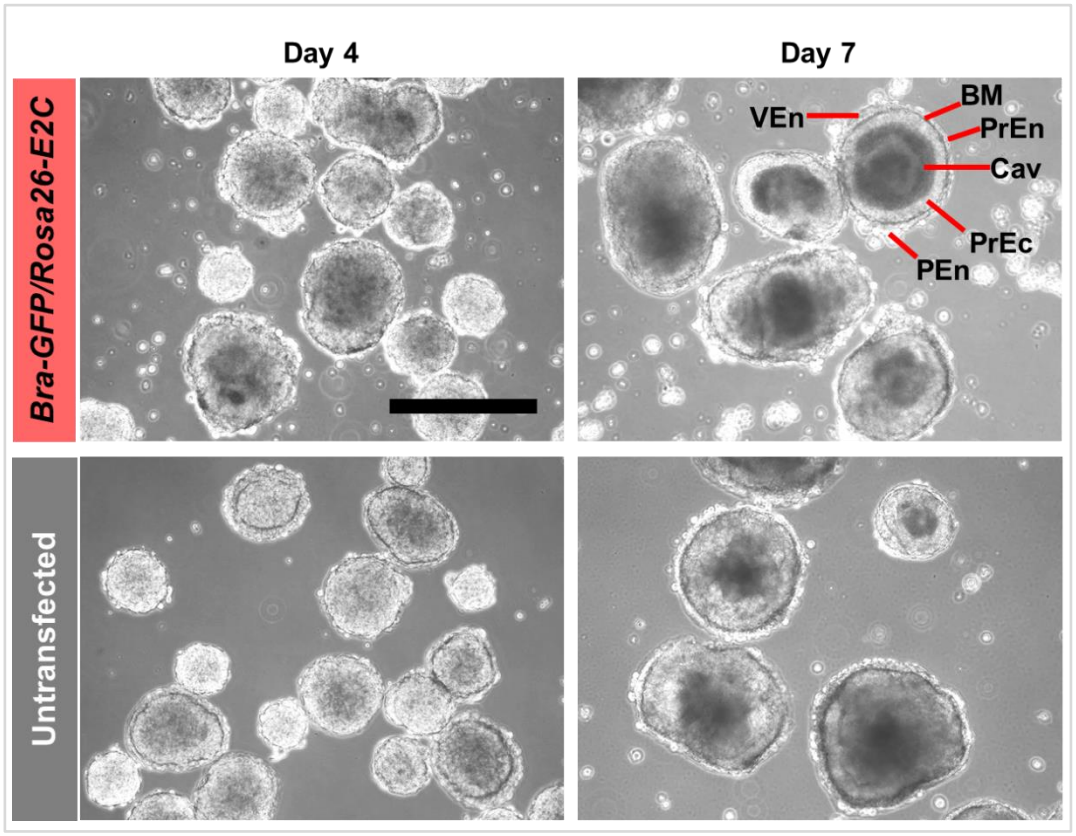

Figure 3.7 Differentiation potential of clone +C4 was confirmed by typical EB formation. Cells were seeded in suspension culture dishes up tol day 7. PrEc, primitive ectoderm; PrEn, primitive endoderm; BM, basement membrane; Cav, cavity; VEn, visceral endoderm; PEn, parietal endoderm. Scale bar, 400 μm (all graphs).

3.3 Discussion

In this study, an E2C-expressing *E14-Bra-GFP* mESC reporter line (clone +C4) was generated by knocking-in *E2C* into the *Rosa26* locus.

Using Soriano's strategy, it has been reported that the targeting efficiency of the *Rosa26* locus is around 20% of drug-resistant colonies (Monticelli, 2010). By using Hohenstein's protocol, the efficiency can be increased to an average of 25%

(Hohenstein *et al*., 2008). However, by using Aizawa's vector that contains longer 5'- and 3'-HAs, it has been reported that the efficiency can be as high as 45%, which is consistent with the results obtained here (i.e., 51% of drug-resistant clones appeared to have undergone correct homologous recombination) (Abe *et al*., 2011). It is likely that the increase in efficiency observed using Aizawa's vector is due to the longer length of the homologous arms (Thomas and Capecchi, 1987; Deng and Capecchi, 1992). Aizawa's vector contains an 8.1 kb 5'-HA and a 3.5 kb 3'-HA whereas the HAs in Hohenstein's vector are only 1 kb for the 5'-HA and 5 kb for the 3'-HA (Abe *et al*., 2011; Hohenstein *et al*., 2008). Although the efficiency appeared to be high within our results, the screening design could be further optimised in order to exclude random vector integration. PCR screening along with Southern blot analysis on 5'-homologous recombination would be of further consideration (Abe *et al*., 2011; Hohenstein *et al*., 2008; Liu *et al*, 2011; Tong *et al*, 2011). This would produce bands for distinguishing whether correct recombination has occurred within the targeted locus. Aside from that, it would be ideal to perform amplicon sequencing comparing between screened clones and non-transfected cells to verify integration integrity (Shen *et al*, 2013).

Interestingly, there were two screened clones which showed positive PCR amplicon bands, but unlike the other positive ones, the intensity was significantly reduced, implying a lower expression level. This might be due to less template DNA of PCR or impurity carried over from genomic DNA. Another possible

reason is that these strains were propagated from a mixture of the correct recombinants and satellite colonies which can be located in the vicinity of the correct recombinant (Friedrich and Soriano, 1991). In addition, DNA methylation may alter the E2C expression level of the transfected mESCs. Different transgene expression patterns of *Rosa26* targeting have been reported, implying complex genomic methylation levels in the generated strains that may result in gene silencing (Dom ńguez-Bendala and McWhir, 2004). Of note, the screened clone +D1 displayed an E2C-expression population of 87%, and moreover, showed a lower mean fluorescence intensity, suggesting that slight DNA methylation might have occurred and hence down-regulated the E2C level. Nevertheless, the reason for the varied expression levels in the *Rosa26* targeted strains is still unclear.

Many mESC lines have been established by viral transduction which results in random insertion of reporter genes into chromosomes leading to different gene copy numbers and integration sites. Although this approach can lead to higher expression levels due the presence of multiple copies of the transgene, the levels of expression can vary considerably between different cells within the transduced population. Furthermore, there is evidence that transgenes introduced into mESCs via viral transduction have a tendency to be silenced following differentiation to specific lineages (Lepperhof *et al*., 2014). Although targeted integration at the *Rosa26* locus generally introduces only a single copy of the transgene into the *Rosa26* allele (Friedrich and Soriano, 1991), leading to lower expression levels

that can be achieved with lentiviral transduction, there is a lower tendency for transgenes within the *Rosa26* locus to become silenced following differentiation of the mESCs (Lepperhof *et al*., 2014). Therefore, this approach could be more suitable for tracking cells over the long-term.

To summarise, in this chapter, we have generated a *Bra-GFP/Rosa26-E2C* mESC reporter line and have shown that these mESCs continue to express key stemness markers and retain the ability to differentiate. This line will be used in subsequent chapters to isolate nascent mesoderm following growth in 3-D as EBs and in 2-D differentiation culture, so that the properties of the mesoderm generated under these different culture conditions can be compared.

Chapter 4

Evaluating the effectiveness of the E2-Crimson fluorescence reporter for tracking *Bra-GFP/Rosa26-E2C* mESCs in living mice

4.1 Introduction

The motivation for generating the *Bra-GFP/Rosa26-E2C* reporter mESC line (see Chapter 3) was to compare the behaviour and differentiation potential of mESC-derived Bra^{+} cells generated under different culture conditions, by monitoring their ability to give rise to renal cell types following (i) administration into adult mouse kidneys, and (ii) incorporation into mouse kidney rudiments *ex vivo* (chapter 6). However, given that fluorescence image of cells within the internal organs of mice can be challenging due to the aforementioned issues with autofluorescence, light absorbance and scattering (Chapter 1), it was first necessary to evaluate the effectiveness of E2C for tracking cells *in vivo* following subcutaneous administration in mice. It has previously been shown that if undifferentiated mESC are injected subcutaneously, they have a tendency to develop teratomas, which are benign tumours that typically contain cell types derived from more than one germ layer (Evans, 2011; Martin, 1981). Our strategy was therefore to assess

whether the presence of E2C in the cells would enable us to monitor teratoma formation *in vivo* with fluorescence imaging following implantation of the cells into the mouse flank. If the E2C reporter line was found to be effective for imaging the cells subcutaneously, we would then progress to monitoring the renal biodistribution and growth of the cells following systemic administration. However, if subcutaneous imaging proved difficult, this would suggest that the E2C would not be effective for detecting cells within the kidneys of mice *in vivo*.

mESC-derived teratomas

Although mESCs can contribute to embryo development following injection into mouse blastocysts, if they are injected into other locations such as retroperitoneum, they can generate non-invasive benign tumours called teratomas, or even malignant teratocarcinomas that resemble tumours formed by embryonal carcinomas and germ cells. Mature teratomas comprise well-differentiated tissues of the three germ layers, such as neural tissue, skin, hair, gland that are of ectoderm origin; adipose, smooth/skeletal/cardiac muscle, bone and cartilage that are of mesoderm origin; as well as gut and pancreas cells that are of endoderm origin (Nussbaum *et al*., 2007; Yamamoto, 2005; Martin, 1980; Stevens, 1970; Solter, 1970). It has also been shown that teratomas can be generated following subcutaneous injection of mESCs into adult mice (Martin, 1981; Wakitani *et al*., 2003). In some cases, additional

undifferentiated stem cells were found in the teratomas, contributing to the malignancy of progressive tumour growth and transplantation, but without metastasis. These teratomas were defined as teratocarcinomas (Martin, 1980). The maturity of the teratomas can be assessed at a histopathological level by their tissue components, particularly by the presence of neuroepithelium which emerges at an early immature stage (Wetherell *et al*., 2014).

Experimental design

Bra-GFP/Rosa26-E2C mESCs were injected subcutaneously into the dorsal flanks of female CB17 severe combined immunodeficient (SCID) mice using the following administration doses: 5×10^6, 7.5×10^6 and 10×10^6. The control comprised untransfected *E14-Bra-GFP* mESCs which were injected at an administration does of 10×10^6 cells. Following injection, fluorescence was detected in living mice using the IVIS Spectrum fluorescence imager on days 0, 1, 4, 7 and 9. Tumour size was also measured at day 4, 7 and 9. On day 9, mice were sacrificed and tumours were fixed and paraffin embedded for histopathology, or frozen for immunohistochemical analyses. Details of protocols are described in Chapter 2.

The specific objectives of this chapter were to:

1. Quantify the intensity of the E2C fluorescence signal *in vitro*;
2. Quantify the intensity of the E2C fluorescence signal *in vivo* over time;

3. Analyse the excised tumours at the study end-point using histopathology and immunofluorescence staining.

4.2 Results

4.2.1 Quantitative analysis of E2C fluorescence signal *in vitro*

Prior to undertaking *in vivo* experiments, it was important to determine the signal intensity of the E2C fluorescence emitted by the newly-established mESC reporter line in order to establish the lower limits of detection. To this end, we assessed the fluorescence intensity of 2×10^6 and 8×10^6 E2C reporter cells *in vitro* by imaging cell pellets using the IVIS Spectrum. The results demonstrated that faint signals from 2×10^6 and 8×10^6 cell pellets were detected by IVIS, showing approximately 1.8- and 4-fold higher intensity than that of the background, respectively (Figure 4.1). This indicated that as expected, the level of E2C fluorescence increased within increasing cell number, but nevertheless, was relatively weak.

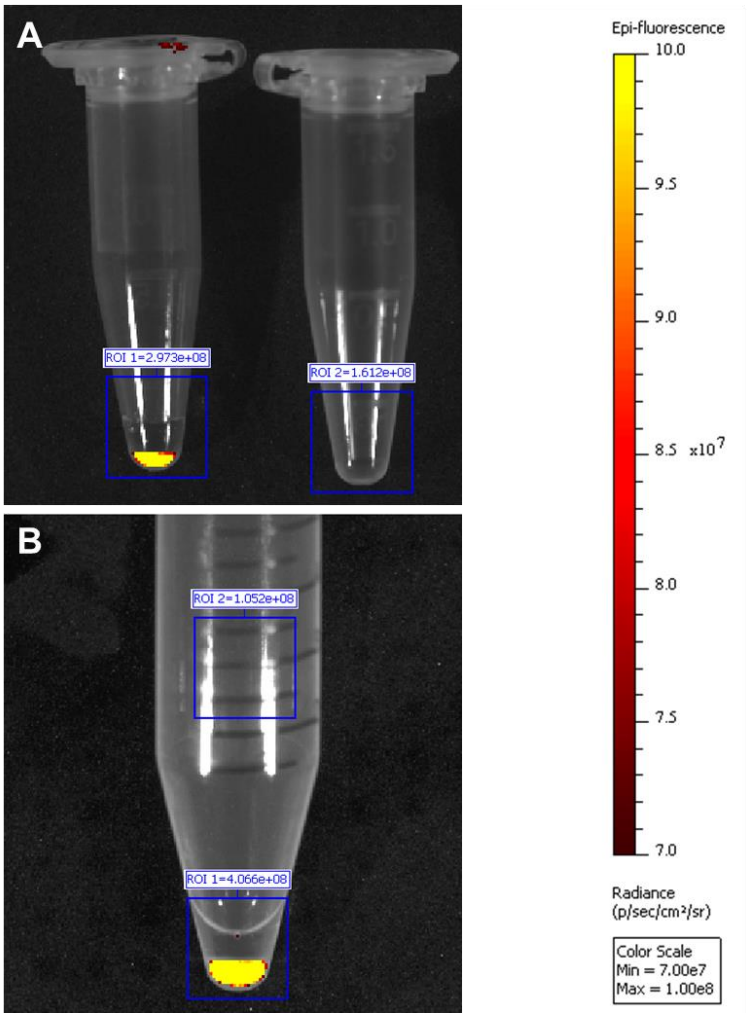

Figure 4.1 IVIS images of E2C$^+$ mESC pellets comprising 2×10^6 (A) and 8×10^6 (B) cells compared to background (microfuge tube wall). Values of the region of interest (ROI) 1 were acquired from *Bra-GFP/Rosa26-E2C* mESC pellets. ROI 2 values were acquired from the background. Data are displayed in radiance units (p/sec/cm^2/sr).

4.2.2 Quantitative analysis of E2C fluorescence signal *in vivo*

Bra-GFP/Rosa26-E2C mESCs suspended in PBS were injected subcutaneously in randomly selected sites in each mouse, at the following doses in an injection volume of 100 µL (5×10^6, 7.5×10^6 and 10×10^6), along

with a control comprising 10×10^6 untransfected mESCs. Palpable tumours were detected in each mouse from day 4. By day 7, several tumours developed reddish-blue discolouration, which was probably due to the high degree of vascularization (Figure 4.2).

E2C fluorescence emitted from the reporter cell line in some injection sites was noticeable *in vivo* immediately following injection (Figure 4.3). In all experimental groups that were administered with *Bra-GFP/Rosa26-E2C* mESCs, the E2C decreased by 24 h post injection. Detectable fluorescence of E2C increased afterwards from this time-point and peaked on day 4. Surprisingly, although visual inspection suggested that the tumours were increasing in size, the E2C signal intensity decreased between days 4 and 9 but remained slightly higher than the control cells. However, there was no significant difference in fluorescence intensity in tumours generated by the reporter cells and untransfected cells (negative controls) within the 9-day growth period (Figure 4.4A).

Quantitative analysis in terms of calculated mean region of interest (ROI) values showed that the E2C signal intensity emitted by the 10×10^6, 7.5×10^6 and 5×10^6 cell doses decreased from $2.3 \pm 0.3 \times 10^8$, $2.2 \pm 0.5 \times 10^8$, and $1.9 \pm 0.2 \times 10^8$ p/sec/cm2/sr, respectively, on day 0 to $1.5 \pm 0.3 \times 10^8$, $1.5 \pm 0.3 \times 10^8$, and $1.5 \pm 0.2 \times 10^8$ p/sec/cm2/sr, respectively, on day 1. The signal then started to

increase and peaked at $2.9 \pm 1.0 \times 10^8$, $2.8 \pm 0.4 \times 10^8$, and $2.6 \pm 0.2 \times 10^8$ p/sec/cm2/sr, respectively, on day 4, before decreasing to $2.5 \pm 0.6 \times 10^8$, $2.8 \pm 0.3 \times 10^8$, $2.4 \pm 0.3 \times 10^8$ p/sec/cm2/sr, respectively, on day 9 (Figure 4.4A and Appendix Table 2).

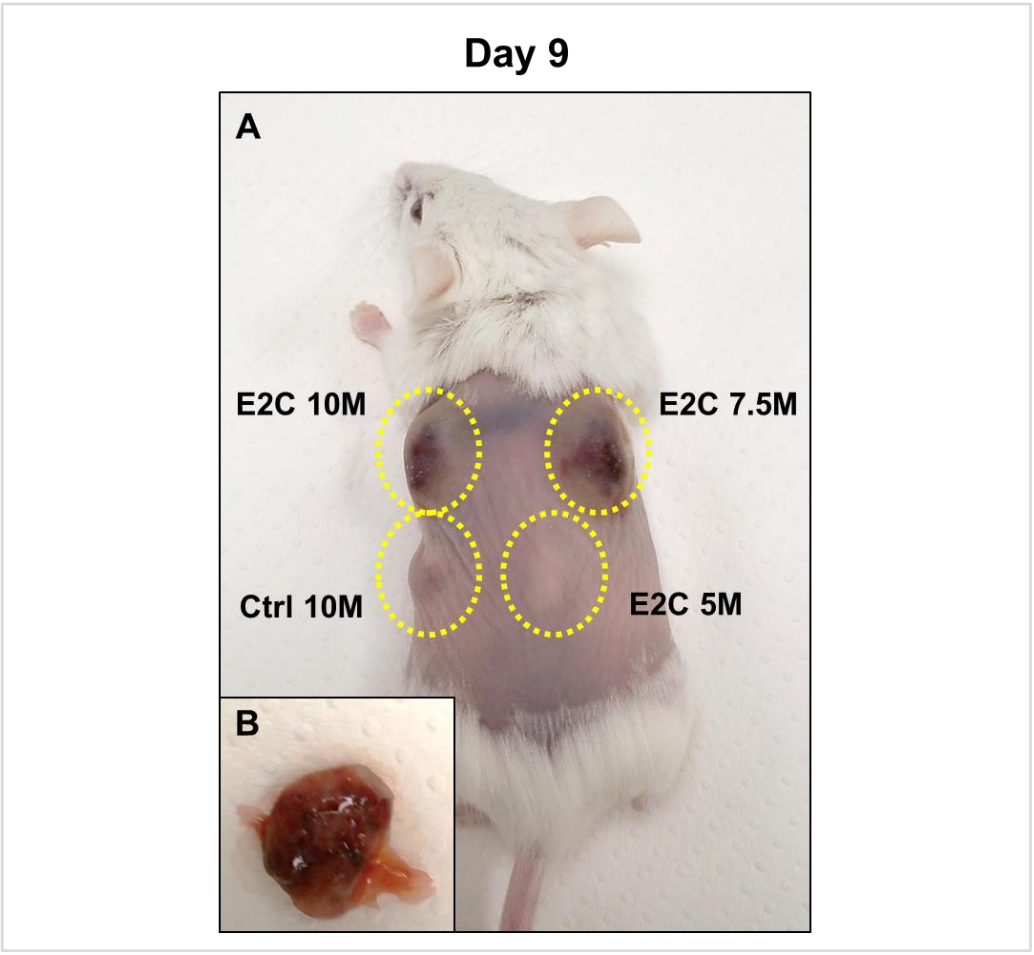

Figure 4.2 Growth of tumours from *Bra-GFP/Rosa26-E2C* mESCs in severe combined immunodeficient (SCID) mice that formed from 5×10^6, 7.5×10^6 and 10×10^6 injected cells. The untransfected *E14-Bra-GFP* cells were used as a negative control (10×10^6 cells). **A**, mouse with tumours in 4 sites on day 9 post injection; **B**, dissected E2C tumour formed on day 9 post injection with 7.5×10^6 cells showing high degree of vascularisation. M represents million ($\times10^6$).

To determine if the emitted fluorescence intensity correlated with tumour size, tumour volume was measured on days 4, 7 and 9. A mathematical model of solid tumour volume calculation has previously been constructed based on the assumption that tumours are hemi-ellipsoid in 3-D shape. Therefore, the volume is calculated from the measurements of tumour length, width and height using the following equation (Dethlefsen *et al*., 1968; Tomayko and Reynolds, 1989):

$$V = \pi lwh/6, \quad (1)$$

where V is the tumour volume, and l, w, h are the length, width, and height of tumour, respectively.

Tumour growth curves were then constructed. The measurement data here displayed a distinct increase in tumour size during day 4 and 9.The increase in tumour volume for the 7.5×10^6 dose of E2C reporter mESCs demonstrated an approximately 4-fold change compared to that of the 5×10^6 cell dose. However, a noticeable increase in tumour volume was observed in all cases, irrespective of the administration dose (Figure 4.4B). Detailed data are shown in the Appendix Tables 1 and 2.

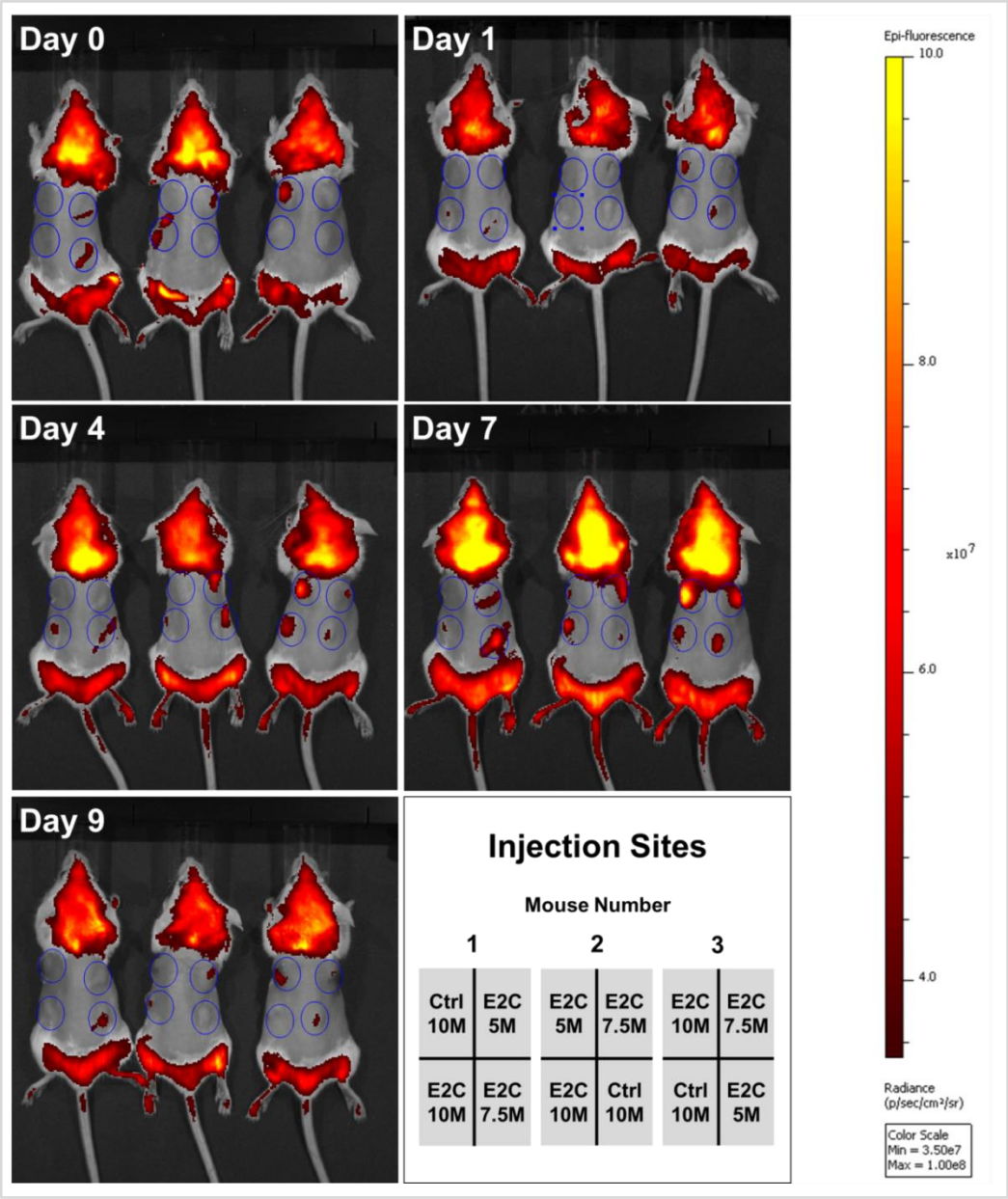

Figure 4.3 IVIS images *in vivo* at days 0, 1, 4, 7 and 9 post injection of E2C$^+$ cells into the dorsal flanks of SCID mice. The emission filter of 605–660 nm wavelengths was applied to detect the fluorescent signal generated from *Bra-GFP/Rosa26-E2C* mESCs. The untransfected *E14-Bra-GFP* cells were used as negative controls. Data are displayed in radiance units (p/sec/cm^2/sr). M represents million ($\times 10^6$).

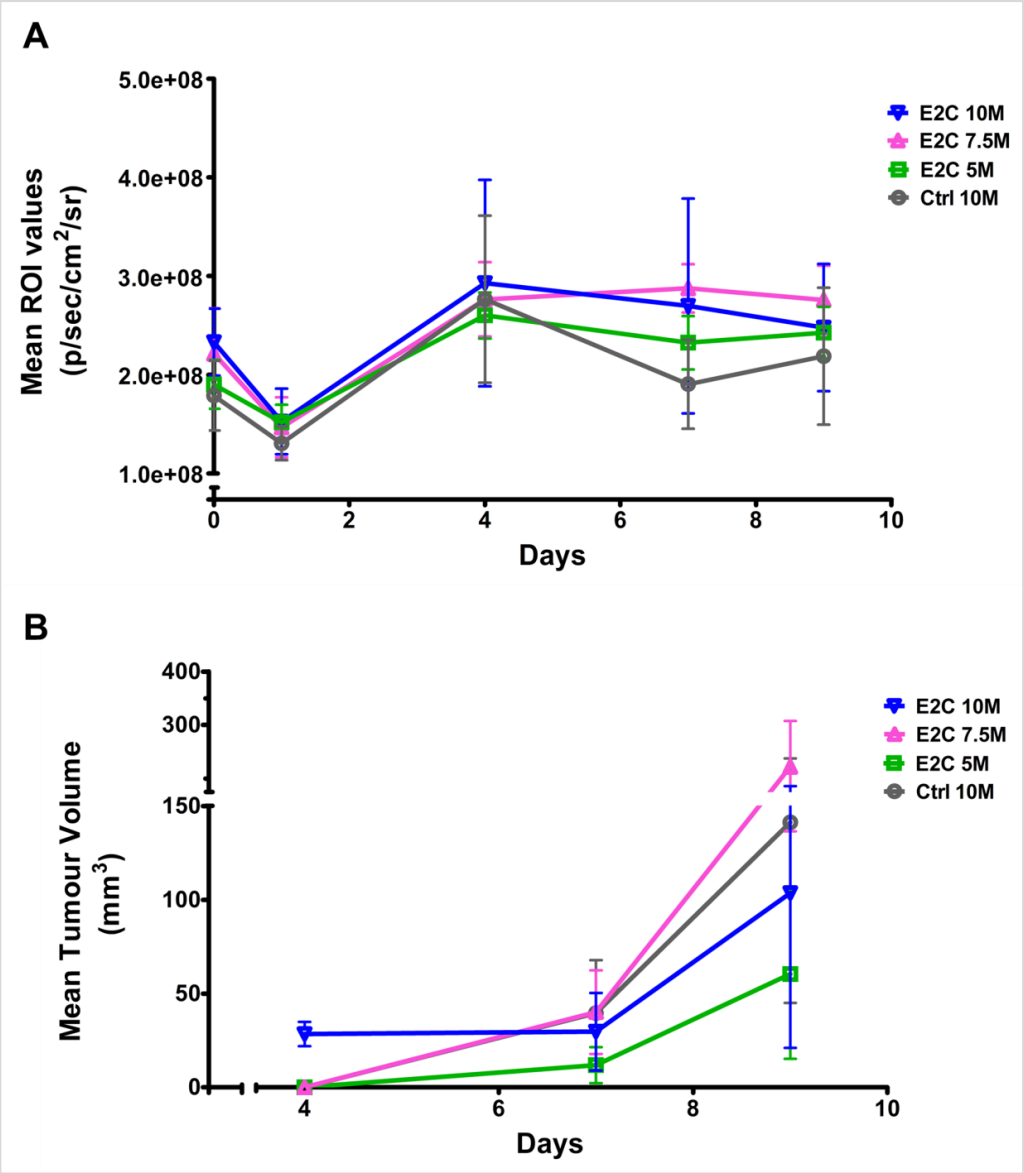

Figure 4.4 Growth curves obtained based on the changes of mean region of interest (ROI) values and tumour volume post injection. (A) ROI values were generated by IVIS software for the time points of day 0, 1, 4, 7 and 9. (B) Tumour volume was calculated based on the manual measurements of tumours on day 4, 7 and 9. Error bars represent ±SD (A) and ±SEM (B), respectively. (n=3). M represents million ($\times 10^6$).

4.2.3 Histopathology and immunofluorescence analyses of tumours

At the study end point, the mESC tumours were harvested and paraffin sections were analyzed by a pathologist to confirm whether the tumours resembled teratomas. Analysis of H&E sections showed that the tumours resembled primitive germ cell tumours and immature teratomas, which typically contain neuroepithelial-like cells and other cell types such as chondrocytes (Figure 4.5). The tumours also appeared to be well-vascularised and contained abundant erythrocytes (Figure 4.5).

To determine if all of the differentiated cells within the tumours continued to express E2C, and whether the tumour vasculature was derived from the mESCs or the host, immunofluorescence staining for E2C and the endothelial marker, PECAM-1, was undertaken. The results showed that most of the tumour cells, including the epithelial and chondrocyte-like cells, expressed E2C, indicating that the transgene expression was stable over this time-frame. As expected, there was no evidence of E2C expression in the control tumours (Figure 4.6). PECAM-1 staining showed that none of the endothelial cells within the tumour stained positively for E2C, indicating that they were all derived from the host (Figure 4.6).

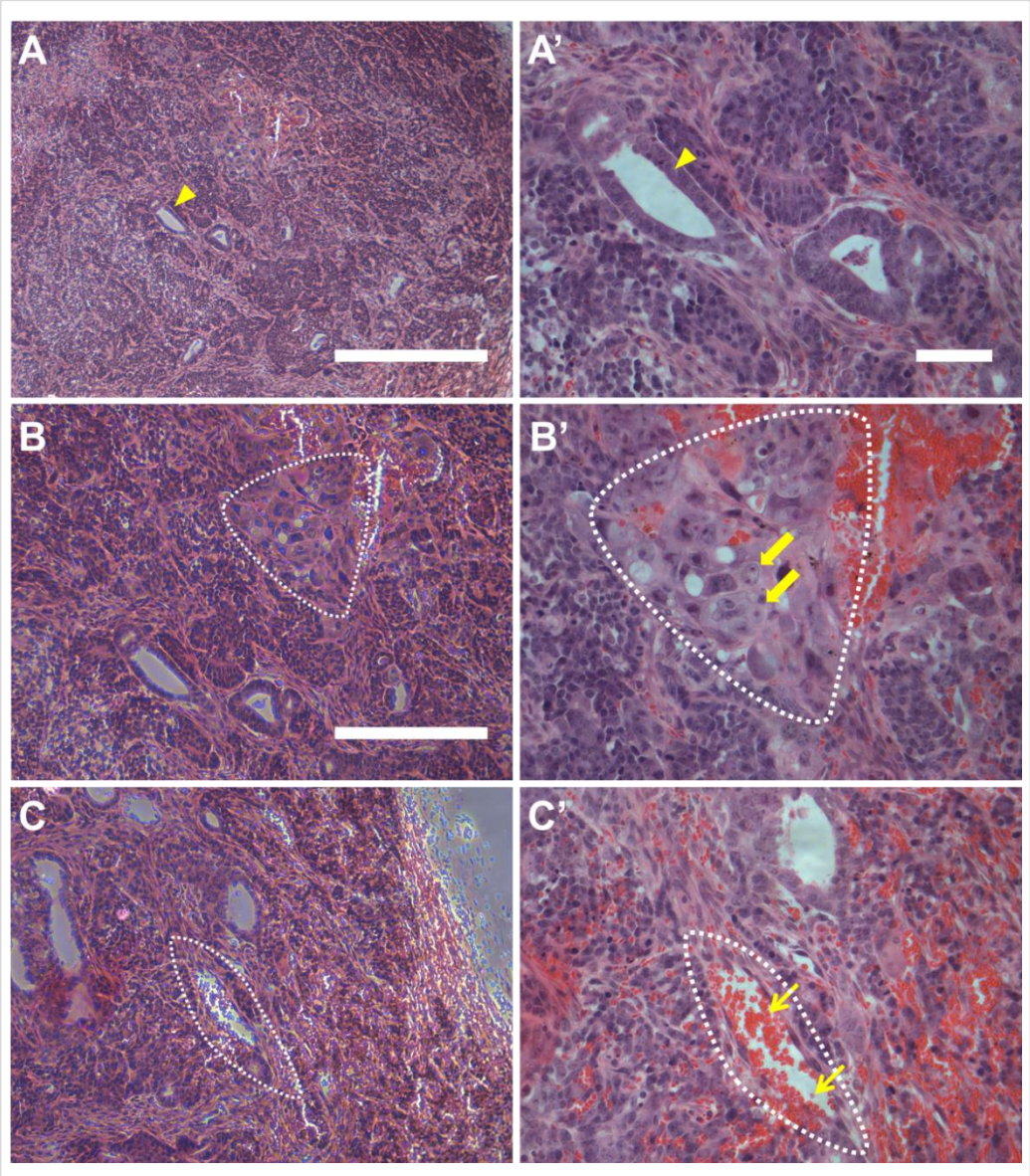

Figure 4.5 Histological analysis of tumours derived from the mESCs. H&E staining was performed on paraffin sections prepared from the day-9 tumours. Arrow heads show epithelial structure (A–A'), thick arrows show chondrocyte-like cells (B–B') and thin arrows show red blood cells (C–C'). Dashed lines show the structures of chondrogenic-like (mesoderm-like) differentiation (B-B') and blood vessels (C–C'). Scale bars, 400 µm (A), 200 µm (B, C); 50 µm (A'–C').

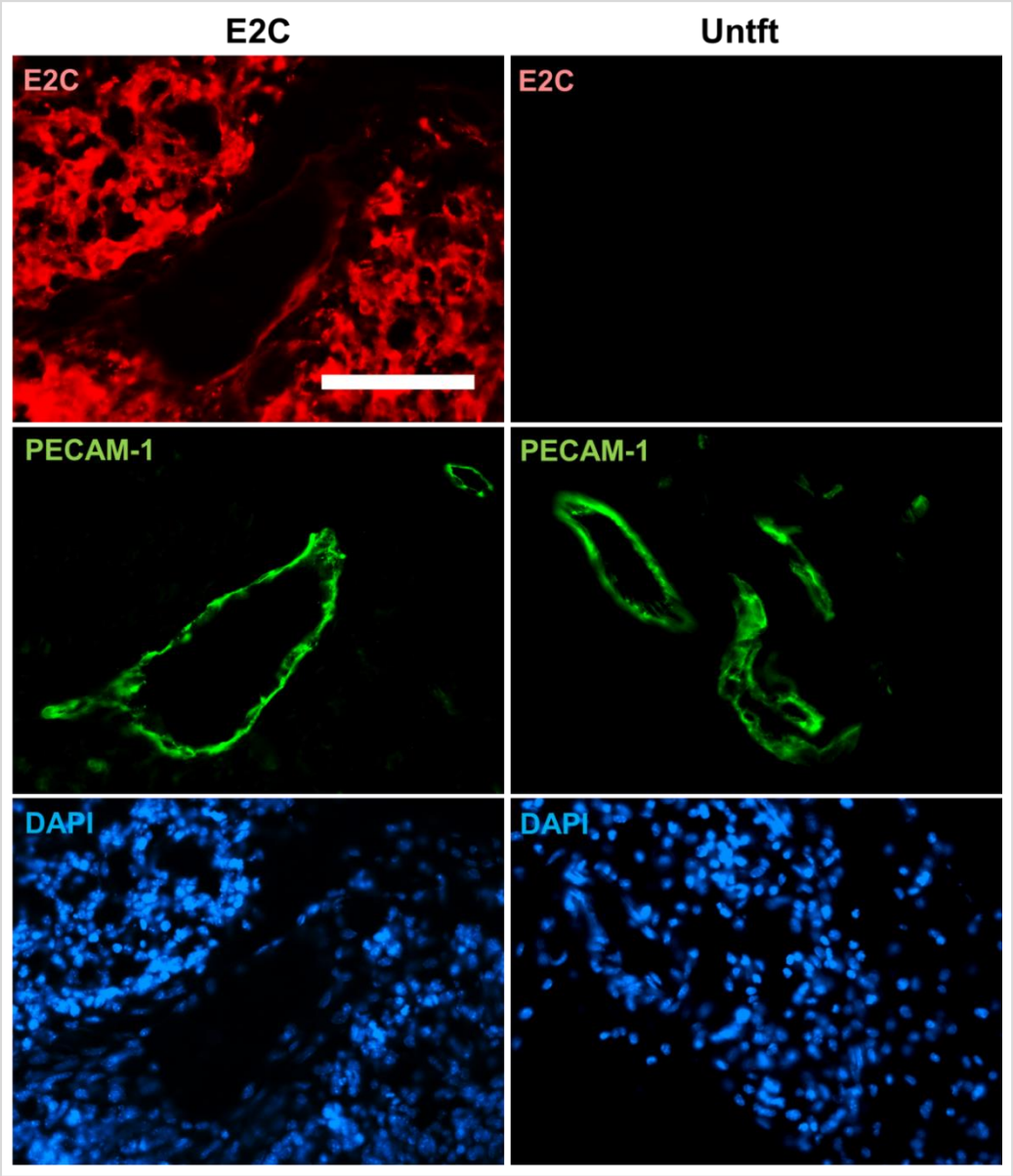

Figure 4.6 Immunostaining for E2C (red) and PECAM-1 (green) in tumours derived from E2C$^+$ mESC reporters (E2C) or untransfected controls (Untft). Dual immunostaining of frozen sections prepared from tumours harvested at day 9 shows that all cells, except the vasculature and blood cells, within the tumours are derived from the E2C$^+$ mESC, which stained positively for E2C. On the other hand, the endothelial cells within the tumours did not stain positively for E2C, indicating they were derived from the host animals. Tumours developed from the untransfected (untft) *E14-Bra-GFP* mESC were used as controls. Scale bar, 100 µm (all graphs).

(continued on next page)

(continued from previous page)

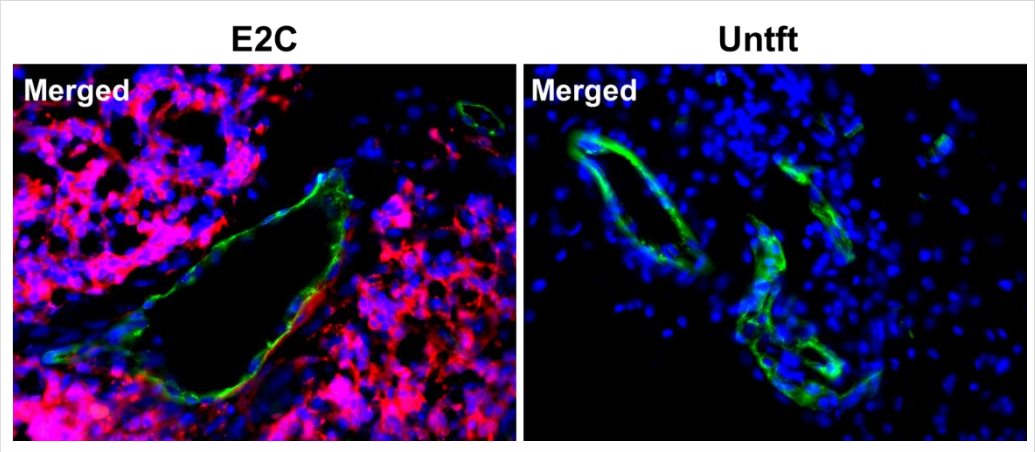

Figure 4.6, continued.

4.3 Discussion

In this chapter, to assess the feasibility of imaging the E2C mESC reporter cells *in vivo* using fluorescence imaging, we injected three cell doses subcutaneously into SCID mice and imaged over a 9-day time course.

It was found that even when the animals were imaged immediately following cell administration, it was not always possible to detect the E2C signal. Thus, the main conclusion from this experiment is that the E2C is not an effective *in vivo* reporter in this context (i.e., when introduced as a single copy into the *Rosa26* locus), and imaging the E2C reporters in the internal organs would not be feasible due to signal attenuation with increasing depth. In contrast to our findings, Christensen and colleagues were able to detectE2C emitted from tumour cells injected into the rat lung (Christensen *et al*., 2015). The likely

explanation is that they used lentiviral technology to generate the reporter cells, which would have introduced multiple copies of the *E2C* transgene into each cell. Furthermore, the E2C was expressed under the strong constitutive cytomegalovirus (CMV) promoter.

In cases where the cells could be detected at day 0, it was found that E2C signal intensity decreased on day 1 before increasing between days 4 and 7. The reduction in signal at day 1 is probably due to cell death. SCID mice are deficient in generating T and B lymphocytes and thus are unable to launch an adaptive immune response. However, they still have an intact innate immune system, comprising neutrophils, macrophages and natural killer cells that might contribute to the death of injected mESCs (Bancroft *et al*., 1989). Another possible reason is that many of the mESCs may simply die due to the sudden change in their micro-environment, as it is well-known that these cells require specific culture conditions for their propagation. The increase in fluorescence observed in most tumours from days 4 to 7 probably reflected the fact that, over this time course, there was an increase in tumour volume. Interestingly, although the tumour volume continued to increase from days 4 to 7, in most cases, there was a decrease in fluorescence. This was most likely due to the fact that the tumours became highly vascularized. H&E staining of tumour sections showed a high number of red blood cells within the blood vessels. Since haemoglobin plays a major role in photon absorption within the <650 nm

wavelength region, it is likely that E2C fluorescence was partially absorbed by the red blood cells in the tumours (Weissleder, 2001).

None of the mice injected with control untransfected mESCs were expected to display any E2C fluorescence signal. Of note, some background signal was observed in the control tumour of mouse number 3 on days 4 and 7 post injection. To confirm whether this was artifactual, or was due to migration of $E2C^+$ mESCs to the control injection site, immunostaining for E2C was performed on frozen sections of the control tumour. No evidence of E2C expression was observed, indicating that the signal observed with IVIS was artifactual background staining. This artifactual signal is likely due to photon scattering and autofluorescence from the skin abutting the tumour (Leblond *et al*., 2010).

H&E histopathological examination of the tumours showed that they resembled immature teratomas, which typically have abundant neuroepithelial cells (Wetherell *et al*., 2014) as well as derivatives of other germ layers, such as chondrocytes (Shaaban *et al*., 2014). The abundant epithelial structures observed in the tumours are likely to resemble either primitive ectoderm epithelia or neuroepithelia. In the developing embryo, some of the primitive ectoderm cells that do not egress through the primitive streak directly give rise to neuroepithelial cells (LaBonne and Bronner-Fraser, 1999). Morphologically,

the primitive ectoderm and early neuroepithelial cells closely resemble each other. Chondrocyte-like cells were also present in the tumours, which would be consistent with them being immature teratomas. Endothelial cells were also identified lining blood vessels, but dual immunostaining for E2C and PECAM-1showed that these cells were derived from the host.

There are numerous reports showing that following subcutaneous implantation or implantation under the kidney capsule, mESCs will typically form mature teratomas that contain various types of well-differentiated cells derived from the three germ layers, and can even generate endothelial cells which form part of the vasculature of the teratoma (Stevens, 1970). However, in these studies the teratomas were allowed to develop over a 4-week period instead of just 9 days. Therefore, the fact that teratomas in this study were immature is probably due to the shorter time that they were allowed to develop *in vivo*.

To summarise, the results obtained from imaging the reporter cells after subcutaneous implantation indicate that the emitted E2C fluorescence is weak and it would not be feasible to image the cells in internal organs such as the kidney. Therefore, the focus of the remaining chapters will be to compare the gene expression profile (Chapter 5) and the behaviour and differentiation potential of the different mESC-derived mesoderm populations in mouse embryo kidneys *ex vivo* (Chapter 6).

Chapter 5

Characterisation of mesoderm derived from the *Bra-GFP/Rosa26-E2C* reporter mESCs cultured under 3-D and 2-D conditions

5.1 Introduction

The next stage of this project aimed to generate nascent mesoderm cells from mESCs cultured under different culture conditions and compare their properties in regard to (i) expression of key genes (this chapter) and (ii) their behaviour and differentiation potential in the *ex vivo* mouse kidney rudiment model (chapter 6). For these characterization studies, the *Bra-GFP/Rosa26-E2C* reporter line was used so that FACS could be used to isolate Bra-GFP$^+$ cells generated under the 3-D and 2-D culture conditions. However, prior to this, it was necessary to first optimize the 3-D and 2-D systems and determine at which point the maximum levels of GFP$^+$ (i.e., Bra$^+$) cells are present within the populations. To facilitate this, for the 3-D EB culture conditions, GFP expression was continually monitored using a real-time fluorescence imager called 'Cell-IQ'.

Characterisation of Bra$^+$ cells: investigating the expression levels of lineage-specific genes

Following gastrulation, the Bra^+ nascent mesoderm generates (i) paraxial mesoderm, which gives rise to the somites; (ii) lateral plate mesoderm, which gives rise to the heart, vessels, haematopoietic stem cells and endothelial cells; and (iii) intermediate mesoderm (IM), which gives rise to the urogenital system. The IM then becomes further specified to anterior IM (AIM) that gives rise to the ureteric bud (UB), and posterior IM (PIM) that gives rise to the metanephric mesenchyme (MM). The UB and MM generate the collecting ducts and nephrons, respectively, of the mature kidney (see chapter 6 Introduction). In the mouse embryo, the fate of the Bra^+ cells is determined by the microenvironment that the cells find themselves in following their migration from the primitive streak (Gilbert, 2010). This cannot be replicated using *in vitro* culture systems, which raises the question of whether the Bra^+ cells generated *in vitro* are equivalent to nascent mesoderm, or instead, are partially committed to a specific mesodermal lineage. For instance, the Little group have previously reported that BRA^+ cells derived from human ESCs have a tendency to spontaneously differentiate into $FOXF1^+$ lateral plate mesoderm when cultured in the absence of exogenous growth factors (Takasato, 2014). This observation highlights the fact that the differentiation potential of Bra^+ cells generated *in vitro* is likely to be influenced by the specific culture conditions used. In this study, our aim was to investigate whether Bra^+ cells generated using two different culture systems express different lineage genes, especially those expressed by specific mesoderm populations (Table 5.1). A brief overview of each of these genes is given below.

The T-box transcription factor gene, *Tbx6,* is expressed in the primitive streak, tail bud and paraxial mesoderm and plays a crucial role in mesoderm specification. *Tbx6* mutations result in disruption of antero-posterior polarity (Papaioannou, 2014; Chapman *et al*., 2003).

Cdx2 is expressed in both the trophectoderm and the nascent mesoderm. Its expression pattern resembles that of *Bra* (Arnold *et al*., 2009; Taguchi *et al*., 2014; Savory *et al*., 2009).

LIM-domain homeobox gene *Lhx1* and odd-skipped-related gene *Osr1* are expressed in lateral plate mesoderm at approximately E8.5. The expression of *Osr1* is observed alongside the antero-posterior axis from the first somite to the caudal region, overlapping the more posterior expression of *Lhx1* which has an anterior boundary at the sixth somite (Dressler, 2009). In addition to being expressed in lateral plate mesoderm, *Osr1* is also expressed in intermediate mesoderm and metanephric mesenchyme and plays an essential role in kidney development (James *et al*., 2006).

The activation of *Pax2* marks the specification of intermediate mesoderm (James and Schultheiss, 2005). *Pax2* is expressed in the intermediate mesoderm and also in the metanephric mesenchyme (Dressler, 2009).

Hox genes encode a family of evolutionary conserved homeobox proteins (Hox) consisting of four clusters: *Hoxa, b, c* and *d* (Di-Po ï*et al*., 2010). They play a role in somite specification along the antero-posterior axis of the mouse embryo (Mallo *et al*., 2010). *Hoxb1* is one of the earliest *Hox* genes to be expressed (Kmita *et al*., 2000; Gadue *et al*., 2006). It was reported in the posterior primitive streak which can give rise to extraembryonic mesoderm (Tam and Loebel, 2007). *Hox10* and *Hox11* genes (*Hoxa10, Hoxa11* and *Hoxd11*) are expressed not only in the posterior paraxial mesoderm but also in the metanephric mesenchyme, and are necessary for metanephros development (Carapu ço *et al*., 2005; Yallowitz *et al*., 2011). *Hoxc9* was reported to be involved in the patterning of the sternum and ribs (Suemori *et al*., 1995); its expression was observed from E8.5 to E16.5 in posterior paraxial mesoderm derivatives, such as the prevertebrae and limb buds. It is also expressed in the developing kidney at E12.5 but the signal is weak (Erselius *et al*., 1990). *Hoxd* cluster genes are involved in limb-specific patterning (Kmita *et al*., 2000).

The *Fox*-encoded forkhead box (Fox) family is another evolutionary conserved group of transcription factors (Jackson, 2010). In the mouse embryo, *Foxf1* is expressed in posterior primitive streak-derived extraembryonic and lateral plate mesoderm at approximately E8.5 (Mahlapuu, 2001). *Foxa2* expression represents the differentiation of anterior primitive streak (Gadue *et al*., 2006). *Foxd1* is known for identifying the metanephric stromal cells following the divergent fate of

Table 5.1 Table of key genes investigated in this study

Genes	Expression Regions	References	Genes	Expression Regions	References
Bra	PS, TB, notocord	a, b	*Foxa2*	Anterior PS	m
Tbx6	PS, PM, TB	a-c	*Foxd1*	MM stroma	n
Cdx2	PS	d-f	*Foxf1*	PS, LPM	0
Lhx1	LPM, IM	g	*Hoxa10*	PM, MM	e, p, q
Osr1	LPM, IM, MM	e, g	*Hoxa11*	PM, MM	e, p, q
Pax2	IM, NC, MM	g, h	*Hoxb1*	Posterior PS	m, r
Wt1	IM, MM	i	*Hoxc9*	Posterior PM	s
Gdnf	MM	j-l	*Hoxd11*	PM, MM	p, q

Notes: PS, primitive streak; PM, paraxial mesoderm; LPM, lateral plate mesoderm; IM, intermediate mesoderm; ND, nephric duct; MM, metanephric mesenchyme; TB, tailbud

a	Papaioannou, 2014	h	James *et al*., 2005	n	Mugford *et al*., 2008
b	Herrmann *et al*., 1990	i	Little, 2015	o	Mahlapuu *et al*., 2001
c	Chapman *et al*., 2003	j	Lin *et al*., 1993	r	Kmita *et al*., 2000
d	Arnold *et al*., 2009	k	Sanchez *et al*., 1996	s	Erselius *et al*., 1990
e	Taguchi *et al*., 2014	l	Basson *et al*., 2006	p	Carapuço *et al*., 2005
f	Savory, *et al*., 2009	m	Gadue *et al*., 2006	q	Yallowitz *et al*., 2011
g	Dressler, 2009				

metanephric mesenchyme (Mugford *et al*., 2008).

Gdnf is a member of the transforming growth factor beta (TGF-beta) family. It is expressed in the metanephric mesenchyme and induces the formation and branching of the ureteric bud, thus serving a critical role in nephrogenesis (Lin *et al*., 1993; Sanchez *et al*., 1996; Basson *et al*., 2006).

Wt1 is expressed in the intermediate mesoderm, metanephric mesenchyme, nascent nephrons, but is restricted to the podocytes as the nephrons mature (Little, 2015).

Objectives

The specific objectives of this chapter were to:

1. Determine the optimal seeding density to generate typical (i.e., cavitating) embryoid bodies (EBs) from the *Bra-GFP/Rosa26-E2C* mESC reporter line;
2. Investigate the expression profile of GFP in EBs derived from the *Bra-GFP/Rosa26-E2C* mESC reporter line using real-time imaging and determine the proportion of GFP^+ cells within the population;
3. Determine the proportion of GFP^+ cells within the population following differentiation of the mESC reporter line to mesoderm using a 2-D culture system;
4. Determine the FACS efficiency and the purity of GFP^+ cells generated from *Bra-GFP/Rosa26-E2C* mESCs cultured under 3-D and 2-D differentiation conditions;
5. Compare the expression profile of key genes in GFP^+ mesodermal cells generated from *Bra-GFP/Rosa26-E2C* mESCs cultured under 3-D and 2-D differentiation conditions.

5.2 Results

5.2.1 Optimisation of mESC seeding density for generating typical EBs

It is known that mESC seeding density used to generate EBs can affect their size and differentiation potential (Koike *et al*., 2007). It was therefore important to

establish the optimal seeding density to promote the generation of typical EBs, that similar to the mouse embryo, generate extraembryonic endoderm, a basement membrane, a primitive ectoderm epithelium and a proamniotic-like cavity prior to undergoing a gastrulation-like process (see Chapter 1). It was also important to ensure that the introduction of E2C within the *Rosa26* locus did not affect the ability of the $E2C^+$ mESCs to form EBs, nor the ability of the mESCs to differentiate to Bra^+ mesoderm. To do this, the *Bra-GFP/Rosa26-E2C* mESCs were plated at different densities (Table 5.2) and cultivated for 7 days in EB medium. At densities of 2.5×10^5 and 1.25×10^5 cells/mL, aggregates were observed during the first 24 h and cavitated EBs were apparent by day 4, with most EBs within the population having cavitated by day 7. However, at the lower seeding density of 6.25×10^4 cells/mL, many EBs did not develop the typical EBs and failed to cavitate (Figure 5.1).

Table 5.2 Optimisation of seeding density in EB culture system

Cell line	Densities (cells/mL)	Time Points (Day)
Bra-GFP/Rosa26-E2C	6.25×10^4 1.25×10^5 2.5×10^5	4, 7

Mesoderm development was identified in all density conditions, but the expression patterns were different. At 6.25×10^4 cells/mL, GFP was expressed at an earlier stage and peaked on day 4 before decreasing. In contrast, at higher densities, GFP became visible at day 4 or later and the fluorescence signal

increased from day 4 to 7, but there appeared to be more GFP^+ cells in the 1.25×10^5 cells/mL EBs (Figure 5.1). Therefore, given that the EBs developing in the 1.25×10^5 cells/mL density cultures appeared to be typical cavitating EBs that contained a high proportion of GFP^+ cells, we used this plating density in all future experiments.

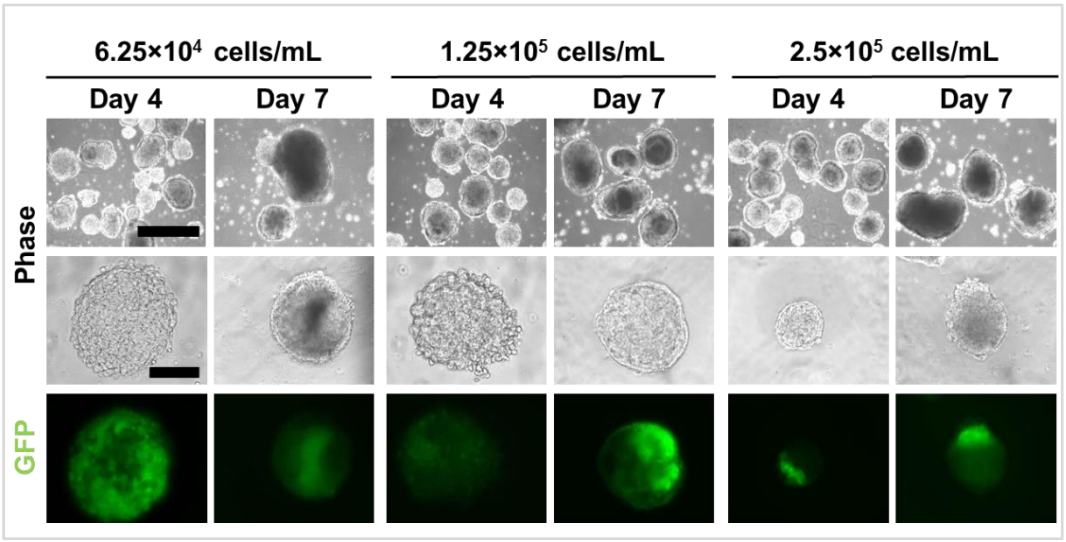

Figure 5.1 Representative fluorescence and phase contrast photomicrographs of EBs derived from E2C mESC reporters at different seeding densities cultured for 7 days. The majority of EBs derived from mESCs plated at densities of 2.5×10^5 and 1.25×10^5 cells/mL showed evidence of cavitation, whereas cavitated EBs were less abundant in the lower density culture (6.25×10^4 cells/mL). Maximal levels of GFP were observed in day 7 EBs derived from the 1.25×10^5 density cultures. Data were collected from three biological replicates. Scale bars, 400 µm (top panel) and 100 µm (middle and bottom panels)

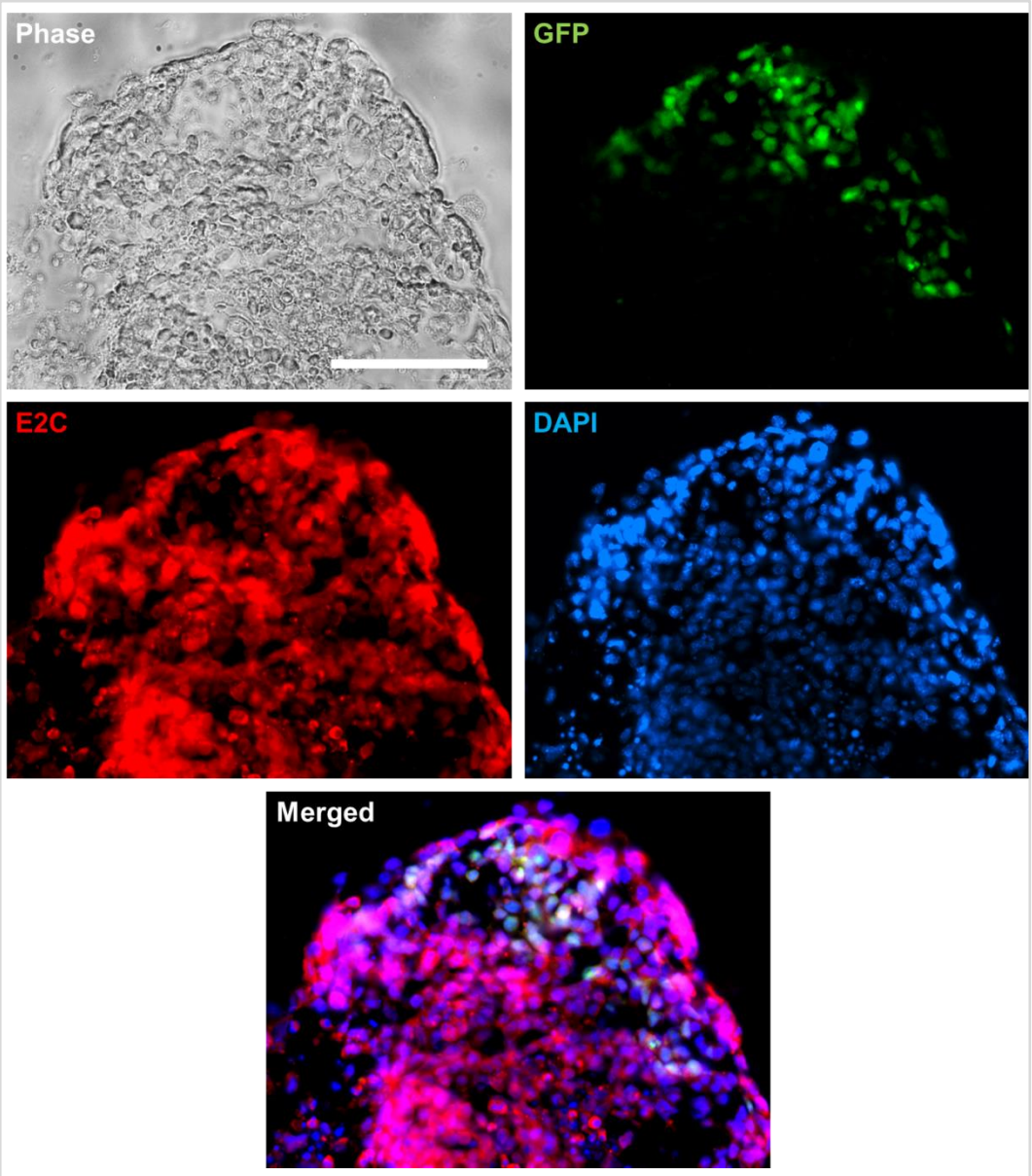

Figure 5.2 Immunostaining for E2C (red) in EBs derived from E2C mESC reporter line. Immunostaining of frozen sections of EBs harvested at day 7 showed that all cells within the EBs derived from the E2C mESCs stained positively for E2C, including the GFP^+ mesodermal cells. Scale bar, 100 μm (all graphs).

To investigate if E2C expression affected mesoderm differentiation, immunostaining of *Bra-GFP/Rosa26-E2C* EB sections was performed to confirm that the GFP^+ cells within the EB expressed E2C. The results showed that all cells within the *Bra-GFP/Rosa26-E2C* EBs expressed E2C, including the GFP^+

mesodermal cells, indicating that E2C expression did not inhibit mesoderm differentiation (Figure 5.2).

5.2.2 Investigating the expression profile of GFP in EBs derived from the *Bra-GFP/Rosa26-E2C* mESC reporter line using real-time imaging and determining of the proportion of GFP^+ cells within the population

In order to accurately monitor changes in GFP expression in the developing EBs over time, *Bra-GFP/Rosa26-E2C* mESCs were plated at a density of 1.25×10^5 cells/mL and at day 3, were embedded in a sandwich-like agarose system (2% agarose bottom layer+EB+1% agarose overlay) and imaged in real-time using the Cell-IQ instrument every hour from day 3 to day 9 post plating. Data were collected from a total of 386 EBs. GFP started to be expressed on day 5, and reached maximum levels on day 6–7. Although expression levels began to decrease at this time point, GFP^+ cells were still present at day 9 (Figure 5.3).

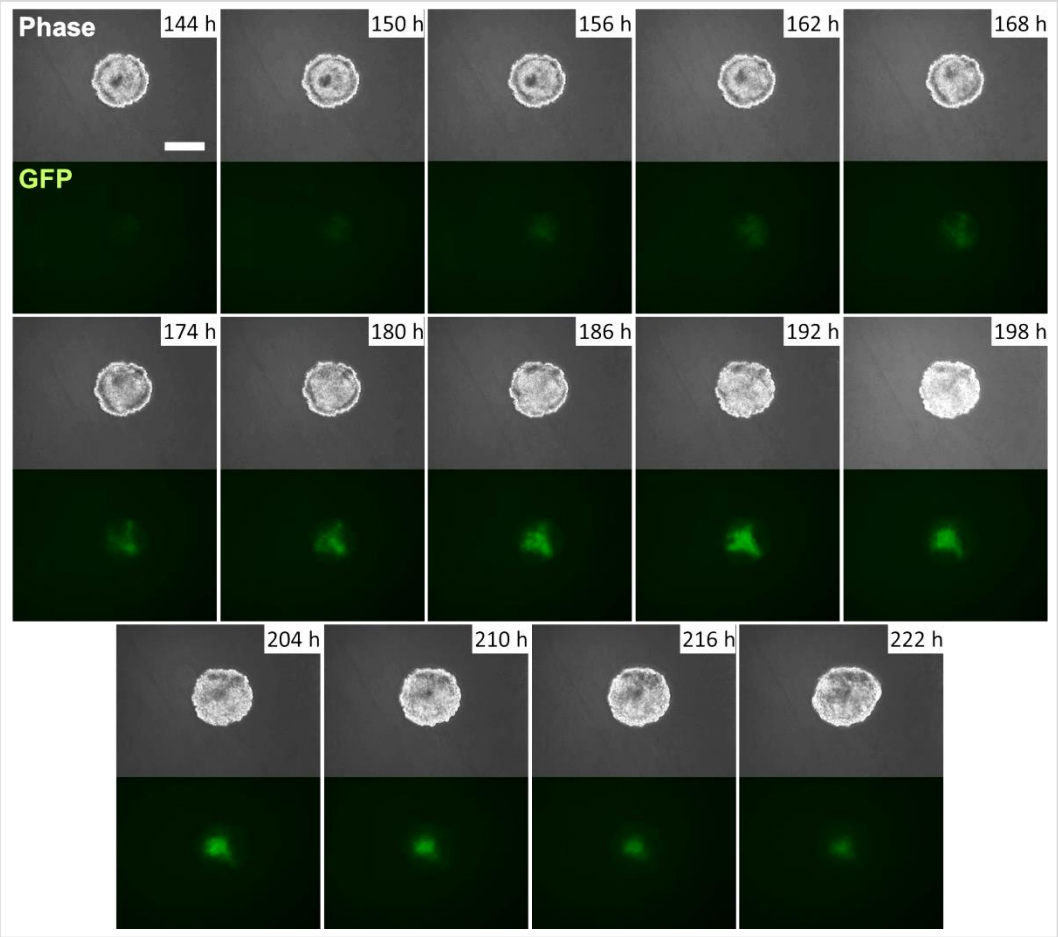

Figure 5.3 Representative fluorescence and phase contrast photomicrographs of EBs derived from *Bra-GFP/Rosa26-E2C* mESCs. Images were taken every hour. 386 EBs were analysed. Scale bar, 200 µm (all graphs).

To quantify the proportion of mesodermal cells within the EBs, flow cytometry analysis was performed. EBs derived from the wild-type E14TG2a mESCs were used as a negative control. The results were consistent with the Cell-IQ data, and showed that the peak GFP expression was day 6, at which time, approximately 39% of the EB population were GFP^+ (Figure 5.4).

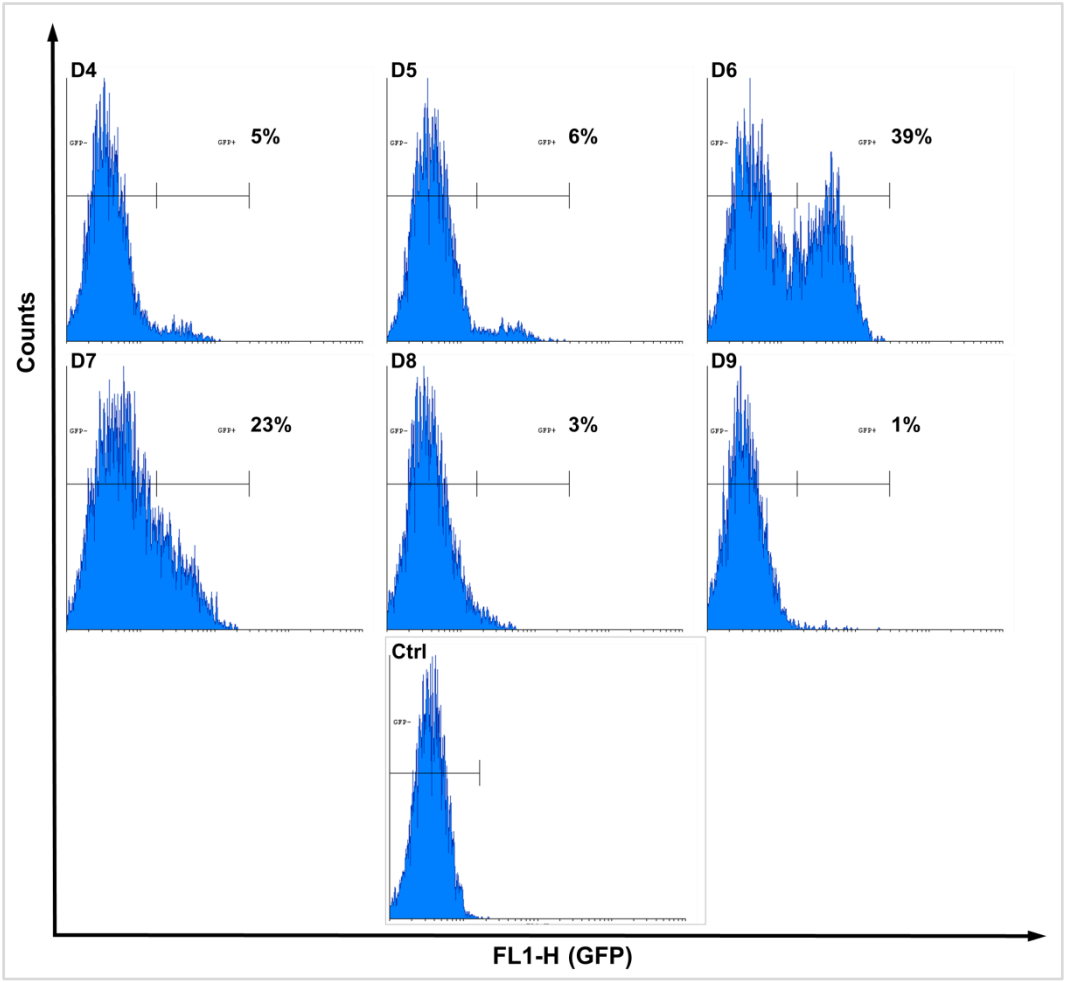

Figure 5.4 Flow cytometry analysis of disaggregated *Bra-GFP/Rosa26-E2C* EBs at different time points. Data showed that GFP started to be expressed on day 5, and reached maximum levels on day 6–7. At the peak of expression (day 6), GFP^+ cells comprised 39% of the population.

5.2.3 Determining the proportion of GFP^+ cells within the population following differentiation of the mESC reporter line to mesoderm using a 2-D culture system

To direct mesoderm differentiation using a 2-D culture system, we followed a method recently published by Turner *et al*, which involves culturing mESCs without feeders in serum free medium containing Activin and Chiron (Turner *et*

al., 2014a). To determine the efficiency of this culture system, the *Bra-GFP/Rosa26-E2C* mESCs were cultured under differentiation conditions for 4 days, and were then screened for GFP expression. Analysis of fixed cells in culture showed that the vast majority of the population expressed GFP. Flow cytometry analysis showed that approximately 89% of the population was GFP^+, which is consistent with the efficiency reported previously with this method (Figure 5.5).

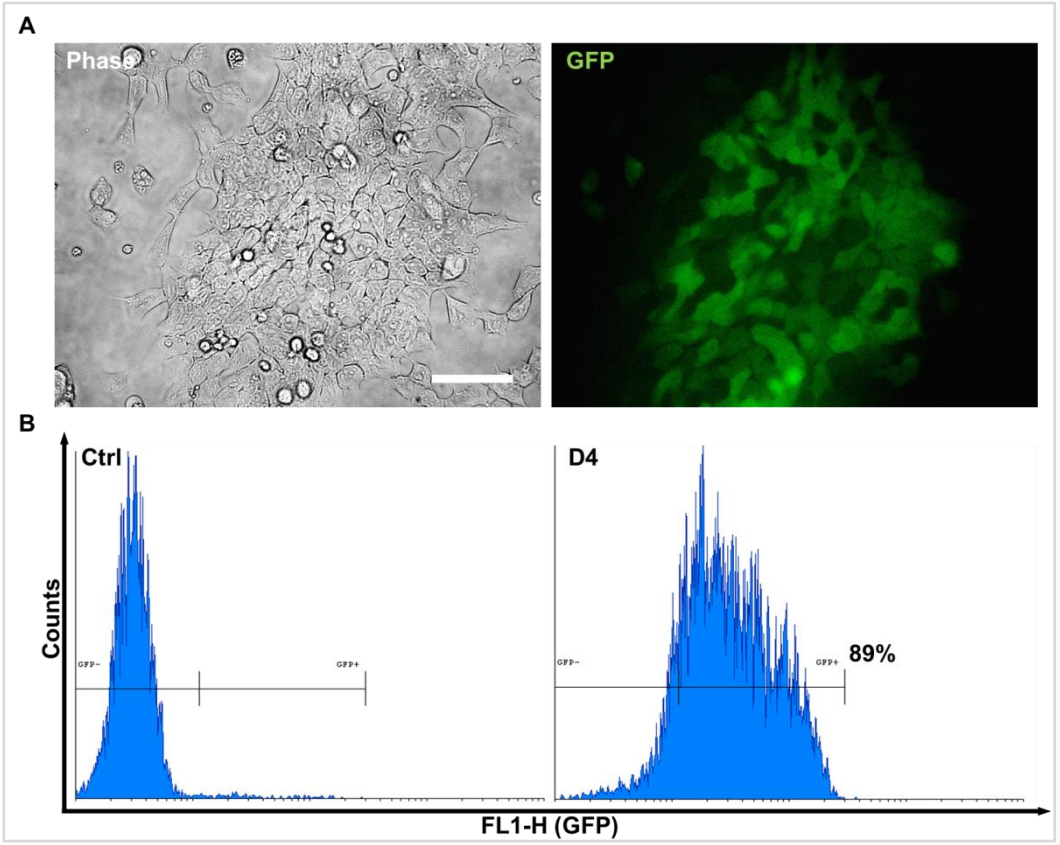

Figure 5.5 Analysis of GFP expression in *Bra-GFP/Rosa26-E2C* mESCs following directed differentiation to mesoderm using a 2-D culture system. (A) Following induction, cells no longer formed colonies, appeared differentiated, and the majority expressed GFP. (B) 4 days following growth under differentiation culture, flow cytometry analysis showed that ~89% of cells expressed GFP. Undifferentiated *Bra-GFP/Rosa26-E2C* mESCs sub-cultured in gelatinised dishes in mESC medium for 24 h prior to induction were used as a negative control. Scale bar, 100 µm (all graphs).

5.2.4 Determining the FACS efficiency and the purity of GFP$^+$ cells generated from *Bra-GFP/Rosa26-E2C* mESCs cultured under 3-D and 2-D differentiation conditions

Before comparing the expression levels of the key target genes in the GFP$^+$ cells isolated from the 3-D and 2-D culture systems, it was first necessary to confirm that the GFP$^+$ cells isolated from each culture system were true mesodermal cells.

Single cell suspensions from day-6 EBs and day-4 2-D monolayer cultures were generated. Both Bra-GFP$^+$ and Bra-GFP$^-$ populations from 3-D and 2-D systems were sorted. At the end of sorting, samples were re-analysed using the same parameters by defining a contamination portion (e.g. Bra-GFP$^-$ cells) comprising less than 1% of the sorted populations (e.g. Bra-GFP$^+$ cells), thus verifying the purity of individual groups. Results showed that sorting purity of GFP$^+$ cells was over 94% (Figure 5.6), confirming they were pure populations.

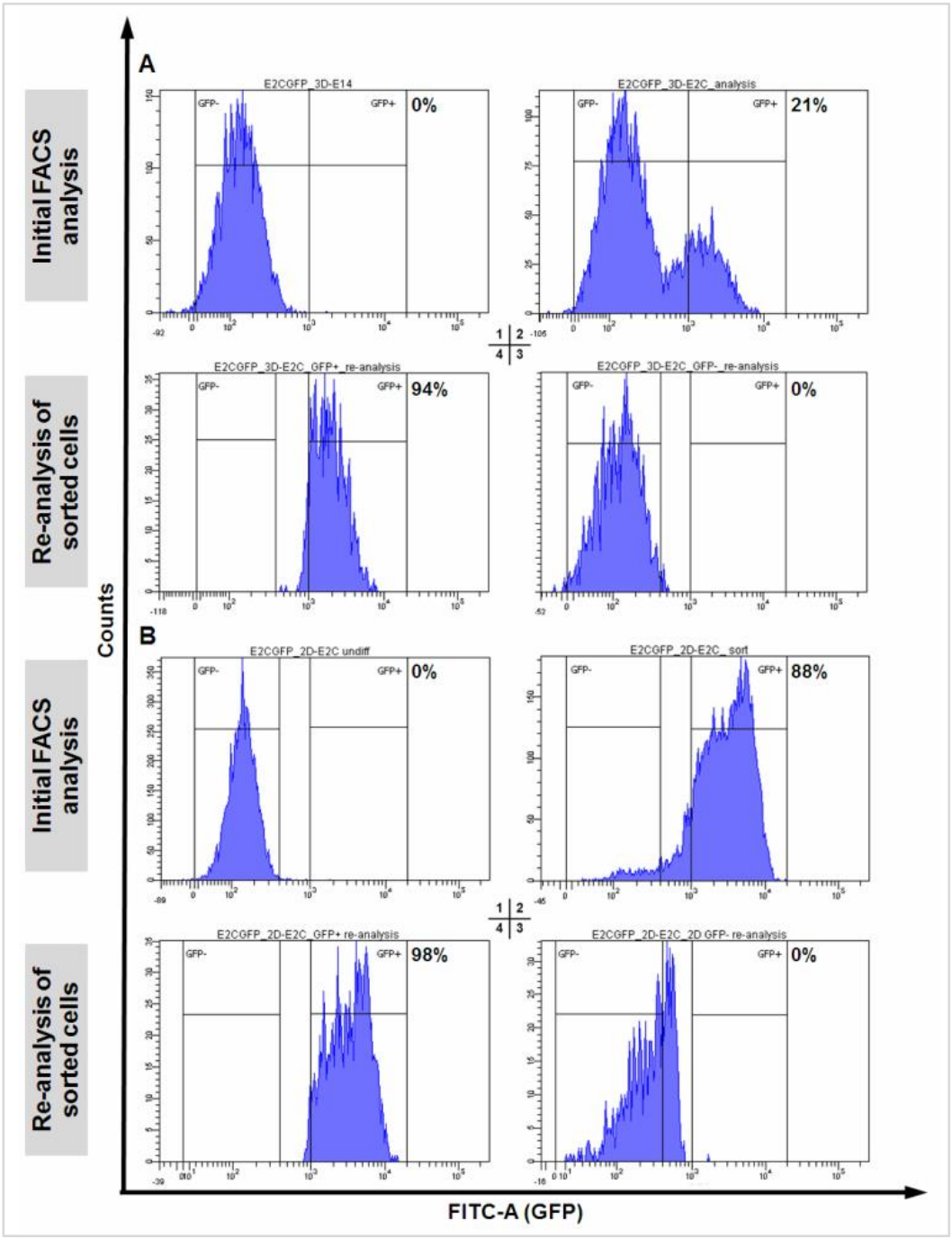

Figure 5.6 Flow cytometry analysis of Bra-GFP$^+$ populations sorted from 3-D (A) and 2-D (B) systems using FACS. Day-6 EBs from E2C reporter mESCs were harvested for sorting (A2). Untransfected day-6 *E14-Bra-GFP* EBs were employed as the negative control (A1). For 2-D, E2C reporter mESCs induced for 48 h were harvested (B2). E2C reporter mESCs maintained undifferentiated in gelatinised dishes in mESC medium for 24 h prior to induction were employed as the negative control (B1). All of the sorted cells using flow cytometry to confirm the purity of the populations isolated using FACS (A3–4, B3–4).

5.2.5 Comparing the expression profile of key genes between the GFP$^+$ mesodermal cells generated from the *Bra-GFP/Rosa26-E2C* mESC reporter line cultured under 3-D and 2-D differentiation conditions

In order to characterize the Bra-GFP$^+$ and Bra-GFP$^-$ populations, RT-qPCR was performed to examine the expression patterns of key genes of mesodermal lineages and of early kidney development. Relative gene expression levels were evaluated and compared between the following groups: (i) the Bra-GFP$^+$ and Bra-GFP$^-$ populations isolated from the EBs (3-D system); (ii) Bra-GFP$^+$ and Bra-GFP$^-$ populations isolated from the 2-D system; and (iii) the Bra-GFP$^+$ populations isolated from the 3-D and 2-D systems. Stemness markers *Oct4* and *Nanog* and the primitive ectoderm marker, *Fgf5*, were also evaluated to assess whether the undifferentiated mESCs and/or ectoderm cells were present.

Firstly, comparisons were made between the key gene expression levels in the Bra-GFP$^+$ cells and the Bra-GFP$^-$ cells isolated from the 3-D and 2-D system, respectively. The results showed that the early mesoderm genes *Bra*, *Cdx2*, *Tbx6*, *Foxf1*, *Foxa2*, *Hoxb1* and *Hoxc9* were expressed by Bra-GFP$^+$ cells isolated from both the 3-D and 2-D systems, but the relative expression levels differed in comparison to the respective Bra-GFP$^-$ populations. For instance, under the 3-D conditions, the expression levels of *Bra*, *Cdx2*, *Tbx6*, *Foxf1*, and *Hoxb1* in the Bra-GFP$^+$ population were approximately 55-, 10- , 40-, 10- and 55-fold higher than in the Bra-GFP$^-$ population, respectively, whereas under the 2-D conditions,

Bra, *Tbx6* and *Hoxb1* levels in the Bra-GFP$^+$ cells were only respectively 2-, 4-, and 5-fold higher than in the Bra-GFP$^-$ cells (Figure 5.7A, C).

There was a 1- to 10-fold up-regulation of Hox10 and Hox11 paralogy groups (*Hoxa10*, *Hoxa11* and *Hoxd11*) in the Bra-GFP$^+$ population compared to the Bra-GFP$^-$ population isolated from cells under 3-D conditions. In contrast, down-regulation of the same genes was observed in the Bra-GFP$^+$ population isolated from cells under 2-D conditions compared to the Bra-GFP$^-$ population (Figure 5.7A, C). This suggested that the status of Bra-GFP$^+$ cells isolated from EBs may be closer to a stage resembling posterior mesoderm, as it has been shown previously that posterior mesoderm, which gives rise to the MM, expresses higher levels of *Hox10* and *11* genes compared to anterior mesoderm (Taguchi *et al*., 2014).

Genes of intermediate mesoderm and metanephric mesenchyme, i.e., *Lhx1*, *Osr1*, *Pax2* and *Wt1*, displayed a similar trend in the change of relative expression levels between the Bra-GFP$^+$ and Bra-GFP$^-$ groups under 3-D and 2-D conditions. It is of note that in the cells isolated from the EBs, *Lhx1* was up-regulated by approximately 10-fold in the Bra-GFP$^+$ cells compared to the Bra-GFP$^-$ cells, whereas there was minimal up-regulation in the Bra-GFP$^+$ cells isolated from the 2-D conditions (Figure 5.7A, C).

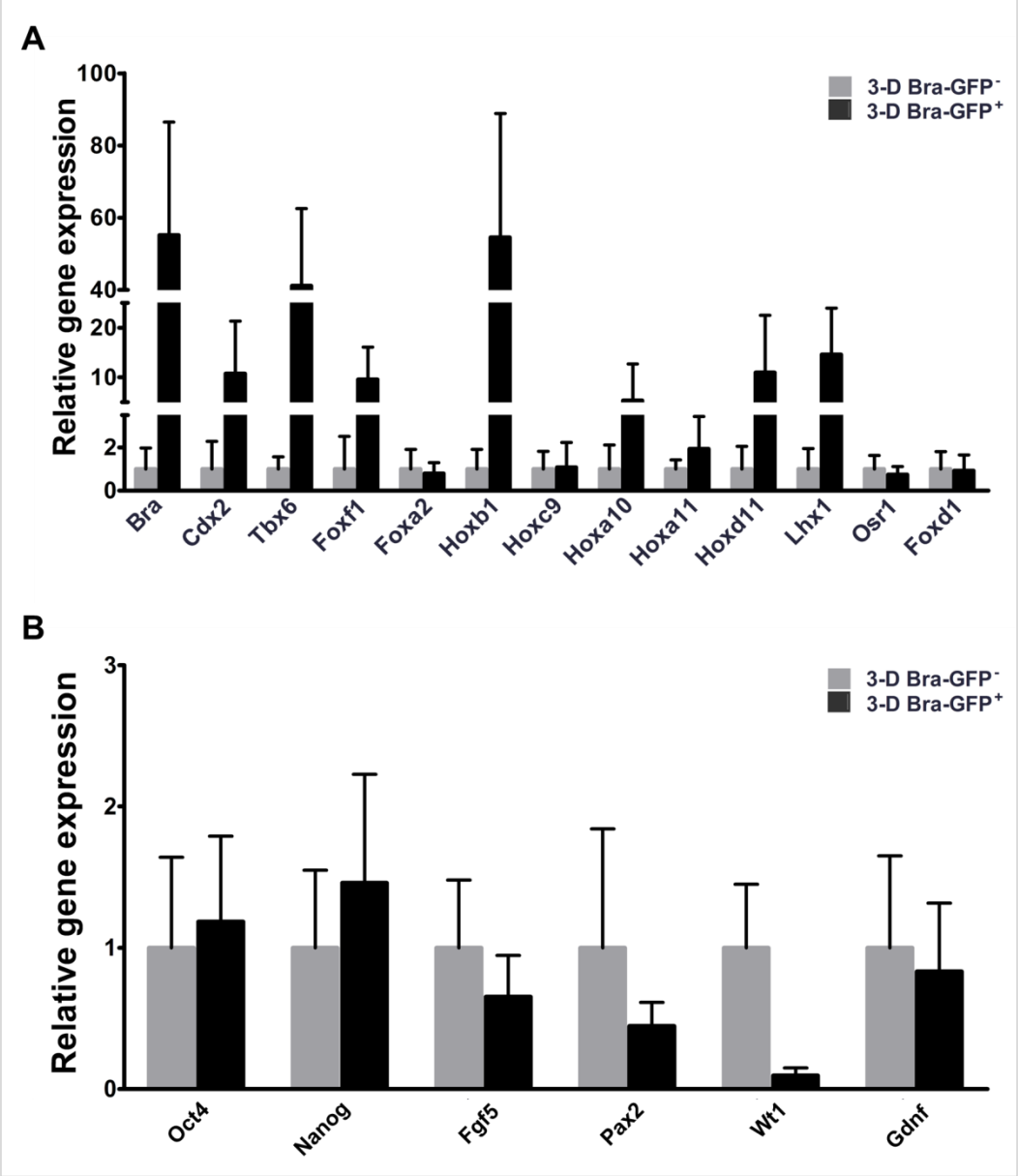

Figure 5.7 Expression levels of mesoderm and early kidney development key genes in the FACS-sorted Bra-GFP$^+$ and Bra-GFP$^-$ populations isolated from 3-D and 2-D systems. Relative expression levels were compared between Bra-GFP$^+$ and Bra-GFP$^-$ populations isolated from 3-D system (A–B, n=2), 2-D system (C–D, n=2). Error bars represent the range of value change.

(continued on next page)

(continued from previous page)

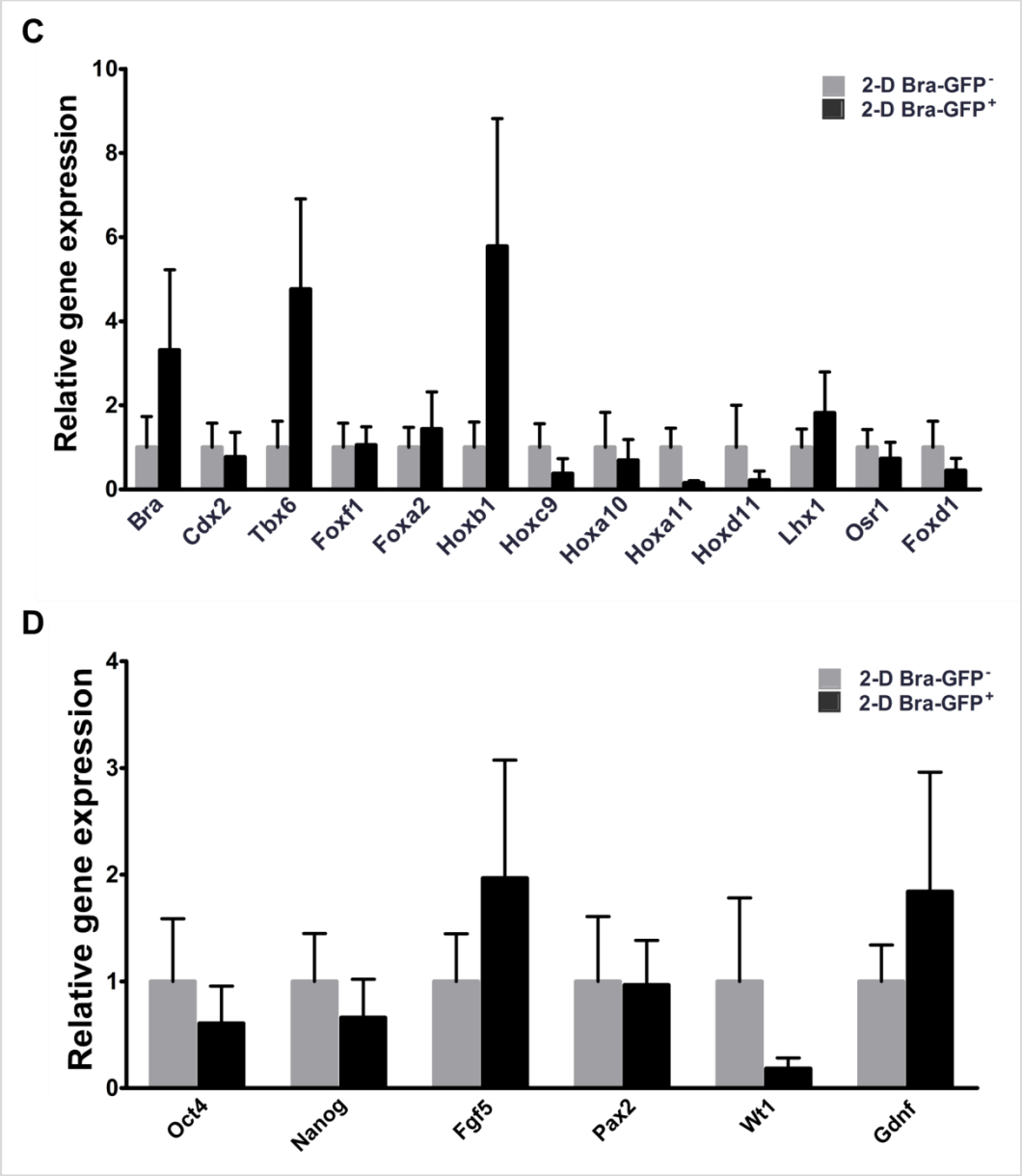

Figure 5.7, continued.

Oct4, Nanog and Fgf5 were also evaluated and the data showed no difference between the Bra-GFP$^+$ cells and Bra-GFP$^-$ cells isolated from both 3-D and 2-D conditions (Figure 5.7B, D).

Next, the relative expression levels of the various genes in Bra-GFP$^+$ cells isolated from 3-D and 2-D system was compared.

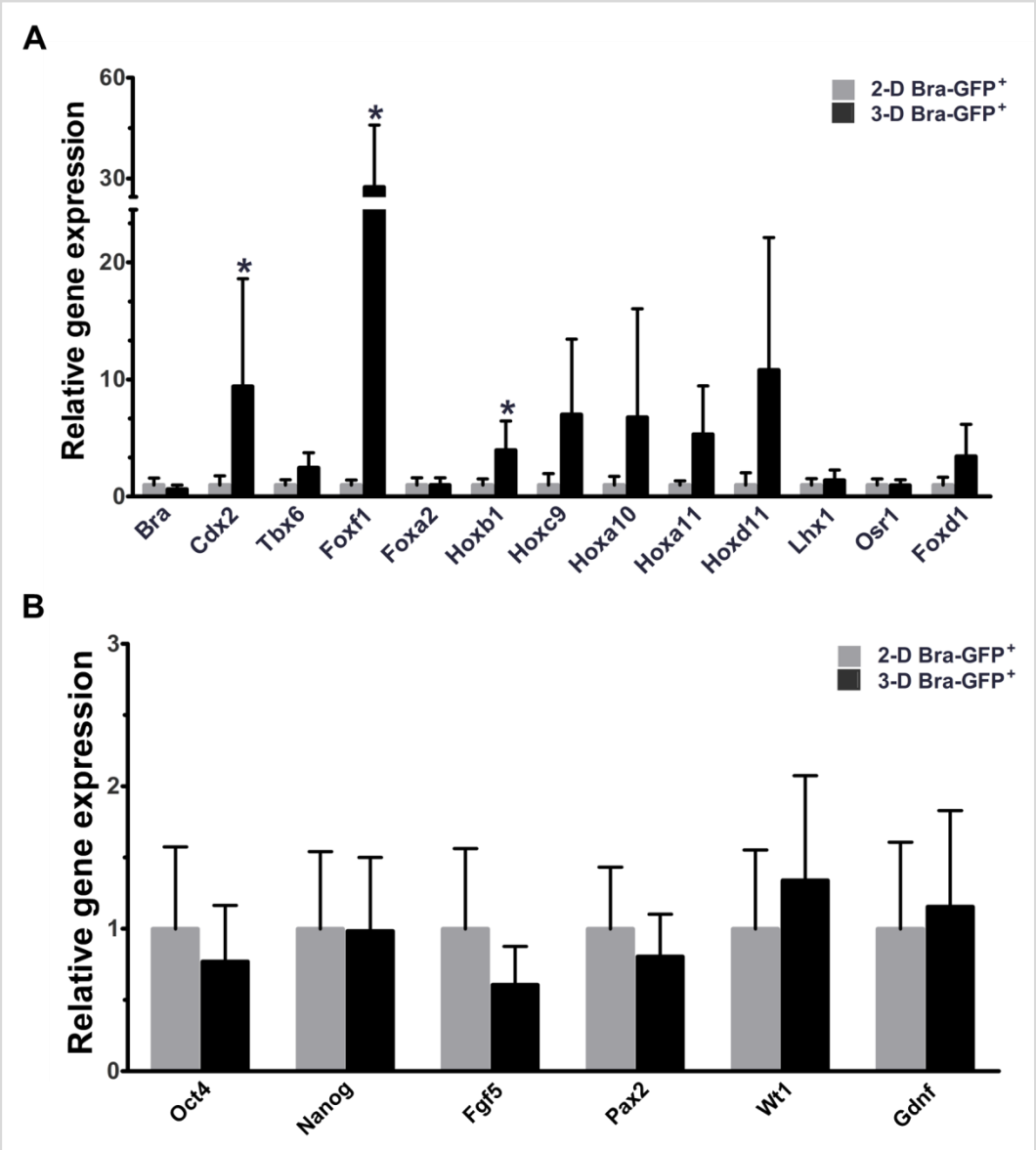

Figure 5.8 Expression levels of mesoderm and early kidney development key genes in the FACS-sorted Bra-GFP$^+$ populations isolated from 3-D and 2-D systems. Relative expression levels were compared between Bra-GFP$^+$ populations isolated from 3-D system (A, n=3) and 2-D system (B, n=3). Error bars represent ±SEM. $p<0.05$ (asterisks) was considered as statistically significant (*t*-test).

There was no significant difference in the expression levels of *Bra* and *Tbx6*,

whereas *Cdx2*, *Foxf1* and *Hoxb1* were significantly up-regulated by 9-, 30-, 5-fold, respectively, in the Bra-GFP$^+$ cells isolated under 3-D conditions. Another early mesoderm gene *Hoxc9* as well as posterior mesoderm genes *Hox10* and *Hox11* were also up-regulated but not significantly. The expression levels of *Lhx1*, *Osr1*, *Pax2*, *Wt1* and *Gdnf* were comparable between the two populations. On the other hand, *Foxd1*, which, is expressed in MM and stroma, showed a slight 2-fold up-regulation in the 3-D Bra-GFP$^+$ cells (Figure 5.8).

5.3 Discussion

In this chapter, mesoderm populations were generated from a *Bra-GFP/Rosa26-E2C* mESC reporter line using 3-D and 2-D differentiation conditions. Bra-GFP$^+$ cells were acquired following the optimisation and evaluation of the culture systems. The expression levels of key genes of mesoderm and early kidney development were then analysed using quantitative RT-PCR.

The dynamics of GFP expression during EB culture was similar to what has been previously observed in our group (Rak-Raszewska, 2010); i.e., at low seeding density, GFP appeared to peak earlier than at higher seeding densities. A possible explanation is that mESCs might express inhibitors of mesoderm differentiation, such as noggin, which would be present at higher levels in higher density cultures, and might therefore delay mesoderm differentiation (GFP expression) (Gratsch

and O'Shea, 2002; Tonegawa and Takahashi, 1998). Also, GFP expression was detected in EBs generated at low density that had not cavitated. This is similar to our lab's previous findings using the same *E14-Bra-GFP* mESC line (Rak-Raszewska, 2010). In that study, GFP was only expressed within the EBs during days 3 to 4 with about 60% of the population expressing GFP at day 4 (Rak-Raszewska, 2010). This is much higher than the proportion we observed in the current study (less than 40%). However, EBs generated using Fehling's method did not form a proamniotic-like cavity, extra-embryonic endoderm or basement membranes. It is therefore envisaged that the properties of Bra^+ mesoderm cells generated from the two types of EBs (i.e., cavitating or non-cavitating), might have different properties and differentiation potential.

An interesting finding from the RT-qPCR analysis was that the expression levels of *Bra* in the GFP^+ cells isolated from the 3-D system were approximately 50 times higher than in the GFP^- cells, but *Bra* levels in GFP^+ cells isolated from the 2-D system were only approximately three times higher than in the corresponding GFP^- cells. Yet despite this, when *Bra* levels in the GFP^+ cells from the 3-D system were directly compared with levels in GFP^+ cells from the 2-D system, there was no significant difference. A possible explanation for this is that the GFP^- cells in the EBs are likely to be endoderm or ectoderm cells that do not express *Bra*, whereas in the 2-D system, it is possible that the GFP^- cells might be committed to the mesodermal lineage and have started to up-regulate *Bra*, but due

to the time-lag between transcription and translation, might not have yet started to produce GFP. If this were the case, such cells would be Bra^+ but GFP^-, and would thus have been sorted into the GFP-negative fraction by FACS.

When comparing the expression levels of key genes between the GFP^+ cells from the 3-D and 2-D systems, there were only three genes that were significantly up-regulated in the cells from 3-D system, namely, *Foxf1*, *Cdx2* and *Hoxb1*. The high expression levels of *Foxf1* might suggest that the GFP^+ cells from the 3-D system might be lateral plate mesoderm cells. It is known that high levels of BMPs promote the differentiation of lateral plate mesoderm, whereas low levels of BMPs promote intermediate mesoderm (Tonegawa and Takahashi, 1998). It is therefore possible that in the larger cavitating EBs, there might be higher levels of BMPs which would then drive the differentiation of lateral plate mesoderm. However, the cells also had significantly higher levels of the nascent mesoderm gene, *Cdx2*, and the posterior mesoderm gene, *Hoxb1*. Furthermore, although not significant, there was a clear trend that the *Hox* genes tested, which are expressed in intermediate mesoderm, were up-regulated in the cells from the 3-D system.

In summary, it can be seen that the expression profiles of some key mesodermal lineage genes are different depending on whether the cells are derived from the 3-D and 2-D culture systems, and are also different from GFP^+ cells isolated previously in our lab from non-cavitating EBs, which expressed very low levels of

Foxf1 (Rak-Raszewska, 2010). In the next chapter, the differentiation potential of the cells will be tested by incorporating them into mouse kidney rudiments *ex vivo*.

Chapter 6

Evaluation of the nephrogenic potential of the mesoderm derived from the *Bra-GFP/Rosa26-E2C* reporter mESCs cultured under the 3-D and 2-D conditions

6.1 Introduction

Mammalian kidney development

Mouse kidney development begins at approximately E8.0 when the intermediate mesoderm gives rise to a pair of nephric ducts which extend along the rostro-caudal axis towards the cloaca (Grote *et al*., 2006; Pedersen *et al*., 2005). It generates three types of excretory organs in a sequential order: the pronephros, the mesonephros and the metanephros. The pronephros form at E8.5 but degenerate by apoptosis (Bouchard *et al*., 2002; Saxén, 1987). The mesonephros arises caudally to the pronephros at around E9.5, but is also transient in mammals and birds (Sainio and Raatikainen-Ahokas, 1999; Saxén, 1987; Tilmann and Capel, 2002). At around E10.5, a region of the intermediate mesoderm at the level of the hindlimb condenses to form the metanephric mesenchyme (MM). The MM cells secrete glial cell-derived neurotrophic factor (Gdnf) that induces outgrowth of the ureteric bud (UB) from the nephric duct (Sainio *et al*., 1997; Hellmich *et al*., 1996). The UB extends into the MM, giving rise to the metanephros (Figure 6.1)

(Saxén, 1987; Costantini and Kopan, 2010).

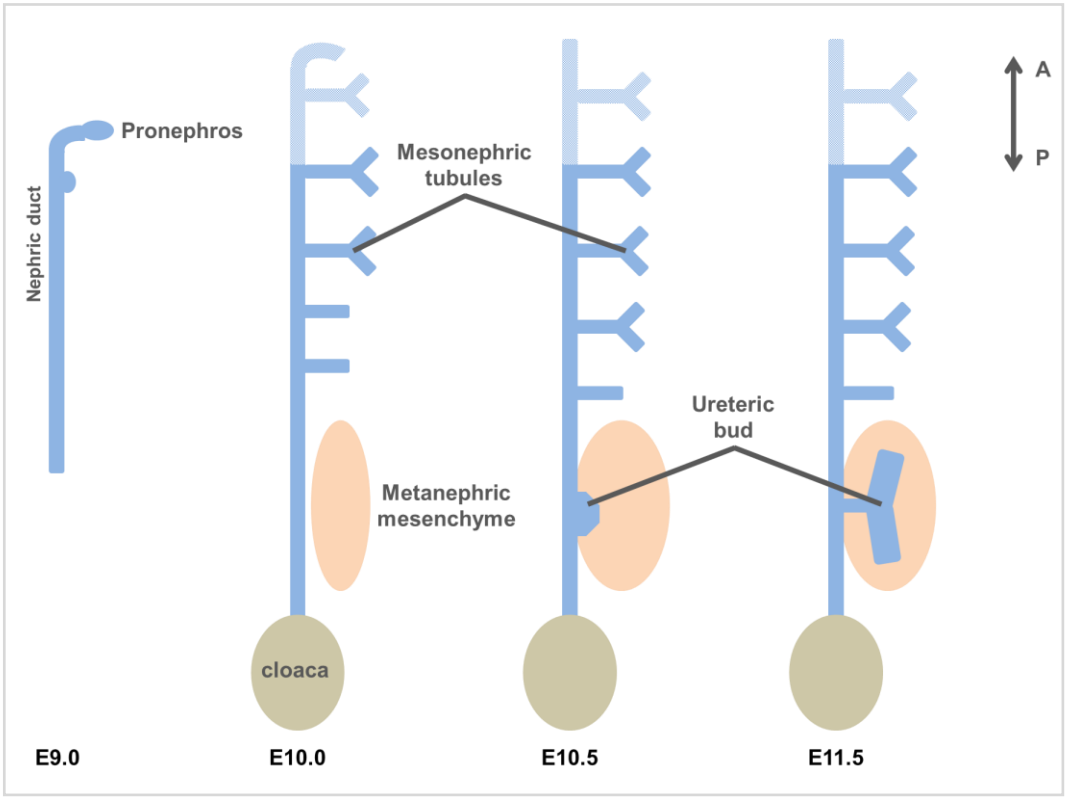

Figure 6.1 Schematic diagram of mouse kidney development from E9.0 to E11.5.

Reciprocal inductive interactions between the UB and the MM lead to repetitive branching of the UB in the MM that respectively develops into the nephrons and collecting duct network of the mature kidney. From E11.5, the MM condenses around the tip of the UBs to form the cap mesenchyme, the progenitor of the nephrons. The MM also gives rise to the kidney stroma. As the UB branches, renal vesicles form from the cap mesenchyme and further generate an epithelial structure called the S-shaped body. The proximal region of the S-shaped body is infiltrated by endothelial cells which develop into a capillary network called the

glomerular tuft. The glomerular tuft comprises afferent and efferent capillaries, the former of which have a larger diameter, thus creating increased pressure within the glomerulus which contributes to glomerular filtration and urine formation. The remaining compartments of the S-shaped body differentiate into proximal and distal tubules of the nephron. The proximal tubules elongate towards the medulla and form Henle's loop which is connected to the distal tubules (Figure 6.2) (Dressler, 2009; Rak-Raszewska *et al*., 2015).

The mechanisms of how the intermediate mesoderm becomes specified as MM and the nephric duct (which gives rise to the UB) are not yet completely defined. It was thought that both the MM and UB were derived from *Osr1*$^{+}$ anterior intermediate mesoderm (Mugford *et al*., 2008). However, recent work from Nishinakamura's group has shown that while the UB and mesonephros are generated from anterior intermediate mesoderm, the MM is derived from *Bra*$^{+}$ posterior mesoderm. This *Bra*$^{+}$*/Osr1*$^{-}$ posterior mesoderm population gives rise to *Bra*$^{-}$*/Osr1*$^{+}$ posterior intermediate mesoderm that expresses *Wt1* and *Hox11*, which gives rise to the MM, which expresses *Pax2* and *Six2* (Taguchi *et al*., 2014).

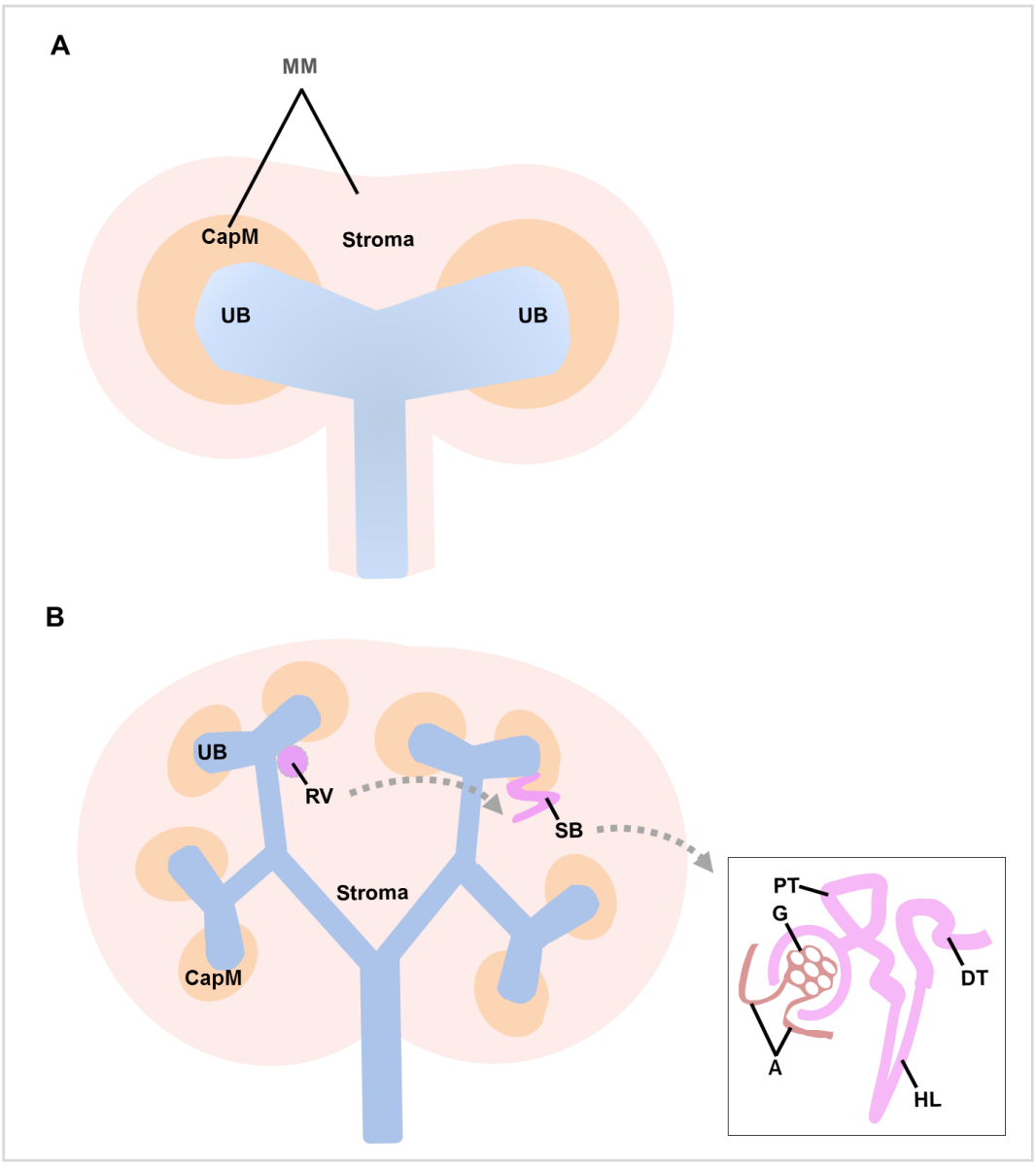

Figure 6.2 Schematic illustration of the early development of metanephric mesenchyme (MM) and ureteric bud (UB) during mouse nephrogenesis. (A) The MM condenses around UBs at E11.5 forming the cap mesenchyme (CapM), while the remaining MM gives rise to the kidney stroma. (B) UBs branch upon reciprocal interaction between themselves and the MM. Renal vesicles (RV) form from the CapM giving rise to the S-shaped body (SB). The SB is infiltrated by endothelial cells which give rise to the glomerular (G) capillary tuft with afferent and efferent arterioles (A). The SB generates all parts of the nephron, including the glomerulus, proximal and distal tubules (PTs, DTs) and Henle's loop (HL).

Testing the nephrogenic potential of stem and progenitor cells

In order to test whether specific types of stem and progenitor cells are able to generate cells of the nephron or UB, our group has previously used an *ex vivo* kidney rudiment culture system developed by the Davies lab (Unbekandt and Davies, 2010). In this system, mouse kidney rudiments are disaggregated to a single cell suspension, mixed with the cell type being tested and centrifuged to promote reaggregation. The chimeric pellet is then cultured on a specific filter membrane at the air–medium interface and the fate of the test cells investigated (Figure 6.3) (Rak-Raszewska *et al*., 2012a; Kuzma-Kuzniarska *et al*., 2012; Ranghini *et al*., 2013; Dauleh *et al*., 2016). Re-aggregated metanephric cells are able to generate nephrons and UBs that appear to undergo the same reciprocal inductive events that occur in intact rudiments, except that there is no longer a contiguous ureteric bud tree. It should also be noted that similarly to intact rudiments, re-aggregated rudiments contain endothelial cells (Halt *et al*., 2016). It was previously thought that endothelial cells rapidly degenerated in kidney rudiments cultured *ex vivo* (Loughna *et al*., 1997), but more recent studies show that endothelial cells are retained and can form networks. However, the endothelial cells do not form typical capillaries with lumen and they do not generate a capillary tuft as they do *in vivo* (Halt *et al*., 2016).

To investigate the fate of any exogenous test cells within chimeric kidney rudiments, it is necessary to introduce a label that enables the cells to be

distinguished from the metanephric cells. Our group has previously labelled the stem or progenitor cells under test with quantum dots (Rak-Raszewska *et al*., 2012a and 2012b; Ranghini *et al*., 2013). However, a disadvantage of quantum dots is that, unlike genetic reporters, they are diluted with each cell division and therefore do not permanently label the cells and their progeny.

Our group has previously used *ex vivo* chimeric kidney rudiments to investigate the nephrogenic potential of Bra^+ mesodermal cells isolated from *E14-Bra-GFP* mESC-derived EBs (Rak-Raszewska *et al*., 2012a). This study showed that the Bra^+ cells could integrate into the developing rudiment and generate functioning proximal tubule cells, podocytes and ureteric bud cells. However, the EBs that were generated in this study were atypical, in that they did not form extraembryonic endodermal cells on their periphery, nor did they form a columnar layer of primitive ectoderm or a proamniotic-like cavity. In the current study, we wished to investigate the nephrogenic potential of Bra^+ cells derived from typical EBs that more closely resemble the early embryo, in that they form extraembryonic endoderm, primitive ectoderm and a proamniotic-like cavity (see Chapter 1). We found in Chapter 5 that, in contrast to atypical EBs where GFP was maximal at day 3−4, GFP expression in the more typical cavitating EBs tended to be expressed later and persist for longer. This led us to hypothesise that GFP^+ cells isolated from the later time points of typical EBs (i.e., day 6) might resemble the posterior mesoderm that gives rise to the MM. If this were the case,

we would expect that these GFP$^+$ cells would only generate MM derivatives and would not integrate into UBs. A further aim of the current study was to assess the nephrogenic potential of Bra$^+$ cells generated from a recently-developed 2-D differentiation system, in order to assess whether their differentiation potential was equivalent to the Bra$^+$ cells generated from the typical EBs.

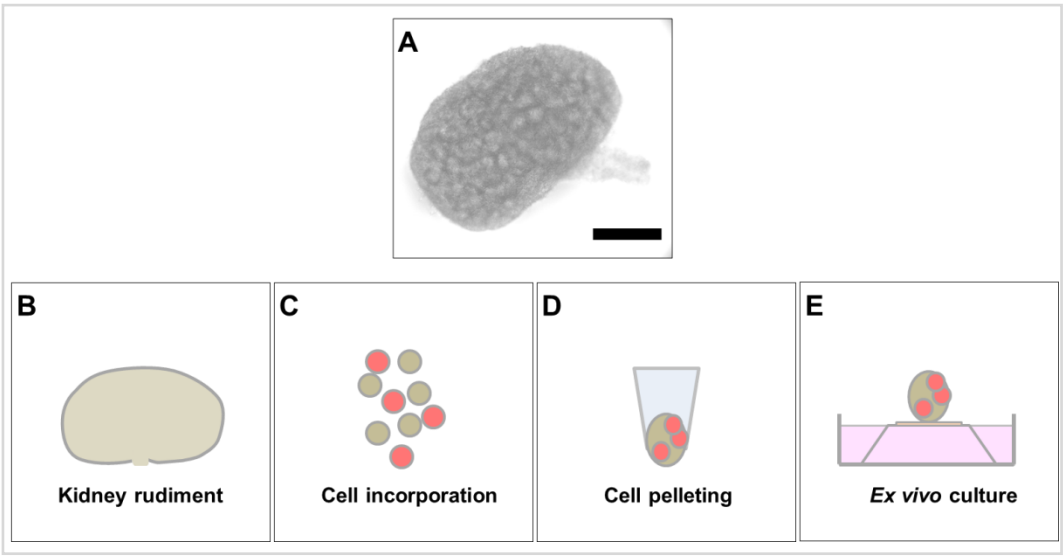

Figure 6.3 Schematic illustration of the method for generating chimeric rudiments *ex vivo* culture. E13.5 embryonic kidneys were dissected (A, bright field). Rudiments were isolated and enzymatically dissociated to form a single cell suspension (B). GFP+ cells were isolated using FACS from either 3-D or 2-D culture systems and were mixed with the dissociated rudiment cells (C) and pelleted (D). The pellets were transferred onto a filter membrane and cultured at the air–medium interface (E). Scale bar, 50 µm.

Experimental design

E13.5 CD1 mouse kidney rudiments were dissociated and Bra-GFP$^+$ cells sorted from either 3-D or 2-D culture systems of the *Bra-GFP/Rosa26-E2C* reporter mESCs. Bra-GFP$^+$ and rudiment cells were mixed at a ratio of 1:9 and centrifuged

to acquire chimeric pellets, each of which comprised 2×10^5 cells. Positive control chimeras comprised GFP^+ mouse neonatal kidney-derived stem cells instead of the Bra-GFP^+ cells, as the former have previously been shown to integrate into developing nephrons and generate podocytes and proximal tubule cells (Ranghini *et al*., 2013) A further control comprised non-chimeric re-aggregated rudiments that did not contain any additional cell types. Pellets were analysed on day 0 and day 5. Intact E13.5 rudiments cultured *ex vivo* for 5 days served as a control for the various immunostainings. Details of protocols are described in Chapter 2.

Objectives

The specific objectives of this chapter were to:

1. Establish the staining pattern of key genes of renal development using intact mouse kidney rudiments cultured *ex vivo*;
2. Confirm that re-aggregated non-chimeric mouse kidney rudiments cultured *ex vivo* develop similarly to intact rudiments;
3. Confirm that positive control chimeric kidney rudiments comprising mouse kidney-derived stem cells develop similarly to intact rudiments;
4. Investigate the behaviour of the two different types of mESC-derived Bra-GFP^+ cells within the chimeric kidney rudiments cultured *ex vivo*.

6.2 Results

6.2.1 *Ex vivo* development of intact kidney rudiments

In order to evaluate how the Bra-GFP$^+$ cells behave in the rudiment culture, it was first necessary to establish the typical staining pattern of various renal cell-specific antibodies in intact kidney rudiments cultured *ex vivo*. Following 5 days of *ex vivo* culture, the rudiments were fixed and immunofluorescence was performed to detect the following markers: megalin, which is expressed on the apical surfaces of proximal tubule cells; Wt1, which is expressed in MM and developing nephrons, and expressed at very high levels in nascent and mature podocytes (Ranghini *et al*., 2013; Taguchi *et al*;., 2014); synaptopodin, which is expressed in mature podocytes. The rudiments were also stained with rhodamine-labeled peanut agglutinin (PNA), which mainly binds to the basement membranes of ureteric buds, and more weakly to those of the developing nephrons (Laitinen *et al*., 1987). PNA staining showed an intact ureteric bud tree and immunostaining for megalin showed typical staining of the apical surfaces of proximal tubule cells (Figure 6.4). As expected, immunostaining for Wt1 showed weaker expression in MM and developing nephrons and intense expression in nascent and mature podocytes, whereas synaptopodin was exclusively expressed in mature podocytes (Figure 6.4).

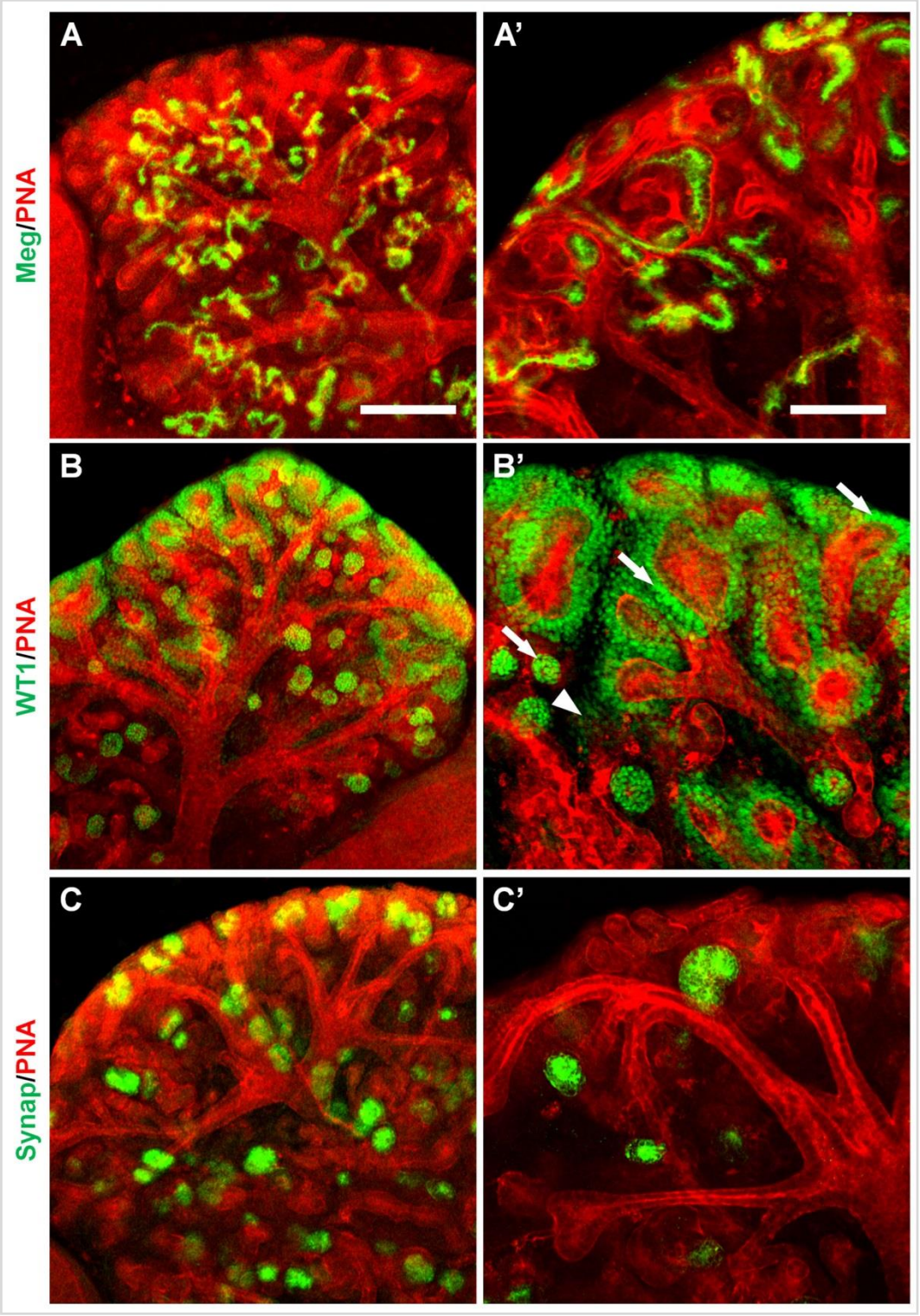

Figure 6.4 Confocal photomicrographs of intact kidney rudiments cultured *ex vivo* for 5 days. Proximal tubules were positively stained for megalin (Meg, green) and PNA (red). Developing glomeruli were immunostained for Wt1 (green) and synaptopodin (Synap, green) positive staining. Arrows point to developing podocytes and arrowheads point to MM. Scale bars, 200 µm (A−C) and 100 µm (A'−C').

6.2.2 *Ex vivo* development of re-aggregated non-chimeric mouse kidney rudiments

To confirm that re-aggregated kidney rudiments could develop nephron and ureteric bud structures as previously reported (Ranghini *et al*., 2013; Rak-Raszewska *et al*., 2011), dissociated kidney rudiment cells were pelleted and cultured *ex vivo* prior to staining with the aforementioned markers. Firstly, it was important to confirm that the disaggregation process was effective and that no non-dissociated renal structures were present at the start of the culture period. Therefore, at day 0, rudiments were stained for megalin and PNA. The results showed that no staining was present at day 0, whereas multiple tubular structures were present by day 5 (Figure 6.5).

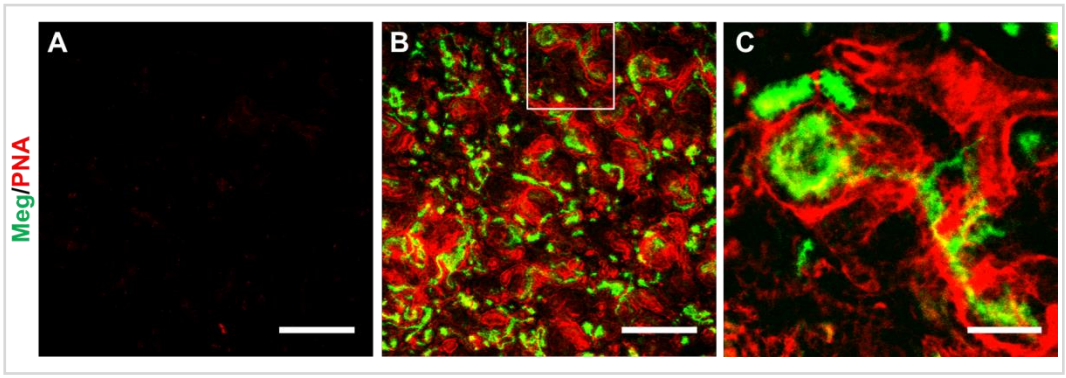

Figure 6.5 Confocal photomicrographs of the re-aggregated non-chimeric rudiments cultured *ex vivo* at day 0 (A) and 5 (B−C). Tubule-like structures formed during the 5-day culture. Meg, megalin (green). Boxed regions outlined are enlarged in the magnified image. Scale bar, 200 µm (A−B) and 50 µm (C).

More detailed analysis of the re-aggregated rudiments showed that the number of tubular structures and nascent glomeruli appeared similar to that of the intact

rudiments, but consistent with previous studies (Ranghini *et al*., 2013; Rak-Raszewska *et al*., 2012a; Kuzma-Kuzniarska *et al*., 2012), although ureteric bud tubules formed, they did not form a contiguous ureteric bud tree (Figure 6.6).

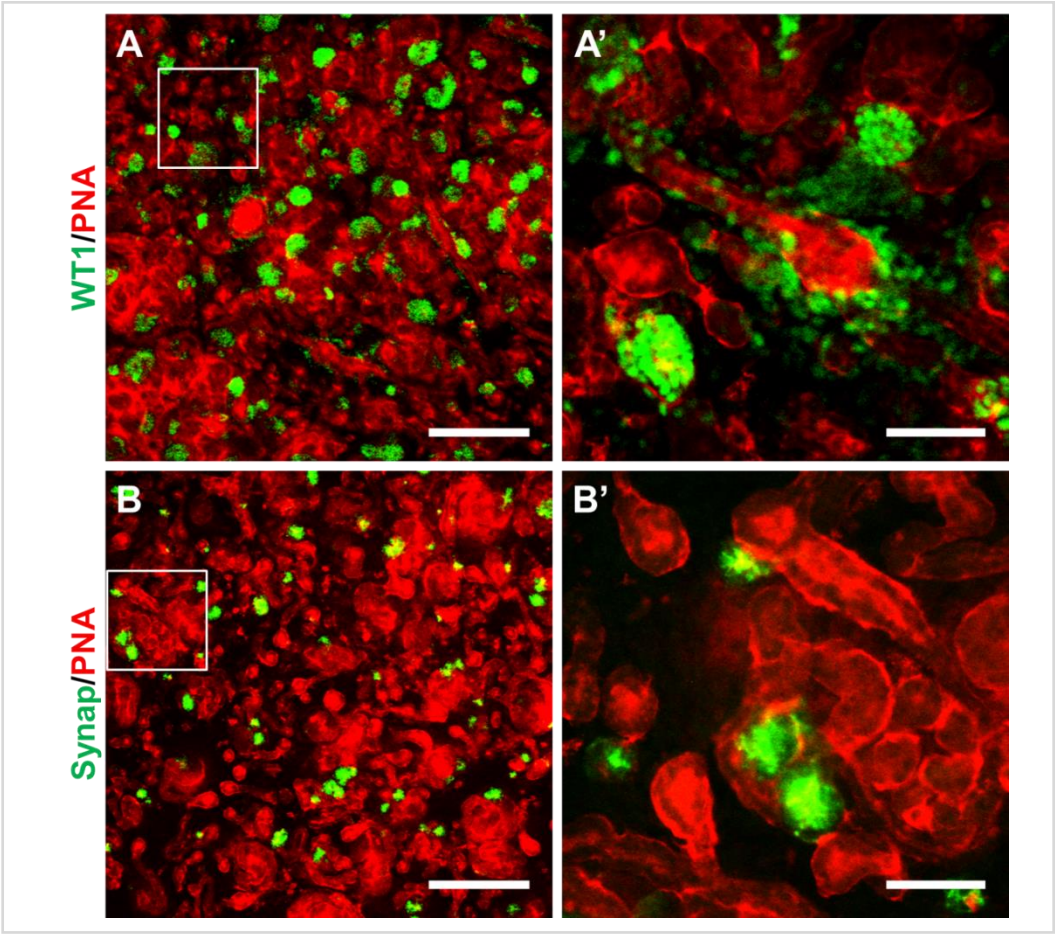

Figure 6.6 Confocal photomicrographs of the re-aggregated non-chimeric rudiments cultured *ex vivo* for 5 days. The re-aggregated rudiments contain tubules and nascent glomerular-like structures that are similar to those of the intact rudiments cultured for 5 days. Meg, megalin (green); Synap, synaptopodin (green). Boxed regions outlined are enlarged in the magnified images. Scale bars, 200 μm (A−B) and 50 μm (A'−B').

6.2.3 *Ex vivo* development of re-aggregated chimeric mouse kidney rudiments comprising mouse kidney-derived stem cells

Before assessing the nephrogenic potential of the mESC-derived Bra^+ cells in the chimeric rudiment assay, it was first necessary to confirm that chimeric rudiments comprising a positive control cell population developed as expected. To this end, chimeric rudiments containing GFP^+ mouse neonatal kidney-derived stem cells (mKSCs) were generated, as we have previously shown that mKSCs can generate proximal tubule cells and podocytes within rudiments (Ranghini *et al.*, 2013). The chimeric rudiments were cultured for 5 days *ex vivo* and analysed as previously using the renal cell-specific markers.

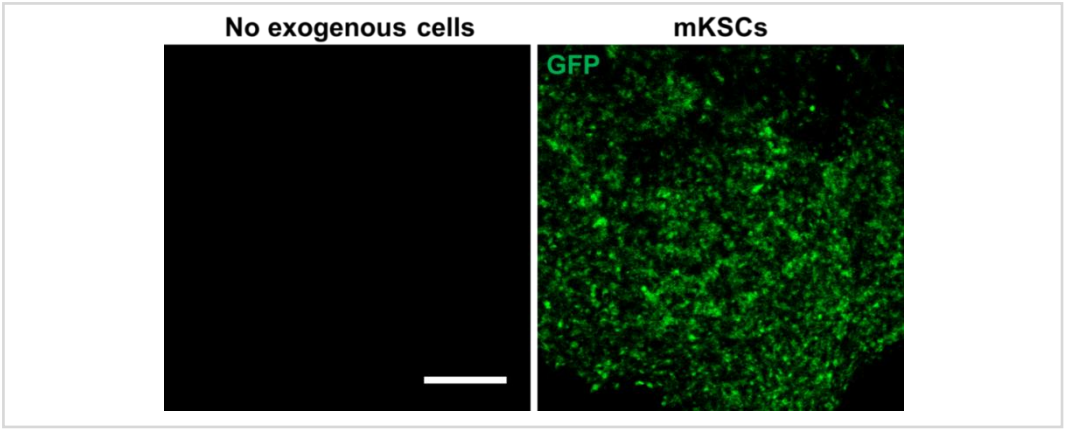

Figure 6.7 Confocal photomicrographs of the re-aggregated pellets at day 0 containing no exogenous cells or GFP^+ mKSCs Positive control GFP+ mKSCs showed even distribution represented by GFP (green) in the pellets at the beginning of the rudiment culture. Scale bar, 200 μm for all images.

On day 0, the mKSCs were evenly distributed in the chimeric rudiments (Figure 6.7). After 5 days of culture, the chimeric rudiments had developed megalin positively-stained proximal tubules as well as nascent glomeruli that contained podocytes, as evidenced by the presence of positive staining for Wt1 and synaptopodin. mKSCs showed integration into the tubules and glomeruli of the

developing nephrons (Figure 6.8).

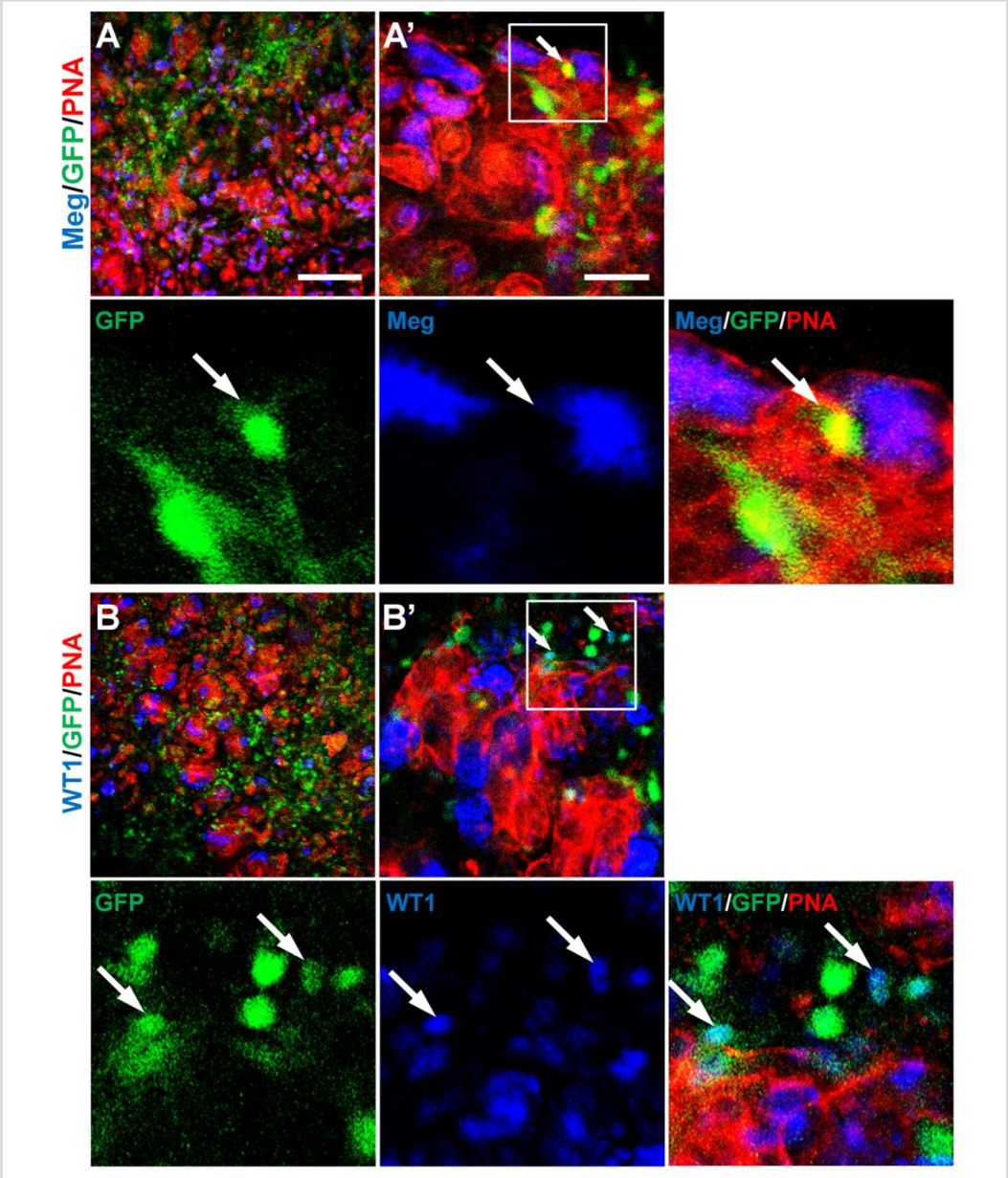

Figure 6.8 Confocal photomicrographs of the GFP$^+$ mKSC chimeric rudiments cultured *ex vivo* for 5 days. mKSCs (green) showed integration into the tubules and glomeruli of the developing nephrons. Arrows point to the integrated KSCs that were GFP-labelled and dual stained by PNA (red), megalin (Meg, blue), Wt1 (blue) or synaptopodin (Synap, blue). Boxed regions outlined in white are represented as the enlargements of the main image frame. Scale bars, 200 μm (A−C) and 50 μm (A'−C').

(continued on next page)

(continued from previous page)

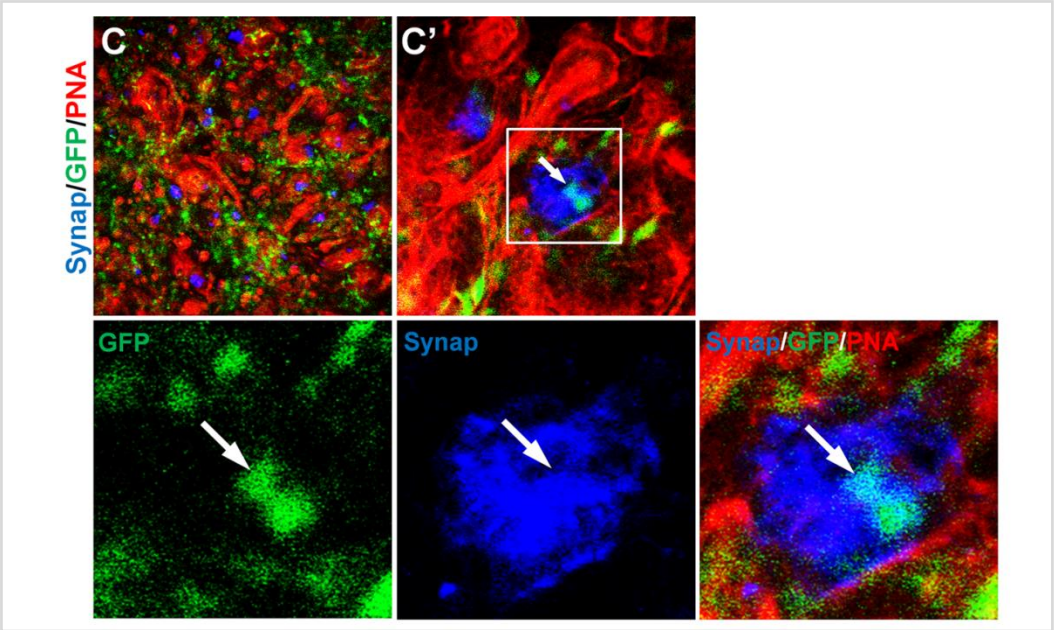

Figure 6.8, continued.

6.2.4 The behaviour of mESC-derived Bra-GFP$^+$ cells within chimeric kidney rudiments cultured *ex vivo*

Firstly, the behaviour of E2-Crimson-expressing (E2C$^+$) Bra-GFP$^+$ cells isolated from mESC-derived EBs (3-D culture system) were investigated in the *ex vivo* rudiment assay. Staining for PNA, megalin, Wt1 and synaptopodin showed that similarly to the positive control chimeras comprising mKSCs, the re-aggregated metanephric cells were able to develop tubular structures and nascent glomeruli (Figure 6.9). However, immunostaining for E2C showed that the EB-derived cells did not integrate into tubules or glomeruli, and instead, appeared to elongate and form interconnected cell networks throughout the rudiment. In many cases, the EB-derived cells appeared to align against the outer surface of developing

glomeruli (Figure 6.9).

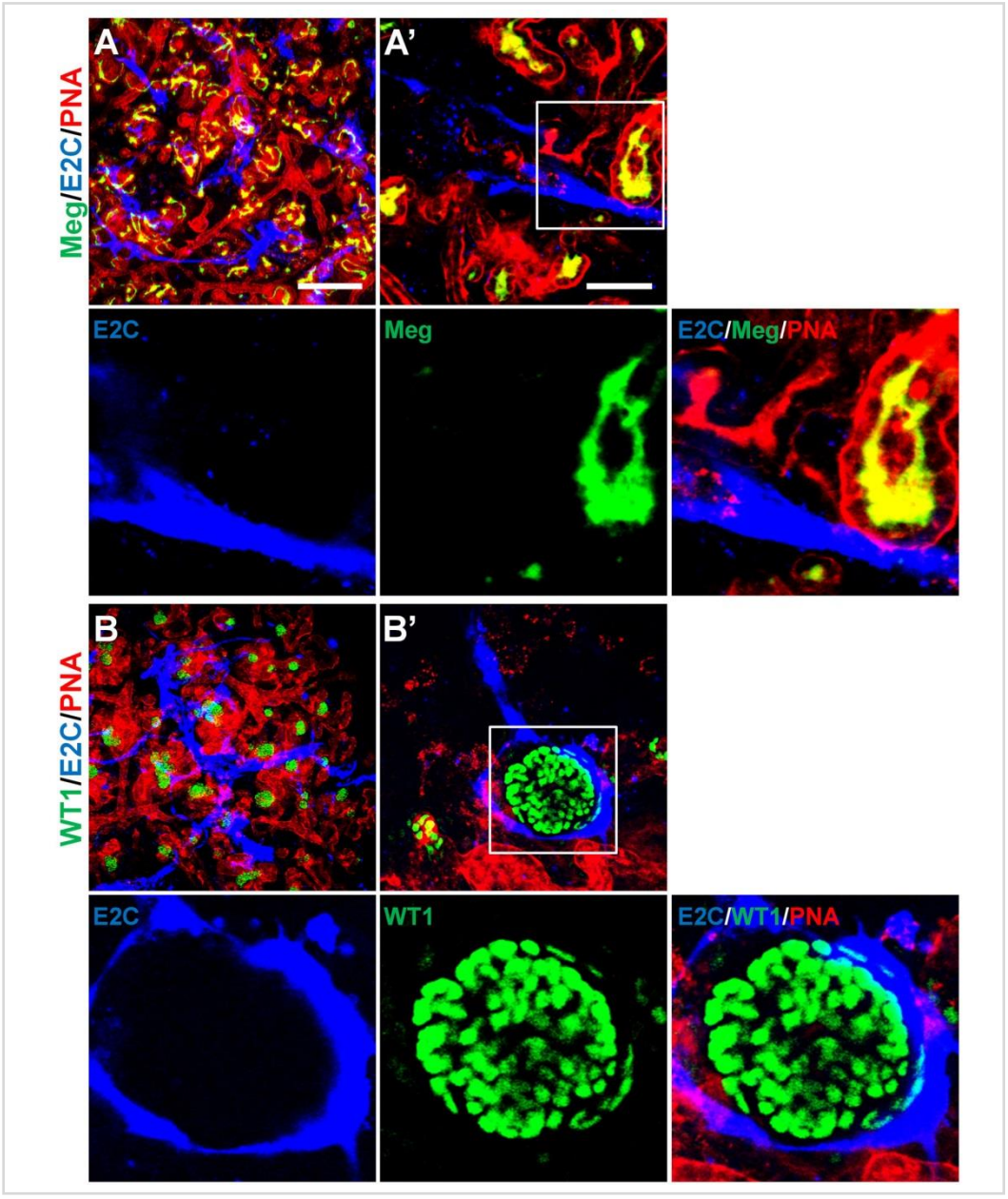

Figure 6.9 Confocal photomicrographs of the day-5 chimeric rudiments comprising Bra-GFP$^+$ cells derived from mESC 3-D system. E2C$^+$ Bra-GFP$^+$ cells (blue) appeared to be elongated and formed an interconnected network within the rudiments. They were often found surrounding the tubules (red) and glomerular structures (green) but did not integrate into them. Meg, megalin (green); Synap, synaptopodin (green). Boxed regions outlined are enlarged in the magnified images. Scale bars, 200 μm (A−C) and 50 μm (A'−C').

(continued on next page)

(continued from previous page)

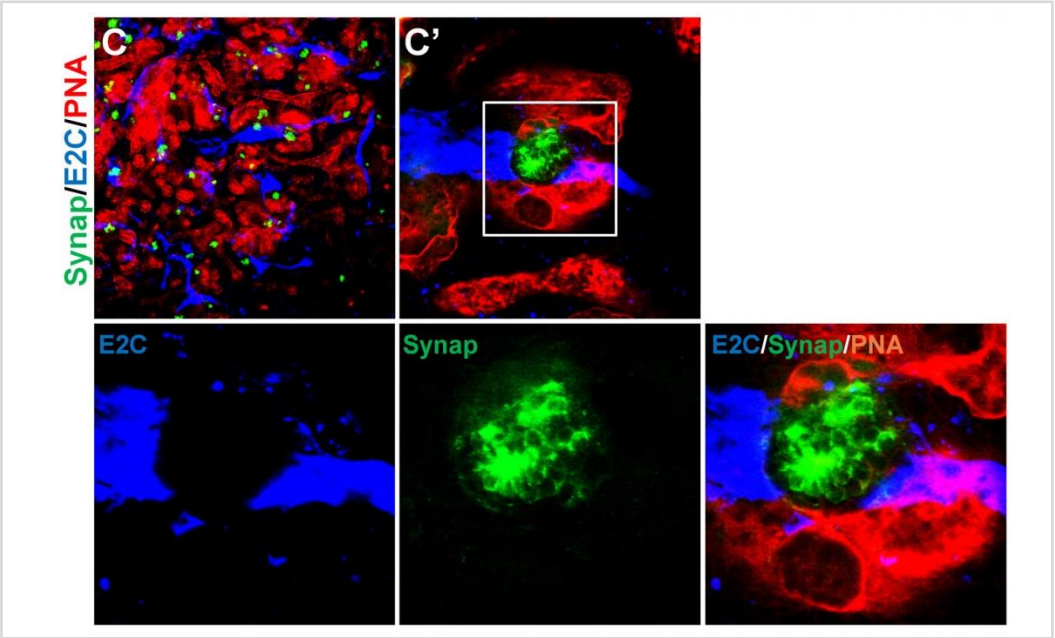

Figure 6.9, continued.

Next, the behaviour of E2C$^+$ Bra-GFP$^+$ cells isolated from the 2-D culture system was investigated using the chimeric rudiment assay. As with the EB-derived Bra-GFP$^+$ chimeras, staining for PNA, megalin, Wt1 and synaptopodin showed that re-aggregated metanephric cells in chimeras comprising Bra-GFP$^+$ cells isolated from the 2-D culture system were able to generate tubular structures and nascent glomeruli (Figure. 6.10). Similarly to the E2C$^+$ EB-derived Bra-GFP$^+$ cells, the cells isolated from the 2-D culture system did not appear to integrate into tubules or glomeruli. However, in contrast to the EB-derived cells, those isolated from 2-D culture tended not to form connections with each other. Although elongated cells were occasionally observed in close proximity to developing glomeruli, the majority of the cells were not elongated and did not

from interconnected cell networks (Figure 6.10). Furthermore, there appeared to be fewer E2C cells present in these chimeras compared to those generated from mESC-derived Bra-GFP$^+$ isolated from EBs.

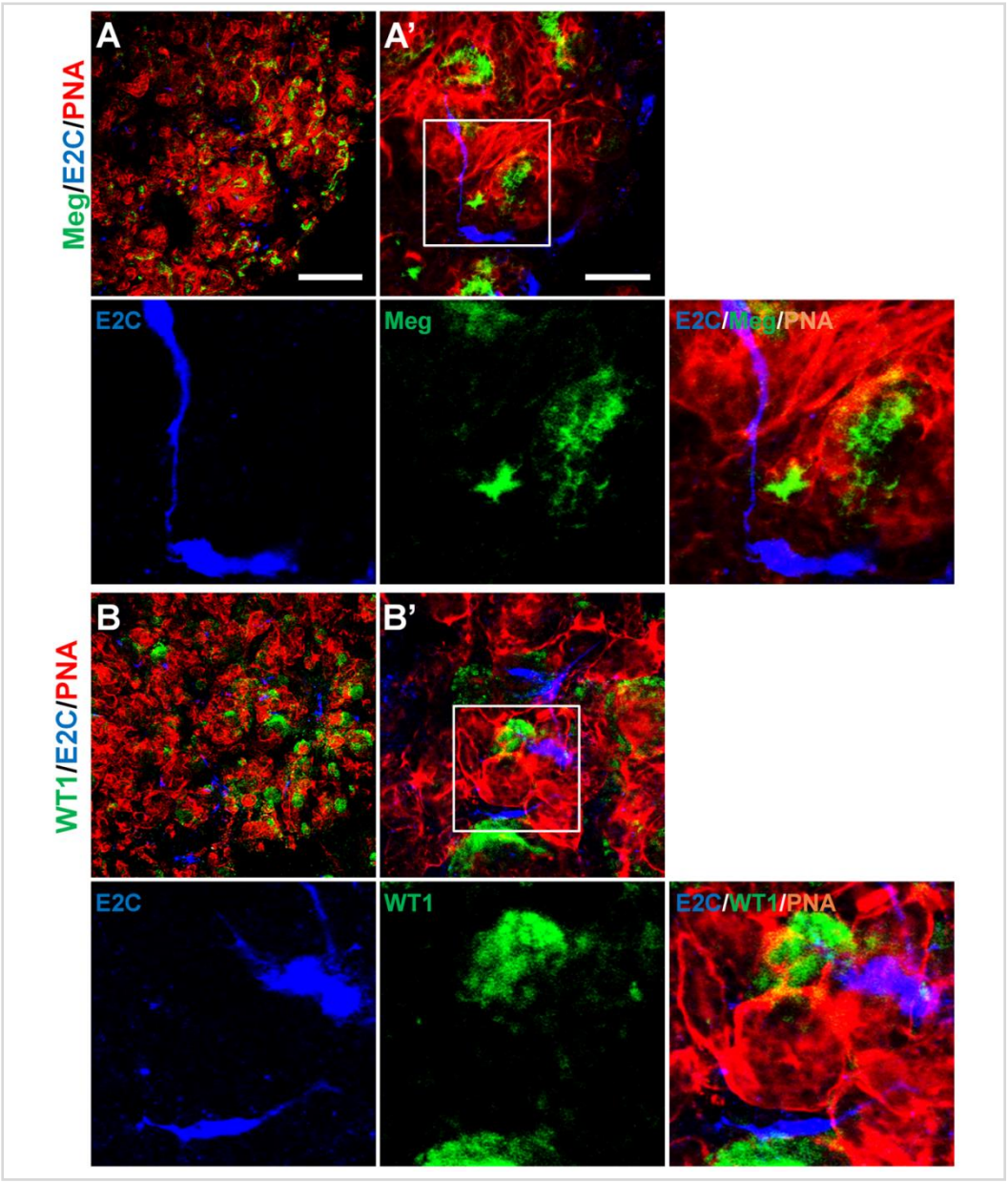

Figure 6.10 Confocal photomicrographs of the day-5 chimeric rudiments comprising Bra-GFP$^+$ cells isolated from mESC 2-D system. Less Bra-GFP$^+$ cells (blue) were observed with limited connections. However, they showed a peripheral distribution similar to the pattern in the day-5 chimeric rudiments with 3-D derived Bra-GFP$^+$ cells. Meg, megalin (green); Synap, synaptopodin (green). Boxed regions outlined are enlarged in the magnified images. Scale bars, 200 μm (A−C) and 50 μm (A'−C'). (continued on next page)

(continued from previous page)

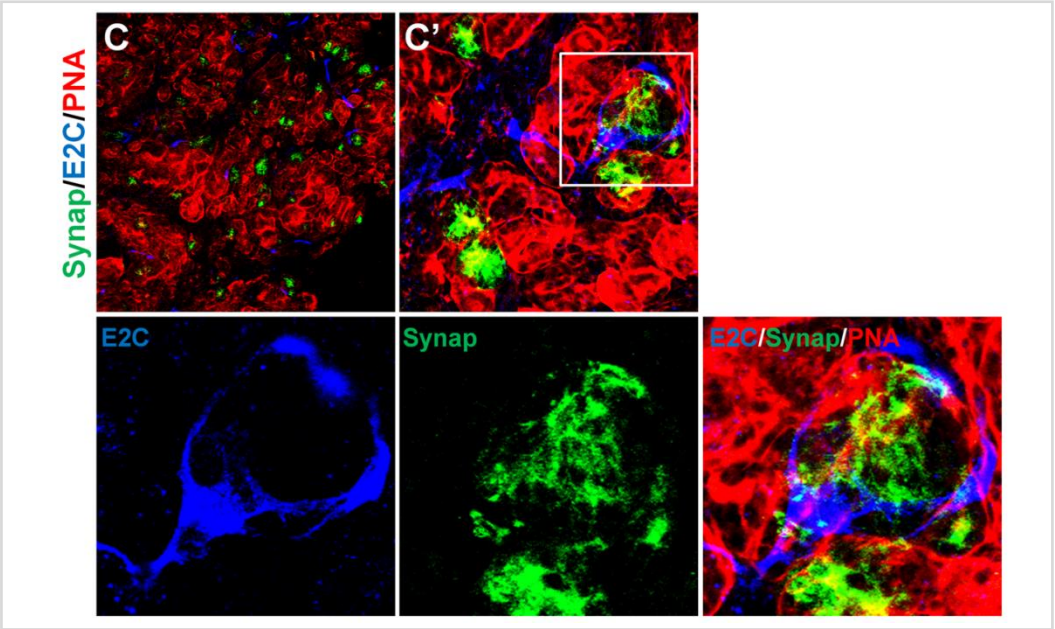

Figure 6.10, continued.

The morphology of E2C$^+$ Bra-GFP$^+$ cells within the chimeras generated from EB-isolated cells appeared similar to that of endothelial cells within *ex vivo* kidney rudiments (Halt *et al*., 2016). To investigate if the E2C$^+$ cells had differentiated into endothelial cells, the rudiments were immunostained for the endothelial marker, PECAM-1 (platelet and endothelial cell adhesion molecule 1) (Kondo *et al*., 2007). It was found that the metanephric cells generated PECAM-1$^+$ interconnected cell networks in both types of chimeric rudiment, indicating that endothelial cells had differentiated. Analysis of E2C$^+$ cells within the chimeric rudiments generated from EB-derived Bra-GFP$^+$ cells showed that the majority of these cells appeared to stain positively for PECAM-1, suggesting that they had differentiated into endothelial cells. In contrast, most of the E2C$^+$

cells within the chimeric rudiments generated from 2-D culture-derived Bra-GFP$^+$ cells did not stain positively for PECAM-1. Instead, only the elongated cells which were occasionally observed within these chimeras were found to stain for PECAM-1 (Figure 6.11).

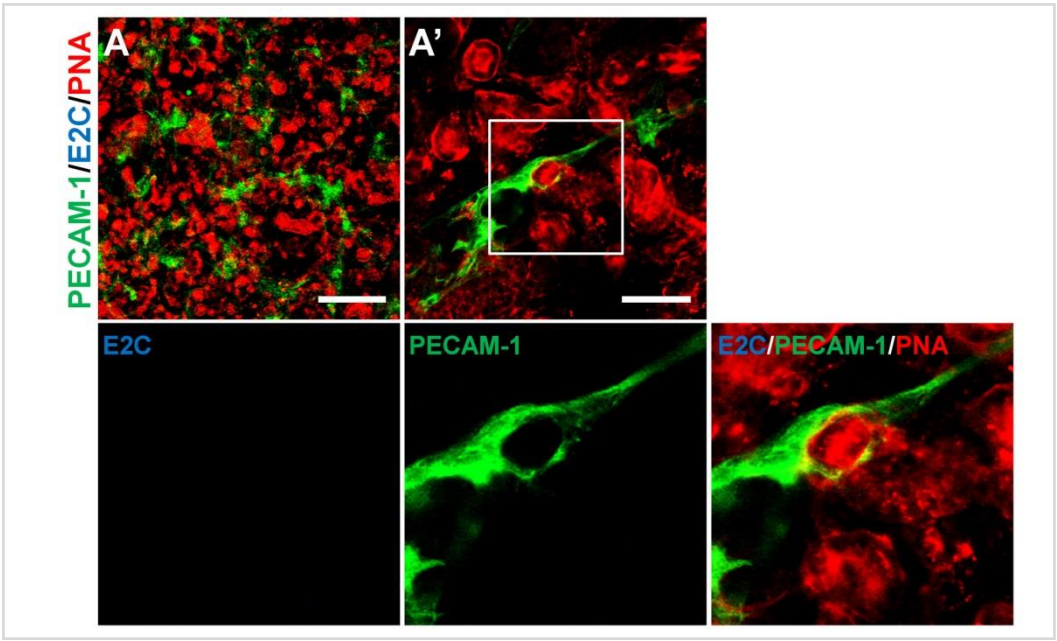

Figure 6.11 Confocal photomicrographs showing PECAM-1 immunostaining within Bra-GFP$^+$ chimeric rudiments. Immunostaining for E2C was undertaken to identify the mesodermal cells and PECAM-1 immunostaining was performed to identify endothelial-like cells. A−A', re-aggregated non-chimeric rudiments; B−B', re-aggregated chimeric rudiments containing E2C$^+$ Bra-GFP$^+$ cells isolated from the 3-D culture system; C−C', re-aggregated chimeric rudiments containing E2C$^+$ Bra-GFP$^+$ cells isolated from the 2-D culture system. Boxed regions outlined are enlarged in the magnified images. Scale bars, 200 μm (A−C) and 50 μm (A'−C').

(continued on next page)

(continued from previous page)

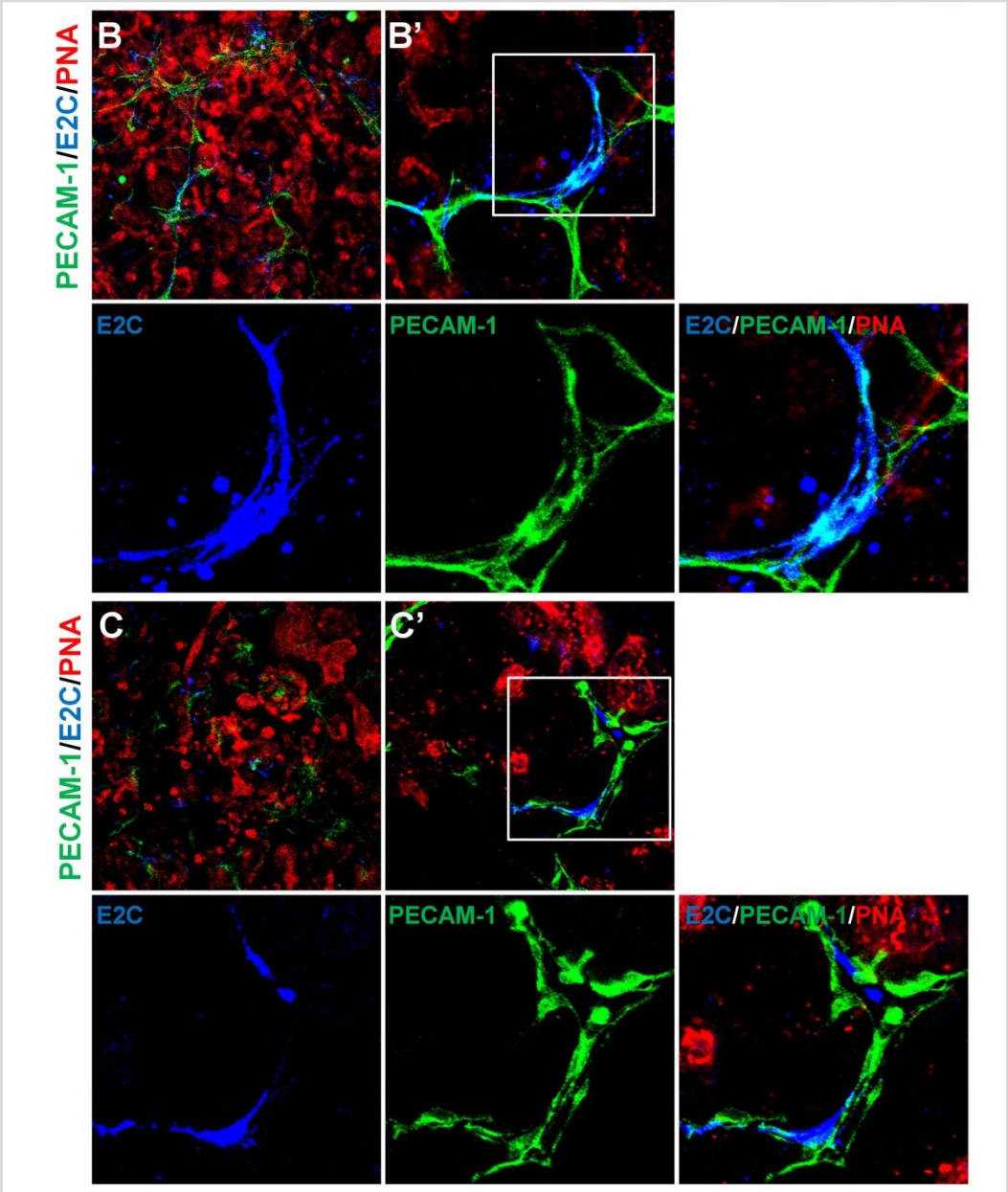

Figure 6.11, continued.

6.3 Discussion

In this chapter, by introducing the E2C-lablled mesodermal cells into the chimeric rudiments *ex vivo*, we showed that neither the Bra-GFP$^+$ cells derived from the

3-D nor 2-D culture systems appeared to integrate into the developing nephrons. The results are strikingly differed from our lab's previous studies that investigated the nephrogenic potential of mKSCs and Bra-GFP$^+$ cells isolated from non-cavitating EBs in the same rudiment culture assay (Ranghini *et al*., 2013; Rak-Raszewska *et al*., 2012a). In these earlier studies, it was found that mKSCs could integrate into developing nephrons and generate proximal tubule cells and podocytes, but did not integrate into the ureteric bud (Ranghini *et al*., 2013). The Bra-GFP$^+$ mESCs derived from non-cavitating EBs were able to integrate into both the developing nephrons and ureteric buds, and could form functional proximal tubule cells and podocytes (Rak-Raszewska *et al*., 2012a). Another study by Vigneau *et al* showed that Bra$^+$ cells derived from mouse EBs contributed to the proximal tubules when injected into the neonatal mouse kidney *in vivo* (Vigneau *et al*., 2007). The results we obtained with the Bra-GFP$^+$ cells obtained from cavitating EBs were surprising. We had expected that as these cells were isolated at a later time point than the Bra-GFP$^+$ cells in the non-cavitating EBs, they might more closely resemble posterior mesoderm, which has recently been shown to generate the MM but not the UB (Taguchi *et al*., 2014). We therefore thought that these cells might integrate into developing nephrons, but not the UBs. However, they did not integrate into either of these structures and instead appeared to differentiate into endothelial cells. There have been contrasting reports concerning the presence of endothelial cells in mouse kidney rudiments cultured *ex vivo*, with some studies suggesting endothelial cells cannot

survive in *ex vivo* rudiments (Loughna *et al*., 1997) and others suggesting they do (Halt *et al*., 2016). Our findings are consistent with the Halt *et al* study that indicates endothelial cells are present in rudiments, and similarly to that study, we found that although the endothelial cells formed interconnected networks, they did not form capillaries with lumen, nor did they invest the developing glomeruli.

The key differences in the gene expression profile of the Bra-GFP$^+$ cells isolated from cavitating EBs (current study) and non-cavitating EBs (previous study) (Rak-Raszewska, 2010) is that in comparison to GFP$^-$ cells, the former expressed much higher levels of *Foxf1*, which is identified in lateral plate mesoderm, and lower levels of the MM genes, *Gdnf* and *Osr1* (Rak-Raszewska, 2010). The high expression levels of *Foxf1* might explain why the EB-derived Bra-GFP$^+$ cells in the current study had a tendency to generate endothelial cells, because it is known that *Foxf1* is essential for vasculogenesis in the developing embryo and is expressed in endothelial cells (Ren *et al*., 2014; Mahlapuu *et al*., 2001).
High level of BMP signals and their receptors ALK3/6 have been shown to promote a lateral plate mesoderm fate (James and Schultheiss, 2005). Due to the heterogeneous nature of the EBs, it is possible that mesoderm niches that resemble dynamic microenvironments of the *in vivo* primitive streak have been formed. Cells residing in the niches that are exposed to high concentrations of BMP signals might, therefore, adopt a lateral plate mesoderm fate. Retinoic acid, FGF and Wnt signals might also affect the cell commitment of lateral plate

mesoderm but their effects may be stochastic within the EBs. Nevertheless, we cannot exclude the possibility that the timing might have been another factor; for instance, Bra-GFP$^+$ cells isolated at slightly earlier or later time-points might have expressed genes of other mesodermal lineages.

Regarding the Bra-GFP$^+$ isolated from the 2-D system, it was found that these also did not integrate into developing nephrons or UBs. Furthermore, only a small proportion of these cells appeared to differentiate into endothelial cells. The majority of the cells did not form interconnected cell networks and appeared to be randomly dispersed throughout the stroma. Similarly to the Bra-GFP$^+$ cells from the cavitating EBs, the Bra-GFP$^+$ cells from the 2-D system did not show any noticeable up-regulation of *Gdnf* or *Osr1* in comparison with the Bra-GFP$^-$ cells. However, in contrast to the EB-derived cells, those isolated from the 2-D system did not show up-regulation of *Foxf1*, which is consistent with their limited tendency to generate endothelial cells. It is possible that the Bra-GFP$^+$ cells from the 2-D system might have differentiated into stromal cells, but it was not possible to test this due to the lack of a stroma-specific antibody. It is interesting to note that the Bra-GFP$^+$ cells from the 2-D system expressed higher levels of the stromal gene, *Foxd1* (Mugford *et al*., 2008) compared to those from the 3-D system, but the results were not statistically significant (chapter 5).

The desirable goal for the Bra-GFP$^+$ cells to incorporate into the kidney rudiments

is to generate functional kidney compartments for use as disease models and for kidney regeneration. However, in the current study, these cells did not appear to be committed to the nephrogenic fate. Nevertheless, they might be a useful tool for generating the vasculature and/or stromal compartments of the kidney which are essential for development and maturation of the kidney *in vivo* (Little, 2016). In addition, a combination of activin A, retinoic acid and BMP7 is able to induce mouse ESCs to generate renal epithelial cells that integrate into tubules (Kim and Dressler, 2005). It is thus possible that applying these molecules to the Bra-GFP^{+} cells could promote their integration into the rudiments.

Chapter 7

General Discussion and Conclusion

The main aim of this work was to explore whether the mesoderm arising in the cavitating 3-D EBs is equivalent to the mesoderm that is generated in the 2-D monolayer culture system. In this project, we generated a *Bra-GFP/Rosa26-E2C* mESC reporter line by knocking an *E2C* transgene into the ubiquitously-expressed *Rosa26* locus. We showed that the reporter cells retained the expression of stemness genes. We also showed that the reporter cells were able to generate typical cavitating EBs *in vitro* and could form teratomas *in vivo*, suggesting that the transgene insertion did not affect their pluripotency.

An initial aim of the study was to track the fate of the E2C reporter cells within the internal organs of adult mice *in vivo* using fluorescence imaging. However, it was found that imaging the E2C reporter cells following subcutaneous injection was extremely difficult and required large numbers of cells. Therefore, it was concluded that in this context (i.e., following insertion of a single copy of the E2C cDNA into the *Rosa26* locus), the E2C is not an effective reporter for *in vivo* imaging. No attempts were made to image the cells following systemic administration in living mice, as it was felt that this would be futile, and therefore,

the use of animals for such an experiment could not be justified.

Although the E2C^{+} reporter cells are not suitable for imaging *in vivo*, it was possible to image them *in vitro*. The targeted *E2C* transgene in the *Rosa26* locus appeared to be stable within the reporter cells during the culture period, implying that this approach would be suitable for tracking cells over the long-term. Indeed, the E2C signal could be detected in histological sections of teratomas generated by injecting the reporter subcutaneously into adult SCID mice. However, the signal intensity was weak and could only be detected using indirect immunofluorescence, using a primary antibody specific to E2C. In addition, despite the fact that we generated a line (clone +C4, Chapter 3) with a purity of 99%, it was still notable that the E2C fluorescence intensity was not high. Data from flow cytometry analysis showed that the maximum E2C intensity was around 10^3 (Figure 3.6). This might be due to low copy number (only a single copy) of the *E2C* in the *Rosa26* allele of the knock-in line (Friedrich and Soriano, 1991). Another possible explanation is the mild strength of the intrinsic *Rosa26* promoter. A comparison between the *Rosa26* endogenous promoter and eight exogenous promoters including β-actin, human cytomegalovirus (CMV), mouse phosphoglycerate kinase (PGK) and CMV early enhancer/chicken β-actin promoter/rabbit β-globin intron composite promoter (CAG) in mESCs revealed that the activity of the endogenous *Rosa26* promoter was similar to that of β-actin, which was 9- to 10- fold less than that of CAG (Chen *et al*., 2011). As the

transgene is placed in the first intron under the direct control of the *Rosa26* endogenous promoter, the lower activity of the native *Rosa26* promoter may result in insufficient E2C expression levels that may not be easy to be detected in deep tissues. To circumvent this, one of the possible solutions could be to insert a transcription enhancer upstream to the transgene within the intron 1; for instance, the successfully used CAG enhancer (Niwa *et al.*, 1991). An alternative option would be to use a luciferase bioluminescent reporter instead of a fluorescent reporter. For *in vivo* animal imaging, bioluminescence provides high sensitivity. (Close *et al.*, 2010). However, although bioluminescence is more sensitive than fluorescence, spatial resolution is poor. Therefore, it would be necessary to confirm cell fate by undertaking immunostaining of histological sections using antibodies that detect luciferase.

Flow cytometry analysis of *Bra* expression in mesoderm populations generated from 3-D and 2-D systems revealed that 2-D induction culture generated a high proportion of GFP^+ cells. In contrast, GFP^+ expression within the EBs was not uniform and fewer GFP^+ cells were present. Although the 2-D system appeared more efficient, the 3-D system remains as a useful tool to generate and isolate cells from EBs, the development of which shows striking similarities to the early embryo. It would therefore be expected that specific cell types isolated from EBs might more closely resemble their counterparts in the developing embryo than would the same cell types isolated from 2-D differentiation culture.

To characterise the two types of mesodermal cells, highly-pure mesoderm and non-mesoderm populations, namely Bra-GFP$^+$ and Bra-GFP$^-$ cells, were isolated from 3-D EB and 2-D monolayer culture conditions and the expression profile of key genes was investigated using quantitative RT-PCR. The results showed that, between the Bra-GFP$^+$ cells isolated from the 3-D and 2-D systems, there was no significant difference in the relative expression levels of key mesodermal genes *Bra* and *Tbx6*, but the nascent mesoderm – lateral plate mesoderm gene *Foxf1* was surprisingly up-regulated by 30-fold in the mesoderm cells isolated from 3-D system. This was a striking difference from our group's previous observations of very low *Foxf1* expression in the mesoderm cells of non-cavitating EBs (Rak-Raszewska, 2010). This could be because the mesoderm cells isolated from the cavitating EBs might already have specified into more differentiated mesodermal lineages, such as the lateral plate mesoderm.

The mouse kidney rudiment assay showed that Bra-GFP$^+$ cells isolated from the 3-D system tended to become endothelial-like cells. This was not observed in our previous study using the non-cavitating EBs (Rak-Raszewska, 2010). Therefore, the immediate future work would be to repeat the assay with mesoderm cells isolated from the non-cavitating EBs derived from this E2C-labelled mESC reporter line to examine whether the previous results can be confirmed, as it cannot be ruled out that the different approaches used to track the fate of the cells (i.e., quantum dots in the previous study compared with the integration of the E2C

reporter gene in the present study), might have effected their behaviour.

Direct reprogramming of kidney lineages provides an alternative approach to regulating mesodermal cell behaviour *in vitro*. Induced pluripotent stem cells (iPSCs) generated from human kidney mesangial and urine-derived renal tubular cells have been shown to have the potential to differentiate into renal podocytes (Li *et al*., 2016; Song *et al*., 2012; Zhou *et al*., 2011). Recent progress of directly reprogramming human adult proximal tubule cells to nephron progenitors by using six genes indicates the great potential of stem cells in kidney regeneration (Hendry *et al.*, 2013).

In conclusion, the mesoderm population isolated from the 3-D (i.e., EBs) system showed different characteristics compared to the mesoderm cells isolated from 2-D mESC culture system in terms of key mesoderm gene expression profiles and differentiation potential. It is possible that, during mesoderm development, slight differences in the timing and/or exposure to regulatory signals lead to divergent differentiation paths. In the current rudiment study, this subtle deviation likely results in varied cell fates *in vitro* and *ex vivo*.

Further work would be needed to monitor mESC differentiation in the 3-D and 2-D cultures in more detail. A possible idea could be to generate dual-reporter mESC lines that enabled the expression of *Bra* and a marker of more

differentiated mesoderm to be monitored simultaneously in real-time during *in vitro* differentiation culture.

References

Abe, K., Niwa, H., Iwase, K., Takiguchi, M., Mori, M., Abé, S., Abe, K. and Yamamura, K. (1996). Endoderm-specific gene expression in embryonic stem cells differentiated to embryoid bodies. *Experimental Cell Research*, 229(1), pp.27-34.

Abe, T., Kiyonari, H., Shioi, G., Inoue, K., Nakao, K., Aizawa, S. and Fujimori, T. (2011). Establishment of conditional reporter mouse lines at ROSA26 locus for live cell imaging. G*enesis*, 49(7), pp.579-590.

Adams, D. and van der Weyden, L. (2008). Contemporary approaches for modifying the mouse genome. *Physiological Genomics*, 34(3), pp.225-238.

Adamson, A., Jackson, D. and Davis, J. (2011). Novel approaches to *in vitro* transgenesis. *Journal of Endocrinology*, 208(3), pp.193-206.

Alford, S., Wu, J., Zhao, Y., Campbell, R. and Knöpfel, T. (2012). Optogenetic reporters. *Biology of the Cell*, 105(1), pp.14-29.

Arnold, S. and Robertson, E. (2009). Making a commitment: cell lineage allocation and axis patterning in the early mouse embryo. *Nature Reviews Molecular Cell Biology*, 10(2), pp.91-103.

Arnold, S., Stappert, J., Bauer, A., Kispert, A., Herrmann, B., and Kemler, R. (2000). *Brachyury* is a target gene of the Wnt/β-catenin signaling pathway. *Mechanisms of Development*, 91(1-2), pp. 249-258.

Artus, J. and Chazaud, C. (2014). A close look at the mammalian blastocyst: epiblast and primitive endoderm formation. *Cellular and Molecular Life Sciences*, 71(17), pp.3327-3338.

Asano, T., Hanazono, Y., Ueda, Y., Muramatsu, S., Kume, A., Suemori, H., Suzuki, Y., Kondo, Y., Harii, K., Hasegawa, M., Nakatsuji, N. and Ozawa, K. (2002). Highly efficient gene transfer into primate embryonic stem cells with a simian lentivirus vector. *Molecular Therapy*, 6(2), pp.162-168.

Ashley, D., Bol, S., Waugh, C. and Kannourakis, G. (1993). A novel approach to the measurement of different *in vitro* leukaemic cell growth parameters: the use of PKH GL fluorescent probes. *Leukemia Research*, 17(10), pp.873-882.

Bancroft, G., Sheehan, K., Schreiber, R. and Unanue ER, E. (1989). Tumor necrosis factor is involved in the T cell-independent pathway of macrophage activation in scid mice. *Journal of Immunology*, 143(1), pp.127-30.

Basilico, C., Ambrosetti, D., Fraidenraich, D. and Dailey, L. (1997). Regulatory mechanisms governing FGF-4 gene expression during mouse development. *Journal of Cellular Physiology*, 173(2), pp.227-232.

Basson, M., Watson-Johnson, J., Shakya, R., Akbulut, S., Hyink, D., Costantini, F., Wilson, P., Mason, I. and Licht, J. (2006). Branching morphogenesis of the ureteric epithelium during kidney development is coordinated by the opposing functions of GDNF and Sprouty1. *Developmental Biology*, 299(2), pp.466-477.

Batlle-Morera, L., Smith, A. and Nichols, J. (2008). Parameters influencing derivation of embryonic stem cells from murine embryos. *Genesis*, 46(12), pp.758-767.

Behringer, R., Bradley, A., Liu, P., Wakamiya, M., Shea, M. and Albrecht, U. (1999). *Nature Genetics*, 22(4), pp.361-365.

Bell, P., Vandenberghe, L., Wu, D., Johnston, J., Limberis, M. and Wilson, J. (2007). A comparative analysis of novel fluorescent proteins as reporters for gene transfer studies. *Journal of Histochemistry and Cytochemistry*, 55(9), pp.931-939.

Bevis, B. and Glick, B. (2002). Corrigendum: Rapidly maturing variants of the Discosoma red fluorescent protein (DsRed). *Nature Biotechnology*, 20(11), pp.1159-1159.

Blancas, A., Shih, A., Lauer, N. and McCloskey, K. (2011). Endothelial cells from embryonic stem cells in a chemically defined medium. *Stem Cells and Development*, 20(12), pp.2153-2161.

Blancas, A., Wong, L., Glaser, D. and McCloskey, K. (2013). Specialized tip/stalk-like and phalanx-like endothelial cells from embryonic stem cells. *Stem Cells and Development*, 22(9), pp.1398-1407.

Bollag, R., Siegfried, Z., Cebra-Thomas, J., Garvey, N., Davison, E. and Silver, L. (1994). An ancient family of embryonically expressed mouse genes sharing a conserved protein motif with the T locus. *Nature Genetics*, 7(3), pp.383-389.

Bouchard, M., Souabni, A., A., Mandler, M.,, M., Neubuser, A.,, A. and Busslinger, M, M. (2002). Nephric lineage specification by Pax2 and Pax8. *Genes & Development*, 16(22), pp.2958-2970.

Bradley, A., Evans, M., Kaufman, M. and Robertson, E. (1984). Formation of germ-line chimaeras from embryo-derived teratocarcinoma cell lines. *Nature*, 309(5965), pp.255-256.

Brook, F. and Gardner, R. (1997). The origin and efficient derivation of embryonic stem cells in the mouse. *Proceedings of the National Academy of Sciences*, 94(11), pp.5709-5712.

Bruce, S., Rea, R., Steptoe, A., Busslinger, M., Bertram, J. and Perkins, A. (2007). *In vitro* differentiation of murine embryonic stem cells toward a renal lineage. *Differentiation*, 75(5), pp.337-349.

Burdon, T., Chambers, I., Stracey, C., Niwa, H. and Smith, A. (1999). Signaling mechanisms regulating self-renewal and differentiation of pluripotent embryonic stem cells. *Cells Tissues Organs*, 165(3-4), pp.131-143.

Campbell, R., Tour, O., Palmer, A., Steinbach, P., Baird, G., Zacharias, D. and Tsien, R. (2002). A monomeric red fluorescent protein. *Proceedings of the National Academy of Sciences*, 99(12), pp.7877-7882.

Canalis, E., Economides, A. and Gazzerro, E. (2003). Bone morphogenetic proteins, their antagonists, and the skeleton. *Endocrine Reviews*, 24(2), pp. 218-235.

Capecchi, M. (1989b). Altering the genome by homologous recombination. *Science*, 244(4910), pp.1288-1292.

Capecchi, M. (1989a). The new mouse genetics: altering the genome by gene targeting.

Trends in Genetics, 5(3), pp.70-76.

Carapuco, M., Navoa, A., Bobola, N. and Mallo, M. (2005). *Hox* genes specify vertebral types in the presomitic mesoderm. *Genes & Development*, 19(18), pp.2116-2121.

Casey, E., O'Reilly, M., Conlon, F. and Smith J. (1998). The T-box transcription factor Brachyury regulates expression of *eFGF* through binding to a non-palindromic response element. *Development*, 125(19), pp. 3887-3894.

Chapman, D., Cooper-Morgan, A., Harrelson, Z. and Papaioannou, V. (2003). Critical role for *Tbx6* in mesoderm specification in the mouse embryo. *Mechanisms of Development*, 120(7), pp.837-847.

Chen, C., Krohn, J., Bhattacharya, S. and Davies, B. (2011). A Comparison of exogenous promoter activity at the *ROSA26* Locus using a PhiC31 integrase mediated cassette exchange approach in mouse ES cells. *PLoS ONE*, 6(8), p.e23376.

Chen, Y., Müller, J., Ruan, Q. and Gratton, E. (2002). Molecular brightness characterization of EGFP *in vivo* by fluorescence fluctuation spectroscopy. *Biophysical Journal*, 82(1), pp.133-144.

Cherry, S., Biniszkiewicz, D., van Parijs, L., Baltimore, D. and Jaenisch, R. (2000). Retroviral expression in embryonic stem cells and hematopoietic stem cells. *Molecular and Cellular Biology*, 20(20), pp.7419-7426.

Christensen, J., Vonwil, D. and Shastri, V. (2015). Non-invasive *in vivo* imaging and quantification of tumor growth and metastasis in rats using cells expressing far-red fluorescence protein. *PLOS ONE*, 10(7), p.e0132725.

Chu, J., Haynes, R., Corbel, S., Li, P., González-González, E., Burg, J., Ataie, N., Lam, A., Cranfill, P., Baird, M., Davidson, M., Ng, H., Garcia, K., Contag, C., Shen, K., Blau, H. and Lin, M. (2014). Non-invasive intravital imaging of cellular differentiation with a bright red-excitable fluorescent protein. *Nature Methods*, 11(5), pp.572-578.

Ciruna, B. and Rossant, J. (2001). FGF Signaling regulates mesoderm cell fate specification and morphogenetic movement at the primitive streak. *Developmental Cell*, 1(1), pp.37-49.

Close, D., Xu, T., Sayler, G. and Ripp, S. (2010). *In vivo* bioluminescent imaging (BLI): noninvasive visualization and interrogation of biological processes in living animals. *Sensors*, 11(1), pp.180-206.

Concepcion, D. and Papaioannou, V. (2014). Nature and extent of left/right axis defects in T^{Wis}/T^{Wis} mutant mouse embryos. *Developmental Dynamics*, 243(8), pp.1046-1053.

Cong, L., Ran, F., Cox, D., Lin, S., Barretto, R., Habib, N., Hsu, P., Wu, X., Jiang, W., Marraffini, L. and Zhang, F. (2013). Multiplex genome engineering using CRISPR/Cas systems. *Science*, 339, pp. 819-823.

Conlon, F., Wright, C. and Robertson, E. (1995). Effects of the T^{Wis} mutation on notochord formation and mesodermal patterning. *Mechanisms of Development*, 49(3), pp.201-209.

Cormack, B., Valdivia, R. and Falkow, S. (1996). FACS-optimized mutants of the green fluorescent protein (GFP). *Gene*, 173(1), pp.33-38.

Costantini, F. and Kopan, R. (2010). Patterning a complex organ: branching morphogenesis and nephron segmentation in kidney development. *Developmental Cell*, 18(5), pp.698-712.

Dauleh, S., Santeramo, I., Fielding, C., Ward, K., Herrmann, A., Murray, P. and Wilm, B. (2016). Characterisation of cultured mesothelial cells derived from the murine adult omentum. *PLOS ONE*, 11(7), p.e0158997.

Davenport, T., Jerome-Majewska, L. and Papaioannou, V. (2003). Mammary gland, limb and yolk sac defects in mice lacking *Tbx3*, the gene mutated in human ulnar mammary syndrome. *Development*, 130(10), pp.2263-2273.

Deng, C. and Capecchi, M. (1992). Reexamination of gene targeting frequency as a function of the extent of homology between the targeting vector and the target locus. *Molecular and Cellular Biology*, 12(8), pp.3365-3371.

Dethlefsen, L., Prewitt, J. and Mendelsohn, M. (1968). Analysis of tumor growth curves. *Jmournal of National Cancer Institute*, 40(2), pp.389-405.

Di-Po ¡ N., Koch, U., Radtke, F. and Duboule, D. (2010). Additive and global functions of *HoxA* cluster genes in mesoderm derivatives. *Developmental Biology*, 341(2), pp.488-498.

Doetschman, T., Eistetter, H., Katz, M., Schmidt, W. and Kemler, R. (1985). The *in vitro* development of blastocyst-derived embryonic stem cell lines: formation of visceral yolk sac, blood islands and myocardium. *J Embryol Exp Morphol*, 87, pp.27-45.

Dom ńguez-Bendala, J. and McWhir, J. (2004). Enhanced gene targeting frequency in ES cells with low genomic methylation levels. *Transgenic Research*, 13(1), pp.69-74.

Doudna, J. and Charpentier, E. (2014). The new frontier of genome engineering with CRISPR-Cas9. *Science*, 346(6213), pp. 1258096.

Dressler, G. (2009). Advances in early kidney specification, development and patterning. *Development*, 136(23), pp.3863-3874.

Dull, T., Zufferey, R., Kelly, M., Mandel, R., Nguyen, M., Trono, D. and Naldini, L. (1998). A third-generation lentivirus vector with a conditional packaging system. *Journal of Virology*, 72(11), pp.8463-8471.

Dunn, S., Martello, G., Yordanov, B., Emmott, S. and Smith, A. (2014). Defining an essential transcription factor program for naive pluripotency. *Science*, 344(6188), pp.1156-1160.

Ema, M., Mori, D., Niwa, H., Hasegawa, Y., Yamanaka, Y., Hitoshi, S., Mimura, J., Kawabe, Y., Hosoya, T., Morita, M., Shimosato, D., Uchida, K., Suzuki, N., Yanagisawa, J., Sogawa, K., Rossant, J., Yamamoto, M., Takahashi, S. and Fujii-Kuriyama, Y. (2008). *Krüppel-like factor 5* is essential for blastocyst development and the normal self-renewal of mouse ESCs. *Cell Stem Cell*, 3(5), pp.555-567.

Erselius, J., Goulding, M. and Gruss, P. (1990). Structure and expression pattern of the

murine *Hox-3.2* gene. *Development*, 110(2), pp.629-642.

Evans, M. (2011). Discovering pluripotency: 30 years of mouse embryonic stem cells. *Nature Reviews Molecular Cell Biology*, 12(10), pp.680-686.

Evans, M. and Kaufman, M. (1981). Establishment in culture of pluripotential cells from mouse embryos. *Nature*, 292(5819), pp.154-156.

Fehling, H., Lacaud, G., Kubo, A., Kennedy, M., Robertson, S., Keller, G. and Kouskoff, V. (2003). Tracking mesoderm induction and its specification to the hemangioblast during embryonic stem cell differentiation. *Development*, 130(17), pp.4217-4227.

Feraud, O., Cao, Y. and Vittet, D. (2001). Embryonic stem cell-derived embryoid bodies development in collagen gels recapitulates sprouting angiogenesis. *Laboratory Investigation*, 81(12), pp.1669-1681.

Fleming, T. (1987). A quantitative analysis of cell allocation to trophectoderm and inner cell mass in the mouse blastocyst. *Developmental Biology*, 119(2), pp.520-531.

Folger, K., Wong, E., Wahl, G. and Capecchi, M. (1983). Patterns of integration of DNA microinjected into cultured mammalian cells: evidence for homologous recombination between Injected plasmid DNA molecules. *Molecular and Cellular Biology*, 3(1), p.147.

Friedrich, G. and Soriano, P. (1991). Promoter traps in embryonic stem cells: a genetic screen to identify and mutate developmental genes in mice. *Genes & Development*, 5(9), pp.1513-1523.

Fu, Y., Foden, J., Khayter, C., Maeder, M., Reyon, D., Joung, J. and Sander, J. (2013). High-frequency off-target mutagenesis induced by CRISPR-Cas nucleases in human cells. *Nature Biotechnology*, 31, pp. 822-826.

Furue, M., Okamoto, T., Hayashi, Y., Okochi, H., Fujimoto, M., Myoishi, Y., Abe, T., Ohnuma, K., Sato, G., Asashima, M. and Sato, J. (2005). Leukemia inhibitory factor as an anti-apoptotic mitogen for pluripotent mouse embryonic stem cells in a serum-free medium without feeder cells. *In Vitro Cellular &*

Developmental Biology - Animal, 41(1), pp.19-28.

Gadue, P., Huber, T., Paddison, P. and Keller, G. (2006). Wnt and TGF-beta signaling are required for the induction of an *in vitro* model of primitive streak formation using embryonic stem cells. *Proceedings of the National Academy of Sciences*, 103(45), pp.16806-16811.

Gardner, R. (1982). Investigation of cell lineage and differentiation in the extraembryonic endoderm of the mouse embryo. *Journal of Embryology & Experimental Morphology*, 68, pp.175-198.

Gilbert, S. (2010). *Developmental Biology*. 9th ed. Sunderland, MA: Sinauer Associates, Inc.

Gratsch, T. and O'Shea, K. (2002). Noggin and chordin have distinct activities in promoting lineage commitment of mouse embryonic stem (ES) cells. *Developmental Biology*, 245(1), pp.83-94.

Grote, D. (2006). Pax2/8-regulated Gata3 expression is necessary for morphogenesis and guidance of the nephric duct in the developing kidney. *Development*, 133(1), pp.53-61.

Guo, G., Yang, J., Nichols, J., Hall, J., Eyres, I., Mansfield, W. and Smith, A. (2009). Klf4 reverts developmentally programmed restriction of ground state pluripotency. *Development*, 136(7), pp.1063-1069.

Gurskaya, N., Fradkov, A., Pounkova, N., Staroverov, D., Bulina, M., Yanushevich, Y., Labas, Y., Lukyanov, S. and Lukyanov, K. (2003). A colourless green fluorescent protein homologue from the non-fluorescent hydromedusa Aequorea coerulescens and its fluorescent mutants. *Biochem. J.*, 373(2), pp.403-408.

Haas, J., Park, E. and Seed, B. (1996). Codon usage limitation in the expression of HIV-1 envelope glycoprotein. *Current Biology*, 6(3), pp.315-324.

Haldi, M., Ton, C., Seng, W. and McGrath, P. (2006). Human melanoma cells transplanted into zebrafish proliferate, migrate, produce melanin, form masses and stimulate angiogenesis in zebrafish. *Angiogenesis*, 9(3), pp.139-151.

Hall, J., Guo, G., Wray, J., Eyres, I., Nichols, J., Grotewold, L., Morfopoulou, S., Humphreys, P., Mansfield, W., Walker, R., Tomlinson, S. and Smith, A. (2009). Oct4 and LIF/Stat3 additively induce krüppel factors to sustain embryonic stem cell self-renewal. *Cell Stem Cell*, 5(6), pp.597-609.

Halt, K., Pärssinen, H., Junttila, S., Saarela, U., Sims-Lucas, S., Koivunen, P., Myllyharju, J., Quaggin, S., Skovorodkin, I. and Vainio, S. (2016). $CD146^{+}$ cells are essential for kidney vasculature development. *Kidney International*, 90(2), pp.311-324.

Hamer, D. and LedeR, P. (1979). Expression of the chromosomal mouse beta maj-globin gene cloned in SV40. *Nature*, 281(5726), pp.35-40.

Hansen, J., Qing, K., Kwon, H., Mah, C. and Srivastava, A. (2000). Impaired intracellular trafficking of adeno-associated virus type 2 vectors limits efficient transduction of murine fibroblasts. *Journal of Virology*, 74(2), pp.992-996.

He, S., Lamers, G., Beenakker, J., Cui, C., Ghotra, V., Danen, E., Meijer, A., Spaink, H. and Snaar-Jagalska, B. (2012). Neutrophil-mediated experimental metastasis is enhanced by VEGFR inhibition in a zebrafish xenograft model. *Journal of Pathology*, 227(4), pp.431-445.

Hellmich, H., Kos, L., Cho, E., Mahon, K. and Zimmer, A. (1996). Embryonic expression of glial cell-line derived neurotrophic factor (GDNF) suggests multiple developmental roles in neural differentiation and epithelial-mesenchymal interactions. *Mechanisms of Development*, 54(1), pp.95-105.

Hendrikx, P., Martens, C., Hagenbeek, A., Keij, J. and Visser, J. (1996). Homing of fluorescently labeled murine hematopoietic stem cells. *Experimental Hematology*, 24(2), pp.129-140.

Hendry, C., Vanslambrouck, J., Ineson, J., Suhaimi, N., Takasato, M., Rae, F. and Little, M. (2013). Direct transcriptional reprogramming of adult cells to embryonic nephron progenitors. *Journal of the American Society of Nephrology*, 24(9), pp. 1424-1434.

Herrmann, B. and Kispert, A. (1994). The *T* genes in embryogenesis. *Trends in Genetics*, 10(8), pp.280-286.

Herrmann, B., Labeit, S., Poustka, A., King, T. and Lehrach, H. (1990). Cloning of the *T* gene required in mesoderm formation in the mouse. *Nature*, 343(6259), pp.617-622.

Hewitson, T. and Darby, I. (2010). *Histology protocols*. 1st ed. New York, N.Y.: Humana Press.

Hicks, A., Lappalainen, R., Narkilahti, S., Suuronen, R., Corbett, D., Sivenius, J., Hovatta, O. and Jolkkonen, J. (2009). Transplantation of human embryonic stem cell-derived neural precursor cells and enriched environment after cortical stroke in rats: cell survival and functional recovery. *European Journal of Neuroscience*, 29(3), pp.562-574.

Hitoshi, N., Ken-ichi, Y. and Jun-ichi, M. (1991). Efficient selection for high-expression transfectants with a novel eukaryotic vector. *Gene*, 108(2), pp.193-199.

Hogan, B., Costantini, F., Beddington, R. and Lacy, E. (1994). *Manipulating the mouse embryo*. 2nd ed. Cold Spring Harbor, N.Y.: Cold Spring Harbor Laboratory Press.

Hohenstein, P., Slight, J., Ozdemir, D., Burn, S., Berry, R. and Hastie, N. (2008). High-efficiency *Rosa26* knock-in vector construction for Cre-regulated overexpression and RNAi. *Pathogenetics*, 1(1), p.3.

Hooper, M., Hardy, K., Handyside, A., Hunter, S. and Monk, M. (1987). HPRT-deficient (Lesch–Nyhan) mouse embryos derived from germline colonization by cultured cells. *Nature*, 326(6110), pp.292-295.

Höpfl, G., Gassmann, M. and Desbaillets, I. (n.d.). Differentiating embryonic stem cells into embryoid bodies. *Germ Cell Protocols*, pp.079-098.

Horan, P. and Slezak, S. (1989). Stable cell membrane labelling. *Nature*, 340(6229), pp.167-168.

Hsu, P., Scott, D., Weinstein, J., Ran, F., Konermann, S., Agarwala, V., Li, Y., Fine,

E.J., Wu, X., Shalem, O., *et al*. (2013). DNA targeting specificity of RNA-guided Cas9 nucleases. *Nature Biotechnology*, 31, pp. 827-832.

Hwang, N., Varghese, S., Theprungsirikul, P., Canver, A. and Elisseeff, J. (2006). Enhanced chondrogenic differentiation of murine embryonic stem cells in hydrogels with glucosamine. *Biomaterials*, 27(36), pp.6015-6023.

Ishino, Y., Shinagawa, H., Makino, K., Amemura, M. and Nakata, A. (1987). Nucleotide sequence of the *iap* gene, responsible for alkaline phosphatase isozyme conversion in *Escherichia coli*, and identification of the gene product. *Journal of Bacteriology*, 169(12), pp. 5429-5433.

Iulianella A., Beckett B., Petkovich M. and Lohnes D. (1999). A molecular basis for retinoic acid-induced axial truncation. *Developmental Biology*, 205(1), pp.33-48.

Jackson, B., Carpenter, C., Nebert, D. and Vasiliou, V. (2010). Update of human and mouse forkhead box (FOX) gene families. *Human Genomics*, 4(5), pp.345-352.

Jaenisch, R., Schnieke, A. and Harbers, K. (1985). Treatment of mice with 5-azacytidine efficiently activates silent retroviral genomes in different tissues. *Proceedings of the National Academy of Sciences of the United States of America*, 82(5), pp.1451-1455.

Jähner, D. and Jaenisch, R. (1985). Retrovirus-induced de novo methylation of flanking host sequences correlates with gene inactivity. *Nature*, 315(6020), pp.594-597.

James, R. and Schultheiss, T. (2005). Bmp signaling promotes intermediate mesoderm gene expression in a dose-dependent, cell-autonomous and translation-dependent manner. *Developmental Biology*, 288(1), pp.113-125.

James, R., Kamei, C., Wang, Q., Jiang, R. and Schultheiss, T. (2006). Odd-skipped related 1 is required for development of the metanephric kidney and regulates formation and differentiation of kidney precursor cells. *Development*, 133(15), pp.2995-3004.

Jiang, J., Chan, Y., Loh, Y., Cai, J., Tong, G., Lim, C., Robson, P., Zhong, S. and Ng, H.

(2008). A core Klf circuitry regulates self-renewal of embryonic stem cells. *Nature Cell Biology*, 10(3), pp.353-360.

Jinek, M., Chylinski, K., Fonfara, I., Hauer, M., Doudna, J. and Charpentier, E. (2012). A programmable dual-RNA-guided DNA endonuclease in adaptive bacterial immunity. *Science*, 337(6096), pp. 816-821.

Jinek, M., East, A., Cheng, A., Lin, S., Ma, E. and Doudna, J. (2013). RNA-programmed genome editing in human cells. *eLife*, 2, e00471.

Johnson, F., Shimomura, O., Saiga, Y., Gershman, L., Reynolds, G. and Waters, J. (1962). Quantum efficiency of *Cypridina* luminescence, with a note on that of *Aequorea*. *Journal of Cellular Physiology*, 60(1), pp.85-103.

Kawase, E., Suemori, H., Takahashi, N., Okazaki, K., Hashimoto, K. and Nakatsuji, N. (1994). Strain difference in establishment of mouse embryonic stem (ES) cell lines. *International Journal of Developmental Biology*, 38(2), pp.385-390.

Kay, M., Glorioso, J. and Naldini, L. (2016). Viral vectors for gene therapy: the art of turning infectious agents into vehicles of therapeutics. *Nature Medicine*, 7(1), pp.33-40.

Keller, G. (2005). Embryonic stem cell differentiation: emergence of a new era in biology and medicine. *Genes & Development*, 19(10), pp.1129-1155.

Keller, G., Kennedy, M., Papayannopoulou, T. and Wiles, M. (1993). Hematopoietic commitment during embryonic stem cell differentiation in culture. *Molecular and Cellular Biology*, 13(1), pp.473-486.

Kim, D. and Dressler, G. (2005). Nephrogenic factors promote differentiation of mouse embryonic stem cells into renal epithelia. *Journal of the American Society of Nephrology*, 16(12), pp. 3527-3534.

King, T., Beddington, R. and Brown, N. (1998). The role of the brachyury gene in heart development and left–right specification in the mouse. *Mechanisms of Development*, 79(1-2), pp.29-37.

Kispert, A. and Herrmann, B. (1993). The *Brachyury* gene encodes a novel DNA binding protein. *The EMBO Journal*, 12(8), pp. 3211-3220.

Kispert, A. and Herrmann, B. (1994). Immunohistochemical analysis of the Brachyury protein in wild-type and mutant mouse embryos. *Developmental Biology*, 161(1), pp.179-193.

Kispert, A., Koschorz, B. and Herrmann, B. (1995). The T protein encoded by Brachyury is a tissue-specific transcription factor. *EMBO Journal*, 14(19), pp.4763–4772.

Klug, M., Soonpaa, M., Koh, G. and Field, L. (1996). Genetically selected cardiomyocytes from differentiating embryonic stem cells form stable intracardiac grafts. *Journal of Clinical Investigation*, 98(1), pp.216-224.

Kmita, M., van Der Hoeven, F., Zákány, J., Krumlauf, R. and Duboule, D. (2000). Mechanisms of *Hox* gene colinearity: transposition of the anterior *Hoxb1* gene into the posterior *HoxD* complex. *Genes & Development*, 14, pp.198-211.

Köhler, A., Schmithorst, V., Filippi, M., Ryan, M., Daria, D., Gunzer, M. and Geiger, H. (2009). Altered cellular dynamics and endosteal location of aged early hematopoietic progenitor cells revealed by time-lapse intravital imaging in long bones. *Blood*, 114(2), pp.290-298.

Koike, M., Kurosawa H, H. and Amano Y, Y. (2005). A Round-bottom 96-well polystyrene plate coated with 2-methacryloyloxyethyl phosphorylcholine as an effective tool for embryoid body formation. *Cytotechnology*, 47(1-3), pp.3-10.

Koike, M., Sakaki, S., Amano, Y. and Kurosawa, H. (2007). Characterization of embryoid bodies of mouse embryonic stem cells formed under various culture conditions and estimation of differentiation status of such bodies. *Journal of Bioscience and Bioengineering*, 104(4), pp.294-299.

Komor, A., Badran, A. and Liu, D. (2017). CRISPR-based technologies for the manipulation of eukaryotic genomes. *Cell*, 168, pp. 20-35.

Kondo, S., Scheef, E., Sheibani, N. and Sorenson, C. (2007). PECAM-1 isoform-specific regulation of kidney endothelial cell migration and capillary morphogenesis. *AJP: Cell Physiology*, 292(6), pp.C2070-C2083.

Konno, T., Akita, K., Kurita, K. and Ito, Y. (2005). Formation of embryoid bodies by mouse embryonic stem cells on plastic surfaces. *Journal of Bioscience and Bioengineering*, 100(1), pp.88-93.

Kurosawa, H. (2007). Methods for inducing embryoid body formation: *in vitro* differentiation system of embryonic stem cells. *Journal of Bioscience and Bioengineering*, 103(5), pp.389-398.

Kusch, T., Storck, T., Walldorf, U. and Reuter, R. (2002). Brachyury proteins regulate target genes through modular binding sites in a cooperative fashion. *Genes & Development*, 16(4), pp. 518-529.

Kuscu, C., Arslan, S., Singh, R., Thorpe, J. and Adli, M. (2014). Genome-wide analysis reveals characteristics of off-target sites bound by the Cas9 endonuclease. *Nature Biotechnology*, 32, pp. 677-683.

Kuzma-Kuzniarska, M., Rak-Raszewska, A., Kenny, S., Edgar, D., Wilm, B., Fuente Mora, C., Davies, J. and Murray, P. (2012). Integration potential of mouse and human bone marrow-derived mesenchymal stem cells. *Differentiation*, 83(3), pp.128-137.

LaBonne, C. and Bronner-Fraser, M. (1999). Molecular mechanisms of neural crest formation. *Annual Review of Cell and Developmental Biology*, 15(1), pp.81-112.

Laitinen, L., Virtanen, I. and Saxen, L. (1987). Changes in the glycosylation pattern during embryonic development of mouse kidney as revealed with lectin conjugates. *Journal of Histochemistry & Cytochemistry*, 35(1), pp.55-65.

Laker, C., Meyer, J., Schopen, A., Friel, J., Heberlein, C., Ostertag, W. and Stocking, C. (1998). Host *cis*-mediated extinction of a retrovirus permissive for expression in embryonal stem cells during differentiation. *Journal of Virology*, 72(1), pp.339-348.

Lane, S., Wang, Y., Lo Celso, C., Ragu, C., Bullinger, L., Sykes, S., Ferraro, F., Shterental, S., Lin, C., Gilliland, D., Scadden, D., Armstrong, S. and Williams, D. (2011). Differential niche and Wnt requirements during acute myeloid

leukemia progression. *Blood*, 118(10), pp.2849-2856.

Leblond, F., Davis, S., Valdés, P. and Pogue, B. (2010). Pre-clinical whole-body fluorescence imaging: Review of instruments, methods and applications. *Journal of Photochemistry and Photobiology B: Biology*, 98(1), pp.77-94.

Lepperhof, V., Polchynski, O., Kruttwig, K., Brüggemann, C., Neef, K., Drey, F., Zheng, Y., Ackermann, J., Choi, Y., Wunderlich, T., Hoehn, M., Hescheler, J. and Šarić, T. (2014). Bioluminescent Imaging of genetically selected induced pluripotent stem cell-derived cardiomyocytes after transplantation into infarcted heart of syngeneic recipients. *PLoS ONE*, 9(9), p.e107363.

Lewandowski, D., Barroca, V., Ducongé, F., Bayer, J., Van Nhieu, J., Pestourie, C., Fouchet, P., Tavitian, B. and Roméo, P. (2010). *In vivo* cellular imaging pinpoints the role of reactive oxygen species in the early steps of adult hematopoietic reconstitution. *Blood*, 115(3), pp.443-452.

Li, D., Wang, L., Hou, J., Shen, Q., Chen, Q., Wang, X., *et al*. (2016). Optimized approaches for generation of integration-free iPSCs from human urine-derived cells with small molecules and autologous feeder. *Stem Cell Reports*, 6(5), 717-728.

Li, P., Zhang, R., Sun, H., Chen, L., Liu, F., Yao, C., Du, M. and Jiang, X. (2013). PKH26 can transfer to host cells *in vitro* and *vivo*. *Stem Cells and Development*, 22(2), pp.340-344.

Li, Y., McClintick, J., Zhong, L., Edenberg, H., Yoder, M. and Cha, R. (2005). Murine embryonic stem cell differentiation is promoted by SOCS-3 and inhibited by the zinc finger transcription factor Klf4. *Blood*, 105(2), pp.635-637.

Lin, L., Doherty, D., Lile, J., Bektesh, S. and Collins, F. (1993). GDNF: a glial cell line-derived neurotrophic factor for midbrain dopaminergic neurons. *Science*, 260(5111), pp.1130-1132.

Lin, S., Xie, X., Patel, M., Yang, Y., Li, Z., Cao, F., Gheysens, O., Zhang, Y., Gambhir, S., Rao, J. and Wu, J. (2007). Quantum dot imaging for embryonic stem cells. *BMC Biotechnology*, 7, p.67.

Link, S. and El-Sayed, M. (2000). Shape and size dependence of radiative, non-radiative and photothermal properties of gold nanocrystals. *International Reviews in Physical Chemistry*, 19(3), pp.409-453.

Little, M. (2015). *Kidney development, disease, repair and regeneration*. 1st ed. San Diego: Elsevier Science Publishing Co Inc.

Little, M. (2016). Generating kidney tissue from pluripotent stem cells. *Cell Death Discovery*, 2, 16053.

Liu, Y., Jiang, P. and Deng, W. (2011). *OLIG* gene targeting in human pluripotent stem cells for motor neuron and oligodendrocyte differentiation. *Nature Protocols*, 6(5), pp.640-655.

Liu, P., Wakamiya, M., Shea, M., Albrecht, U., Behringer, R. and Bradley, A. (1999). Requirement for *Wnt3* in vertebrate axis formation. *Nature Genetics*, 22(4), pp. 361-365.

Lo Celso, C., Fleming, H., Wu, J., Zhao, C., Miake-Lye, S., Fujisaki, J., Côté, D., Rowe, D., Lin, C. and Scadden, D. (2008). Live-animal tracking of individual haematopoietic stem/progenitor cells in their niche. *Nature*, 457(7225), pp.92-96.

Lois, C., Hong, E., Pease, S., Brown, E. and Baltimore, D. (2002). Germline transmission and tissue-specific expression of transgenes delivered by lentiviral vectors. *Science*, 295(5556), pp.868-872.

Loughna, S., Hardman, P., Landels, E., Jussila, L., Alitalo, K. and Woolf, A. (1997). A molecular and genetic analysis of renalglomerular capillary development. *Angiogenesis*, 1(1), pp.84-101.

Luo, J., Giguère, V., Sladek, R., Bader, J., Matthyssen, A. and Rossant, J. (1997). Placental abnormalities in mouse embryos lacking the orphan nuclear receptor ERR-beta. *Nature*, 388(6644), pp.778-782

Lyons, A. and Parish, C. (1994). Determination of lymphocyte division by flow cytometry. *Journal of Immunological Methods*, 171(1), pp.131-137.

Mahlapuu, M., Ormestad, M., Enerbäck, S. and Carlsson, P. (2001). The forkhead transcription factor *Foxf1* is required for differentiation of extra-embryonic and lateral plate mesoderm. *Development*, 128(2), pp.155-66.

Mali, P., Yang, L., Esvelt, K., Aach, J., Guell, M., DiCarlo, J., Norville, J. and Church, G. (2013). RNA-guided human genome engineering via Cas9. *Science*, 339, pp. 823-826.

Mallo, M., Wellik, D. and Deschamps, J. (2010). *Hox* genes and regional patterning of the vertebrate body plan. *Developmental Biology*, 344(1), pp.7-15.

Mansour, S., Thomas, K. and Capecchi, M. (1988). Disruption of the proto-oncogene *int-2* in mouse embryo-derived stem cells: a general strategy for targeting mutations to non-selectable genes. *Nature*, 336(6197), pp.348-352.

Martin, G. (1980). Teratocarcinomas and mammalian embryogenesis. *Science*, 209(4458), pp.768-776.

Martin, G. (1981). Isolation of a pluripotent cell line from early mouse embryos cultured in medium conditioned by teratocarcinoma stem cells. *Proceedings of the National Academy of Sciences*, 78(12), pp.7634-7638.

Martin, B. and Kimelman, D. (2010). Brachyury establishes the embryonic mesodermal progenitor niche. *Genes & Development*, 24(24), pp. 2778–2783.

Martin, G. and Evans, M. (1975). Differentiation of clonal lines of teratocarcinoma cells: formation of embryoid bodies *in vitro*. *Proceedings of the National Academy of Sciences*, 72(4), pp.1441-1445.

Matsuda, T., Nakao, K., Arai, T., Katsuki, M., Heike, T. and Yokota, T. (2016). STAT3 activation is sufficient to maintain an undifferentiated state of mouse embryonic stem cells. *EMBO Journal*, 2(18), pp.4261-4269.

Matz, M., Fradkov, A., Labas, Y., Savitsky, A., Zaraisky, A., Markelov, M. and Lukyanov, S. (1999). Fluorescent proteins from nonbioluminescent *Anthozoa* species. *Nature Biotechnology*, 17(10), pp.969-973.

McMahon, A. and Bradley, A. (1990). The *Wnt-1 (int-1)* proto-oncogene is required for development of a large region of the mouse brain. *Cell*, 62(6), pp.1073-1085.

Mempel, T., Pittet, M., Khazaie, K., Weninger, W., Weissleder, R., von Boehmer, H. and von Andrian, U. (2006). Regulatory T cells reversibly suppress cytotoxic t cell function independent of effector differentiation. *Immunity*, 25(1), pp.129-141.

Merzlyak, E., Goedhart, J., Shcherbo, D., Bulina, M., Shcheglov, A., Fradkov, A., Gaintzeva, A., Lukyanov, K., Lukyanov, S., Gadella, T. and Chudakov, D. (2007). Bright monomeric red fluorescent protein with an extended fluorescence lifetime. *Nature Methods*, 4(7), pp.555-557.

Mitsui, K., Tokuzawa, Y., Itoh H, H., Segawa, K., Murakami, M., Takahashi, K., Maruyama, M., Maeda, M. and Yamanaka, S. (2003). The homeoprotein Nanog is required for maintenance of pluripotency in mouse epiblast and ES cells. *Cell*, 113(5), pp.631-642.

Mohamed, M., Volkov, V., Link, S. and El-Sayed, M. (2000). The `lightning' gold nanorods: fluorescence enhancement of over a million compared to the gold metal. *Chemical Physics Letters*, 317(6), pp.517-523.

Monticelli, S. (2010). *MicroRNAs and the immune system*. New York, NY: Humana Press.

Mugford, J., Sipilä, P., McMahon, J. and McMahon, A. (2008). *Osr1* expression demarcates a multi-potent population of intermediate mesoderm that undergoes progressive restriction to an *Osr1*-dependent nephron progenitor compartment within the mammalian kidney. *Developmental Biology*, 324(1), pp.88-98.

Muller-Borer, B., Collins, M., Gunst, P., Cascio, W. and Kypson, A. (2007). Quantum dot labeling of mesenchymal stem cells. *Journal of Nanobiotechnology*, 5(1), p.9.

Mundel, P., Heid, H., Mundel, T., Krüger, M., Reiser, J. and Kriz, W. (1997). Synaptopodin: An Actin-associated protein in telencephalic dendrites and renal podocytes. *J Cell Biol*, 139(1), pp.193-204.

Murray, P. and Edgar, D. (2000). Regulation of programmed cell death by basement membranes in embryonic development. *Journal of Cell Biology*, 150(5), pp.1215-1221.

Nadijcka, M. and Hillman, N. (1974). Ultrastructural studies of the mouse blastocyst substages. *Journal of Embryology & Experimental Morphology*, 32(3), pp.675-695.

Nagy, A., Marina, G., Kristina, V. and Richard, B. (2003). *Manipulating the mouse embryo*. Cold Spring Harbor, N.Y.: Cold Spring Harbor Laboratory Press.

Naldini, L., Blömer, U., Gallay, P., Ory, D., Mulligan, R., Gage, F., Verma, I. and Trono, D. (1996). *In vivo* gene delivery and stable transduction of nondividing cells by a lentiviral vector. *Science*, 272(5259), pp.263-267.

Narducci, M., Fiorenza, M., Kang, S., Bevilacqua, A., Di Giacomo, M., Remotti, D., Picchio, M., Fidanza, V., Cooper, M., Croce, C., Mangia, F. and Russo, G. (2002). TCL1 participates in early embryonic development and is overexpressed in human seminomas. *Proceedings of the National Academy of Sciences*, 99(18), pp.11712-11717.

Narkilahti, S., Rajala, K., Pihlajamäki, H., Suuronen, R., Hovatta, O. and Skottman, H. (2007). Monitoring and analysis of dynamic growth of human embryonic stem cells: comparison of automated instrumentation and conventional culturing methods. *BioMedical Engineering OnLine*, 6, p.11.

Nat, R., Nilbratt M, M., Narkilahti, S., Winblad, B., Hovatta, O. and Nordberg, A. (2007). Neurogenic neuroepithelial and radial glial cells generated from six human embryonic stem cell lines in serum-free suspension and adherent cultures. *GLIA*, 55(4), pp.385-399.

Neumann, E., Schaefer-Ridder, M., Wang, Y. and Hofschneider, P. (1982). Gene transfer into mouse lyoma cells by electroporation in high electric fields. *EMBO Journal*, 1(7), pp.841–845.

Nichols, J. and Smith, A. (2012). Pluripotency in the embryo and in culture. *Cold Spring Harbor Perspectives in Biology*, 4(8), p.a008128.

Niwa, H., Yamamura, K. and Miyazaki, J. (1991). Efficient selection for high-expression transfectants with a novel eukaryotic vector. *Gene*, 108(2), pp. 193-199.

Niwa, H., Burdon, T., Chambers, I. and Smith, A. (1998). Self-renewal of pluripotent embryonic stem cells is mediated via activation of STAT3. *Genes & Development*, 1(12), pp.2048-2060.

Nussbaum, J., Minami, E., Laflamme, M., Virag, J., Ware, C., Masino, A., Muskheli, V., Pabon, L., Reinecke, H. and Murry, C. (2007). Transplantation of undifferentiated murine embryonic stem cells in the heart: teratoma formation and immune response. *FASEB Journal*, 21(7), pp.1345-1357.

Oeda, S., Hayashi, Y., Chan, T., Takasato, M., Aihara, Y., Okabayashi, K., Ohnuma, K. and Asashima, M. (2013). Induction of intermediate mesoderm by retinoic acid receptor signaling from differentiating mouse embryonic stem cells. *The International Journal of Developmental Biology*, 57(5), pp.383-389.

Org, T., Duan, D., Ferrari, R., Montel-Hagen, A., Van Handel, B., Kerényi, M., et al. (2015). Scl binds to primed enhancers in mesoderm to regulate hematopoietic and cardiac fate divergence. *The EMBO Journal*, 34(6), pp. 759-777.

Papaioannou, V. (2014). The T-box gene family: emerging roles in development stem cells and cancer. *Development*, 141(20), pp.3819-3833.

Parish, C. (1999). Fluorescent dyes for lymphocyte migration and proliferation studies. *Immunology and Cell Biology*, 77(6), pp.499-508.

Park, C., Afrikanova, I., Chung, Y., Zhang, W., Arentson, E., Fong, G., Rosendahl, A. and Choi, K. (2004). A hierarchical order of factors in the generation of FLK1- and SCL-expressing hematopoietic and endothelial progenitors from embryonic stem cells. *Development*, 131(11), pp.2749-2762.

Pedersen, A., Skjong, C. and Shawlot, W. (2005). *Lim1* is required for nephric duct extension and ureteric bud morphogenesis. *Developmental Biology*, 288(2), pp.571-581.

Pfeifer, A., Ikawa, M., Dayn, Y. and Verma, I. (2002). Transgenesis by lentiviral

vectors: lack of gene silencing in mammalian embryonic stem cells and preimplantation embryos. *Proceedings of the National Academy of Sciences of the United States of America*, 99(4), pp.2140-2145.

Plachta, N. (2004). Developmental potential of defined neural progenitors derived from mouse embryonic stem cells. *Development*, 131(21), pp.5449-5456.

Pollard, J. and Walker, J. (1997). *Basic cell culture protocols*. 1st ed. Totowa, N.J.: Humana Press, pp.173-184.

Ragnarson, B., Bengtsson, L. and Haegerstrand, A. (1992). Labeling with fluorescent carbocyanine dyes of cultured endothelial and smooth muscle cells by growth in dye-containing medium. *Histochemistry*, 97(4), pp.329-333.

Rak-Raszewska, A. (2010). *Investigating the nephrogenic potential of mouse embryonic stem cells and their derivatives*. Doctoral thesis. University of Liverpool.

Rak-Raszewska, A., Hauser, P. and Vainio, S. (2015). Organ*In vitro*Culture: What have we learned about early kidney development? *Stem Cells International*, 2015, pp.1-16.

Rak-Raszewska, A., Marcello, M., Kenny, S., Edgar, D., Sœ, V. and Murray, P. (2012b). Quantum dots do not affect the behaviour of mouse embryonic stem cells and kidney stem cells and are suitable for short-term tracking. *PLoS ONE*, 7(3), p.e32650.

Rak-Raszewska, A., Wilm, B., Edgar, D., Kenny, S., Woolf, A. and Murray, P. (2012a). Development of embryonic stem cells in recombinant kidneys. *Organogenesis*, 8(4), pp.125-136.

Ran, F., Cong, L., Yan, W., Scott, D.A., Gootenberg, J., Kriz, A., Zetsche, B., Shalem, O., Wu, X., Makarova, K., *et al*. (2015). *In vivo* genome editing using *Staphylococcus aureus* Cas9. *Nature*, 520, pp. 186-191.

Ranghini, E., Mora, C., Edgar, D., Kenny, S., Murray, P. and Wilm, B. (2013). Stem cells derived from neonatal mouse kidney generate functional proximal tubule-like cells and integrate into developing nephrons *In vitro*. *PLoS ONE*,

8(5), p.e62953.

Ren, X., Ustiyan, V., Pradhan, A., Cai, Y., Havrilak, J., Bolte, C., Shannon, J., Kalin, T. and Kalinichenko, V. (2014). FOXF1 Transcription Factor Is Required for Formation of Embryonic Vasculature by Regulating VEGF Signaling in Endothelial Cells. *Circulation Research*, 115(8), pp.709-720.

Risau, W., Sariola, H., Zerwes, H., Sasse, J., Ekblom, P., Kemler, R. and Doetschman, T. (1988). Vasculogenesis and angiogenesis in embryonic-stem-cell-derived embryoid bodies. *Development*, 102, pp.471-478.

Rivera-Pérez, J. and Magnuson, T. (2005). Primitive streak formation in mice is preceded by localized activation of *Brachyury* and *Wnt3*. *Developmental Biology*, 288(2), pp.363-371.

Robertson, E. (1987). *Teratocarcinomas and embryonic stem cells*. Oxford: IRL Press.

Robertson, E., Bradley, A., Kuehn, M. and Evans, M. (1986). Germ-line transmission of genes introduced into cultured pluripotential cells by retroviral vector. *Nature*, 323(6087), pp.445-448.

Rodriguez, T., Srinivas, S., Clements, M., Smith, J. and Beddington, R. (2005). Induction and migration of the anterior visceral endoderm is regulated by the extra-embryonic ectoderm. *Development*, 132(11), pp.2513-2520.

Roe, T., Reynolds, T., Yu, G. and Brown, P. (1993). Integration of murine leukemia virus DNA depends on mitosis. *EMBO Journal*, 12(5), pp.2099-2108.

Rosen, A., Kelly, D., Schuldt, A., Lu, J., Potapova, I., Doronin, S., Robichaud, K., Robinson, R., Rosen, M., Brink, P., Gaudette, G. and Cohen, I. (2007). Finding fluorescent needles in the cardiac haystack: tracking human mesenchymal stem cells labeled with quantum dots for quantitative *in vivo* three-dimensional fluorescence analysis. *Stem Cells*, 25(8), pp.2128-2138.

Rusk, N. (2009). *Milestone 4: Nature Milestones in Light Microscopy*. [online] Nature.com. Available at: http://www.nature.com/milestones/milelight/full/milelight04.html [Accessed 10 Nov. 2016].

Sainio, K. and Raatikainen-Ahokas, A. (1999). Mesonephric kidney--a stem cell factory? *The International Journal of Developmental Biology*, 43(2), pp.435-9.

Sainio, K., Suvanto, P., Davies, J., Wartiovaara, J., Wartiovaara, K., Saarma, M., Arumäe, U., Meng, X., Lindahl, M., Pachnis, V. and Sariola, H. (1997). Glial-cell-line-derived neurotrophic factor is required for bud initiation from ureteric epithelium. *Development*, 124(20), pp.4077-4087.

Sakurai, H., Inami, Y., Tamamura, Y., Yoshikai, T., Sehara-Fujisawa, A. and Isobe, K. (2009). Bidirectional induction toward paraxial mesodermal derivatives from mouse ES cells in chemically defined medium. *Stem Cell Research*, 3(2-3), pp.157-169.

Salamat, M., Miosge, N. and Herken, R. (1995). Development of Reichert's membrane in the early mouse embryo. (1995). *Anatomy and Embryology* (Berl), 192(3), pp.275-281.

Sánchez, M., Silos-Santiago, I., Frisén, J., He, B., Lira, S. and Barbacid, M. (1996). Renal agenesis and the absence of enteric neurons in mice lacking GDNF. *Nature*, 382(6586), pp.70-73.

Sanchez-Aguilera, A., Lee, Y., Lo Celso, C., Ferraro, F., Brumme, K., Mondal, S., Kim, C., Dorrance, A., Luo, H., Scadden, D. and Williams, D. (2011). Guanine nucleotide exchange factor Vav1 regulates perivascular homing and bone marrow retention of hematopoietic stem and progenitor cells. *Proceedings of the National Academy of Sciences of the United States of America*, 108(23), pp.9607-9612.

Savory, J., Bouchard, N., Pierre, V., Rijli, F., De Repentigny, Y., Kothary, R. and Lohnes, D. (2009). *Cdx2* regulation of posterior development through non-Hox targets. *Development*, 136(24), pp.4099-4110.

Saxén, L. (1987). *Organogenesis of the kidney*. Cambridge [Cambridgeshire]: Cambridge University Press.

Serbedzija, G., Bronner-Fraser, M., Bronner-Fraser, M. and Fraser, S. (1989). A vital dye analysis of the timing and pathways of avian trunk neural crest cell

migration. *Development*, 106(4), pp.809-16.

Shaaban, A., Rezvani, M., Elsayes, K., Baskin, H., Mourad, A., Foster, B., Jarboe, E. and Menias, C. (2014). Ovarian malignant germ cell tumors: cellular classification and clinical and imaging features. *RadioGraphics*, 34(3), pp.777-801.

Shaner, N., Campbell, R., Steinbach, P., Giepmans, B., Palmer, A. and Tsien, R. (2004). Improved monomeric red, orange and yellow fluorescent proteins derived from *Discosoma sp*. red fluorescent protein. *Nature Biotechnology*, 22(12), pp.1567-1572.

Shcherbo, D., Merzlyak, E., Chepurnykh, T., Fradkov, A., Ermakova, G., Solovieva, E., Lukyanov, K., Bogdanova, E., Zaraisky, A., Lukyanov, S. and Chudakov, D. (2007). Bright far-red fluorescent protein for whole-body imaging. *Nature Methods*, 4(9), pp.741-746.

Shcherbo, D., Murphy, C., Ermakova, G., Solovieva, E., Chepurnykh, T., Shcheglov, A., Verkhusha, V., Pletnev, V., Hazelwood, K., Roche, P., Lukyanov, S., Zaraisky, A., Davidson, M. and Chudakov, D. (2009). Far-red fluorescent tags for protein imaging in living tissues. *Biochem. J.*, 418(3), pp.567-574.

Shen, M. and Leder, P. (1992). Leukemia inhibitory factor is expressed by the preimplantation uterus and selectively blocks primitive ectoderm formation *in vitro*. *Proceedings of the National Academy of Sciences*, 89(17), pp.8240-8244.

Shen B., Zhang J., Wu H., Wang J., Ma K., Li Z., Zhang X., Zhang P. and Huang X. (2013). Generation of gene-modified mice via Cas9/RNA-mediated gene targeting. *Cell Research*, 23(5), pp.720-723.

Shimomura, O., Johnson, F. and Saiga, Y. (1962). Extraction, purification and properties of aequorin, a bioluminescent protein from the luminous hydromedusan, *Aequorea*. *Journal of Cellular Physiology*, 59(3), pp.223-239.

Shinji, T., Koide, N. and Tsuji, T. (1988). Glycosaminoglycans partially substitute for proteoglycans in spheroid formation of adult rat hepatocytes in primary

culture. *Cell Structure and Function*, 13(2), pp.179-188.

Showell, C., Binder, O. and Conlon, F. (2003). T-box genes in early embryogenesis. *Developmental Dynamics*, 229(1), pp.201-218.

Smith, A. (2001). Embryo-derived stem cells: of mice and men. *Annual Review of Cell and Developmental Biology*, 17(1), pp.435-462.

Smith-Arica, J., Thomson, A., Ansell, R., Chiorini, J., Davidson, B. and McWhir, J. (2003). Infection efficiency of human and mouse embryonic stem cells using adenoviral and adeno-associated viral vectors. *Cloning Stem Cells*, 5(1), pp.51-62.

Solter, D., Škreb, N. and Damjanov, I. (1970). Extrauterine Growth of Mouse Egg-cylinders results in Malignant Teratoma. *Nature*, 227(5257), pp.503-504.

Song, B., Smink, A., Jones; C., Callaghan, J., Firth, S., Bernard, C., Laslett A., Kerr, P. and Ricardo, S. (2012). The directed differentiation of human iPS cells into kidney podocytes. *PLoS One*, 7(9), e46453.

Soriano, P. (1999). Generalized lacZ expression with the ROSA26 Cre reporter strain. *Nature Genetics*, 21(1), pp.70-71.

Stern, C. (2004). *Gastrulation*. 1st ed. Cold Spring Harbor, N.Y.: Cold Spring Harbor Laboratory Press.

Stevens, L. (1970). The development of transplantable teratocarcinomas from intratesticular grafts of pre- and postimplantation mouse embryos. *Developmental Biology*, 21(3), pp.364-382.

Strack, R., Hein, B., Bhattacharyya, D., Hell, S., Keenan, R. and Glick, B. (2009). A Rapidly maturing far-red derivative of DsRed-Express2 for whole-cell labeling. *Biochemistry*, 48(35), pp.8279-8281.

Strack, R., Strongin, D., Bhattacharyya, D., Tao, W., Berman, A., Broxmeyer, H., Keenan, R. and Glick, B. (2008). A noncytotoxic DsRed variant for whole-cell labeling. *Nature Methods*, 5(11), pp.955-957.

Suemori, H., Takahashi, N. and Noguchi, S. (1995). *Hoxc-9* mutant mice show anterior transformation of the vertebrae and malformation of the sternum and ribs.

Mechanisms of Development, 51(2-3), pp.265-273.

Suslov, O., Kukekov, V., Ignatova, T. and Steindler, D. (2002). Neural stem cell heterogeneity demonstrated by molecular phenotyping of clonal neurospheres. *Proceedings of the National Academy of Sciences*, 99(22), pp.14506-14511.

Suzuki, O., Matruda, J., Takano, K., Yamamoto, Y., Asano, T., Naiki, M. and Kusanagi, M. (1999). Effect of genetic background on establishment of mouse embryonic stem cells. *Experimental Animals*, 48(3), pp.213-216.

Taguchi, A., Kaku, Y., Ohmori, T., Sharmin, S., Ogawa, M., Sasaki, H. and Nishinakamura, R. (2014). Redefining the *in vivo* origin of metanephric nephron progenitors enables generation of complex kidney structures from pluripotent stem cells. *Cell Stem Cell*, 14(1), pp.53-67.

Takada, S., Stark, K., Shea, M., Vassileva, G., McMahon, J. and McMahon, A. (1994). *Wnt-3a* regulates somite and tailbud formation in the mouse embryo. *Genes & Development*, 8(2), pp.174-189.

Takasato, M., Er, P., Becroft, M., Vanslambrouck, J., Stanley, E., Elefanty, A. and Little, M. (2014). Directing human embryonic stem cell differentiation towards a renal lineage generates a self-organizing kidney. *Nature Cell Biology*, 16(1), pp.118-126.

Tam, P. and Beddington, R. (1987). The formation of mesodermal tissues in the mouse embryo during gastrulation and early organogenesis. *Development*, 99(1), pp.109-126.

Tam, P. and Behringer, R. (1997). Mouse gastrulation: the formation of a mammalian body plan. *Mechanisms of Development*, 68(1-2), pp.3-25.

Tam, P. and Loebel, D. (2007). Gene function in mouse embryogenesis: get set for gastrulation. *Nature Reviews Genetics*, 8(5), pp.368-381.

Tarkowski, A. and Wróblewska, J. (1967). Development of blastomeres of mouse eggs isolated at the 4- and 8-cell stage. *Journal of Embryology & Experimental Morphology*, 18(1), pp.155-180.

Thomas, K. and Capecchi, M. (1987). Site-directed mutagenesis by gene targeting in

mouse embryo-derived stem cells. *Cell*, 51(3), pp.503-512.

Thomas, K. and Capecchi, M. (1990). Targeted disruption of the murine int-1 proto-oncogene resulting in severe abnormalities in midbrain and cerebellar development. *Nature*, 346(6287), pp.847-850.

Tilmann, C. (2002). Cellular and molecular pathways regulating mammalian sex determination. *Recent Progress in Hormone Research*, 57(1), pp.1-18.

Tomayko, M. and Reynolds, P. (1989). Determination of subcutaneous tumor size in athymic (nude) mice. *Cancer Chemotherapy and Pharmacology*, 24(3), pp.148–154.

Tonegawa, A. and Takahashi, Y. (1998). Somitogenesis controlled by Noggin. *Developmental Biology*, 202(2), pp.172-182.

Tong, C., Huang, G., Ashton, C., Li, P. and Ying, Q. (2011). Generating gene knockout rats by homologous recombination in embryonic stem cells. *Nature Protocols*, 6(6), pp.827-844.

Trono, D. (2000). Lentiviral vectors: turning a deadly foe into a therapeutic agent. *Gene Therapy*, 7(1), pp.20-23.

Tsakiridis, A. and Wilson, V. (2015). Assessing the bipotency of in vitro-derived neuromesodermal progenitors. *F1000Research*, 4, 100.

Turksen, K. (2002). *Embryonic stem cells*. 1st ed. Totowa, N.J.: Humana Press, pp.17-26.

Turner, D., Ruḛ P., Mackenzie, J., Davies, E. and Martinez Arias, A. (2014a). Brachyury cooperates with Wnt/β-catenin signalling to elicit primitive-streak-like behaviour in differentiating mouse embryonic stem cells. *BMC Biology*, 12(1).

Turner, D., Trott, J., Hayward, P., Rue, P. and Martinez Arias, A. (2014b). An interplay between extracellular signalling and the dynamics of the exit from pluripotency drives cell fate decisions in mouse ES cells. *Biology Open*, 3(7), pp.614-626.

Unbekandt, M. and Davies, J. (2010). Dissociation of embryonic kidneys followed by

reaggregation allows the formation of renal tissues. *Kidney International*, 77(5), pp.407-416.

Vasquez, K., Marburger, K., Intody, Z. and Wilson, J. (2001). Manipulating the mammalian genome by homologous recombination. *Proceedings of the National Academy of Sciences*, 98(15), pp.8403-8410.

Vigneau, C., Polgar, K., Striker, G., Elliott, J., Hyink, D., Weber, O., Fehling, H., Keller, G., Burrow, C. and Wilson, P. (2007). Mouse embryonic stem cell-derived embryoid bodies generate progenitors that integrate long term into renal proximal tubules *in vivo*. *Journal of the American Society of Nephrology*, 18(6), pp.1709-1720.

Wagner, D., Delk, N., Lukianova-Hleb, E., Hafner, J., Farach-Carson, M. and Lapotko, D. (2010). The *in vivo* performance of plasmonic nanobubbles as cell theranostic agents in zebrafish hosting prostate cancer xenografts. *Biomaterials*, 31(29), pp.7567-7574.

Wang, H., Yang, H., Shivalila, C., Dawlaty, M., Cheng, A., Zhang, F. and Jaenisch, R. (2013). One-step generation of mice carrying mutations in multiple genes by CRISPR/Cas-mediated genome engineering. *Cell*, 153, pp. 910-918.

Wakitani, S., Takaoka, K., Hattori, T., Miyazawa, N., Iwanaga, T., Takeda, S., Watanabe, T. and Tanigami, A. (2003). Embryonic stem cells injected into the mouse knee joint form teratomas and subsequently destroy the joint. *Rheumatology*, 42(1), pp.162-165.

Walter, M., Wright, K., Fuller, H., MacNeil, S. and Johnson, W. (2010). Mesenchymal stem cell-conditioned medium accelerates skin wound healing: an *in vitro* study of fibroblast and keratinocyte scratch assays. *Experimental Cell Research*, 316(7), pp.1271-1281.

Wang, L. and Wu, H. (2007). *Biomedical optics*. 1st ed. Hoboken, N.J.: Wiley-Interscience.

Wang, L., Jackson, W., Steinbach, P. and Tsien, R. (2004). Evolution of new nonantibody proteins via iterative somatic hypermutation. *Proceedings of the*

National Academy of Sciences, 101(48), pp.16745-16749.

Wartenberg, M., Günther, J., Hescheler, J. and Sauer, H. (1998). The embryoid body as a novel *in vitro* assay system for antiangiogenic agents. *Laboratory Investigation*, 78(10), pp.1301-1214.

Weissleder, R. (2001). A clearer vision for *in vivo* imaging. *Nature Biotechnology*, 19(4), pp.316-317.

Wetherell, D. (2014). Mature and immature teratoma: a review of pathological characteristics and treatment options. *Medical & Surgical Urology*, 03(01).

Wickham, T., Mathias, P., Cheresh, D. and Nemerow, G. (1993). Integrins alpha v beta 3 and alpha v beta 5 promote adenovirus internalization but not virus attachment. *Cell*, 73(2), pp.309-319.

Wiedenheft, B., Zhou, K., Jinek, M., Coyle, S., Ma, W. and Doudna, J. (2009). Structural basis for DNase activity of a conserved protein implicated in CRISPR-mediated genome defense. *Structure*, 17(6), pp. 904-912.

Wiedenheft, B., Sternberg, S. and Doudna, J. (2012). RNA-guided genetic silencing systems in bacteria and archaea. *Nature*, 482, pp. 331-338.

Wilkinson, D., Bhatt, S. and Herrmann, B. (1990). Expression pattern of the mouse *T* gene and its role in mesoderm formation. *Nature*, 343(6259), pp.657-659.

Winnier, G., Blessing, M., Labosky, P. and Hogan, B. (1995). Bone morphogenetic protein-4 is required for mesoderm formation and patterning in the mouse. *Genes & Development*, 9(17), pp.2105-2116.

Wobus, A., Holzhausen, H., Jäkel, P. and Schöneich, J. (1984). Characterization of a pluripotent stem cell line derived from a mouse embryo. *Experimental Cell Research*, 152(1), pp.212-219.

Wray, J., Kalkan, T. and Smith, A. (2010). The ground state of pluripotency. *Biochemical Society Transactions*, 38(4), pp.1027-1032.

Yagi, T., Ikawa, Y., Yoshida, K., Shigetani, Y., Takeda, N., Mabuchi, I., Yamamoto, T. and Aizawa, S. (1990). Homologous recombination at *c-fyn* locus of mouse embryonic stem cells with use of diphtheria toxin A-fragment gene in negative

selection. *Proceedings of the National Academy of Sciences*, 87(24), pp.9918-9922.

Yagi, T., Nada, S., Watanabe, N., Tamemoto, H., Kohmura, N., Ikawa, Y. and Aizawa, S. (1993). A novel negative selection for homologous recombinants using diphtheria toxin A fragment gene. *Analytical Biochemistry*, 214(1), pp.77-86.

Yallowitz, A., Hrycaj, S., Short, K., Smyth, I. and Wellik, D. (2011). *Hox10* Genes function in kidney development in the differentiation and integration of the cortical stroma. *PLoS ONE*, 6(8), p.e23410.

Yamagata, Y., Parietti, V., Stockholm, D., Corre, G., Poinsignon, C., Touleimat, N., Delafoy, D., Besse, C., Tost, J., Galy, A. and Paldi, A. (2012). Lentiviral transduction of $CD34^{+}$ cells induces genome-wide epigenetic modifications. *PLoS ONE*, 7(11), p.e48943.

Yamaguchi, T., Harpal, K., Henkemeyer, M., and Rossant, J. (1994). fgfr-1 is required for embryonic growth and mesodermal patterning during mouse gastrulation. *Genes & Development*, 8(24), pp. 3032-3044.

Yamaguchi, T., Takada, S., Yoshikawa, Y., Wu, N. and McMahon, A. (1999). *T* (Brachyury) is a direct target of Wnt3a during paraxial mesoderm specification. *Genes & Development*, 13(24), 3185-3190.

Yamamoto, M. (2005). Branching ducts similar to mesonephric ducts or ureteric buds in teratomas originating from mouse embryonic stem cells. *AJP: Renal Physiology*, 290(1), pp.F52-F60.

Yang, T., Cheng, L. and Kain, S. (1996). Optimized codon usage and chromophore mutations provide enhanced sensitivity with the green fluorescent protein. *Nucleic Acids Research*, 24(22), pp.4592-4593.

Yang, H., Wang, H. and Jaenisch, R. (2014). Generating genetically modified mice using CRISPR/Cas-mediated genome engineering. *Nature Protocols*, 9(8), pp. 1956-1968.

Yanushevich, Y., Staroverov, D., Savitsky, A., Fradkov, A., Gurskaya, N., Bulina, M., Lukyanov, K. and Lukyanov, S. (2001). A strategy for the generation of

non-aggregating mutants of *Anthozoa* fluorescent proteins. *FEBS Letters*, 511(1-3), pp.11-14.

Ying, Q. and Smith, A. (2003). Defined conditions for neural commitment and differentiation. *Methods in EnzymologY*, 365(2), pp.327-341.

Yoder, J., Walsh, C. and Bestor, T. (1997). Cytosine methylation and the ecology of intragenomic parasites. *Trends in Genetics*, 13(8), pp.335-340.

Yoshikawa, Y., Fujimori, T., McMahon, A. and Takada, S. (1997). Evidence that absence of *Wnt-3a* signaling promotes neuralization instead of paraxial mesoderm development in the mouse. *Developmental Biology*, 183(2), pp. 234-242.

Yusuf, R. and Scadden, D. (2009). Homing of hematopoietic cells to the bone marrow. *Journal of Visualized Experiments*, (25).

Zambrowicz, B., Imamoto, A., Fiering, S., Herzenberg, L., Kerr, W. and Soriano, P. (1997). Disruption of overlapping transcripts in the ROSA β-geo 26 gene trap strain leads to widespread expression of β-galactosidase in mouse embryos and hematopoietic cells. *Proceedings of the National Academy of Sciences*, 94(8), pp.3789-3794.

Zhang, H., Nieves, J., Fraser, S. T., Isern, J., Douvaras, P., Papatsenko, D., *et al*. (2014). Expression of Podocalyxin separates the hematopoietic and vascular potentials of mouse ES cell-derived mesoderm. *Stem Cells*, 32(1), pp. 191-203.

Zhu, X., Fang, C., Jia, H., Huang, Y., Cheng, C., Ko, C., Chen, Z., Wang, J. and Wang, Y. (2014). Cellular uptake behaviour, photothermal therapy performance, and cytotoxicity of gold nanorods with various coatings. *Nanoscale*, 6(19), pp.11462-11472.

Zhou, T., Benda, C., Duzinger, S., Huang, Y., Li, X., Li, Y., *et al*. (2011). Generation of induced pluripotent stem cells from urine. *Journal of the American Society of Nephrology*, 22(7), pp. 1221-1228.

Zinder, N. and Lederberg, J. (1952). Genetic exchange in *Salmonella*. *Journal of Bacteriology*, 64(5), pp.679–699.

Appendix

Table 1 Tumour Monitoring Record Post Injection of *Bra-GFP/Rosa26-E2C* mESCs

Mouse No.	Cell Lines	Cell No. (Mil.)	Day 4				Day 7				Day 9			
			W (g)	L (mm)	W (mm)	H (mm)	W (g)	L (mm)	W (mm)	H (mm)	W (g)	L (mm)	W (mm)	H (mm)
1	E2C	10	19.34	5.1	6.2	2.0	19.15	N/A	N/A	N/A	19.52	N/A	N/A	N/A
		7.5		N/A	N/A	N/A		N/A	N/A	N/A		6.4	4.5	3.5
		5		N/A	N/A	N/A		N/A	N/A	N/A		4.4	4.4	2.2
	Ctrl	10		N/A	N/A	N/A		6.8	6.7	4.0		9.2	9.0	7.7
2	E2C	10	17.00	3.4	4.4	2.0	17.55	3.6	3.5	3.0	17.72	5.6	4.7	3.2
		7.5		N/A	N/A	N/A		5.2	5.3	3.0		9.6	8.9	6.4
		5		N/A	N/A	N/A		4.0	4.9	3.0		9.0	6.8	4.7
	Ctrl	10		N/A	N/A	N/A		3.6	3.3	3.0		5.4	5.4	3.0
3	E2C	10	18.20	5.8	6.0	2.0	20.45	8.5	5.2	3.0	20.88	9.9	9.7	5.3
		7.5		N/A	N/A	N/A		7.0	7.0	3.0		9.7	9.6	6.7
		5		N/A	N/A	N/A		3.0	3.0	1.0		4.8	3.4	1.0
	Ctrl	10		N/A	N/A	N/A		3.0	3.0	1.0		5.5	4.8	3.2

(W, weight; L, length; W, width; E2C, *Bra-GFP/Rosa26-E2C* mESCs; Ctrl, untransfected *E14-Bra-GFP* mESCs)

Table 2 Tumour Volume and *In Vivo* Monitoring Record Post Injection of *Bra-GFP/Rosa26-E2C* mESCs

Cell Lines	Cell No. ($\times 10^6$)	Mouse No.	**ROI values** (e+08) (radiance: p/sec/cm^2/sr)					**Volume** (mm^3)		
			Day 0	**Day 1**	**Day 4**	**Day 7**	**Day 9**	**Day 4**	**Day 7**	**Day 9**
E2C	10	1	2.127	1.368	2.376	1.881	1.834	33.11	0.00	0.00
		2	2.142	1.305	2.275	2.276	2.480	15.67	19.79	44.10
		3	2.723	1.908	4.135	3.933	3.122	36.44	69.43	266.49
		Mean	2.331	1.527	2.929	2.697	2.479	28.41	29.74	103.53
			±0.340	±0.331	±1.046	±1.089	±0.644	±11.159	±35.768	±142.840
	7.5	1	2.657	1.780	2.981	3.129	3.109	0.00	0.00	52.78
		2	2.243	1.447	2.983	2.639	2.749	0.00	43.29	286.31
		3	1.742	1.174	2.330	2.860	2.416	0.00	76.97	326.68
		Mean	2.214	1.467	2.813	2.876	2.758	0.00	40.09	221.92
			±0.458	±0.303	±0.376	±0.245	±0.347	±0.000	±38.584	±147.866
	5	1	2.180	1.580	2.459	2.528	2.546	0.00	0.00	22.30
		2	1.821	1.318	2.869	2.017	2.127	0.00	30.79	150.61
		3	1.705	1.659	2.475	2.429	2.608	0.00	4.71	8.55
		Mean	1.902	1.519	2.601	2.325	2.427	0.00	11.83	60.48
			±0.248	±0.178	±0.232	±0.271	±0.262	±0.000	±16.583	±78.351
Ctrl	10	1	1.419	1.115	1.849	1.459	1.475	0.00	95.42	333.83
		2	1.826	1.448	2.933	1.895	2.227	0.00	18.66	45.80
		3	2.122	1.357	3.517	2.361	2.861	0.00	4.71	44.23
		Mean	1.789	1.307	2.766	1.905	2.188	0.00	39.60	141.29
			±0.353	±0.172	±0.846	±0.451	±0.694	±0.000	±48.844	±166.744

(ROI, region of interest; E2C, *Bra-GFP/Rosa26-E2C* mESCs; Ctrl, untransfected *E14-Bra-GFP* mESCs)

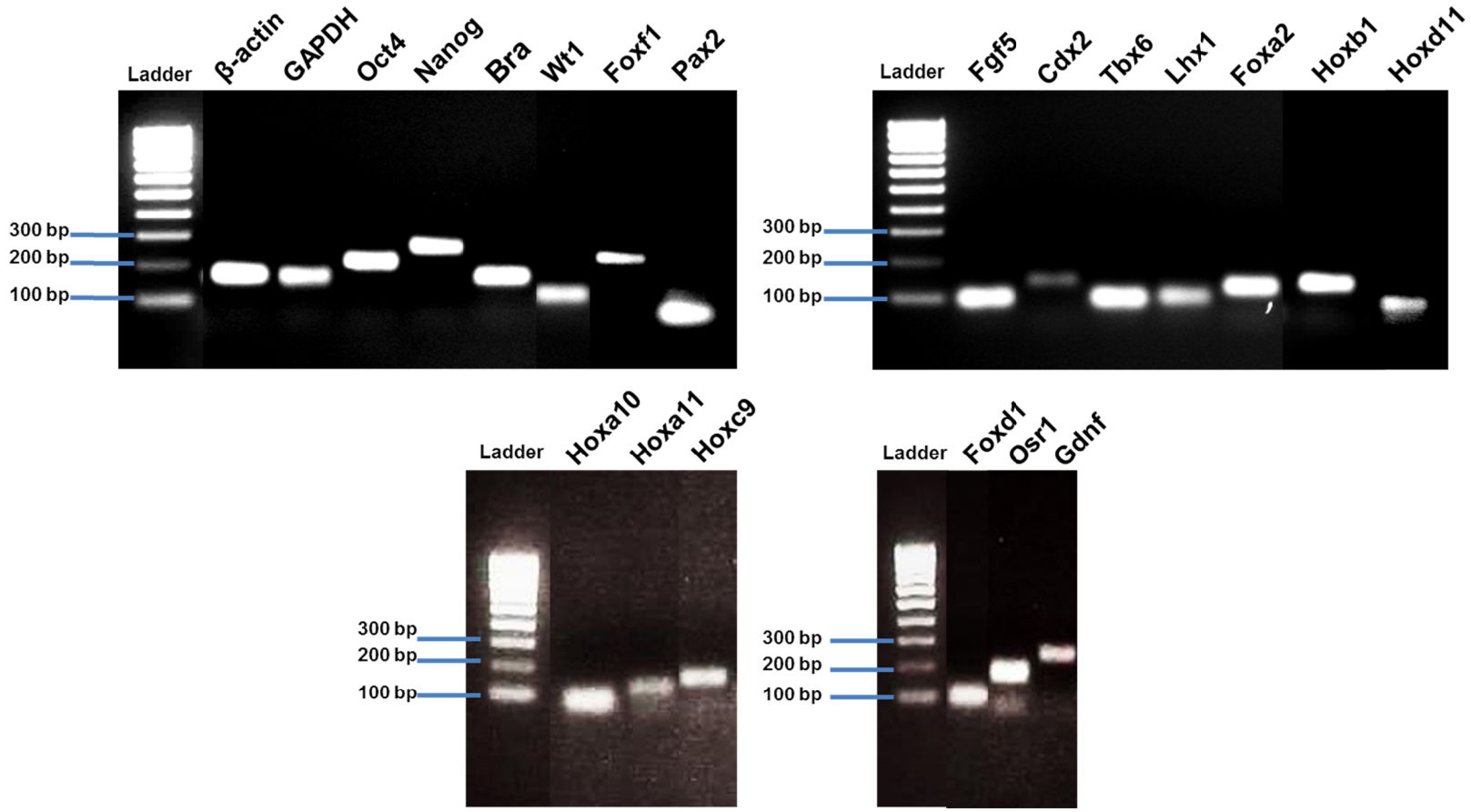

Figure 1 2% agarose gel electrophoresis of RT-qPCR amplicons from key mesodermal and kidney gene mRNAs. Expected size of amplicons are as follows: *β-actin*, 145 bp; *GAPDH*, 150 bp; *Bra*, 136 bp; *Cdx2*, 114 bp; *Fgf5*, 88 bp; *Foxa2*, 115 bp; *Foxd1*, 88 bp; *Foxf1*, 191 bp; *Gdnf*, 222 bp; *Hoxa10*, 61 bp; *Hoxa11*, 97 bp; *Hoxb1*, 128 bp; *Hoxc9*, 138 bp; *Hoxd11*, 97 bp; *Lhx1*, 87 bp; *Nanog*, 232 bp; *Oct4*, 188 bp; *Osr1*, 161 bp; *Pax2*, 104 bp; *Tbx6*, 80,80,157 bp; *WT1*, 116 bp.

Video 1 Stitched growth video of Day 3–Day 7 EBs derived from *Bra-GFP/Rosa26-E2C* mESCs using the Cell-IQ imaging facility, showing cavitating progress during the culture period. EBs were imaged on an hourly basis.